

1 Comments on NO₂ and HCHO measurements in Moore's from 2012 to 2016 from Pandora
2 spectrometer instruments compared with OMI retrieval and with aircraft measurements during
3 the Korus-AQ campaign by Jay Herman et al.

4
5
6
7 General comments.

8
9 This paper is about observations of tropospheric columns of HCHO and NO₂ in 8 sites located in
10 Korea, by using a Ground Based-direct Sun spectrometric instrument prior and during a study
11 about Air Quality called KORUS-AQ. Observations have a different temporal extension
12 depending on the site and varies from 1 to 5 years.

13
14 Comparisons to NO₂ OMI-Aura OMNO₂ V03 and to measurements made by using the CAMS
15 instrument on board of an aircraft are also presented in this work.

16
17 Ground based (GB) data are very valuable and interesting and this paper states the importance
18 of GB measurements in comparison to satellite measurements available at the moment of the
19 campaign that cannot capture the diurnal variation of pollution, necessary to state the Air
20 Quality. It is also very valuable the effort devoted to keep operative 9 different instruments
21 during one to five years.

22
23 In my opinion the work is very descriptive with a lack of interpretation of the measurements,
24 instead, this article is in the scope of AMT journal and it should be published after taking into
25 account some specific comments and technical corrections.

26
27 Specific comments.

28
29 Please note: the colors used – Green for changes to the paper; Yellow for my comments in
30 reply to your review; No color for your review text

31
32 Introduction.

33
34 It would be clarifying if a brief introduction of the campaign, why in Korea, objectives, and kind
35 of instrumentation or citation of other works done during this campaign (if it is the case) would
36 be included in the introduction. Also why the target gases to be measured are HCHO and NO₂.
37 Previous works in AQ in Asian megacities (i.e., using MAXDOAS technique) should be also
38 mentioned in the introduction to put these measurements in context.

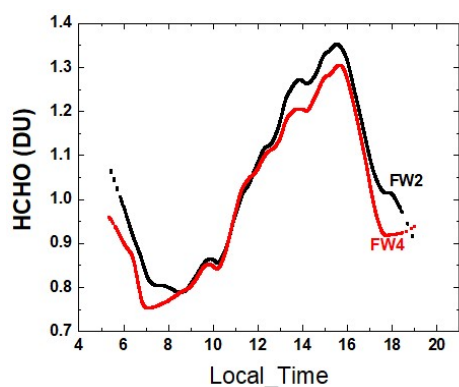
39
40 The introduction now reads

41
42 The purpose of this paper is to present the retrieved amounts of nitrogen dioxide and
43 formaldehyde, NO₂ and HCHO, obtained from Pandora Spectrometer instruments (PSI) during the
44 KORUS-AQ campaign (Korea US Air Quality: May – June 2016). Quoting from a NASA website: "Korea
45 U.S.-Air Quality (KORUS-AQ) is a joint field study between NASA and the Republic of Korea to advance
46 the ability to monitor air pollution from space. The campaign will assess air quality across urban, rural
47 and coastal South Korea using observations from aircraft, ground sites, ships and satellites to test air

48 quality models and remote sensing methods. Findings will help develop observing systems using models
49 and data to improve air quality assessments for decision makers.” A thorough description of the KORUS-
50 AQ campaign and its motivations is given in a pre-campaign white paper, [https://espo.nasa.gov/korus-
ag/content/KORUS-AQ_White_Paper](https://espo.nasa.gov/korus-
51 ag/content/KORUS-AQ_White_Paper).

52 Assessing air quality in South Korea is of interest because of the levels of pollution arising from
53 high densities of population and intense industrial activity associated with the production of NO₂.
54 Recent measurements of surface concentrations of NO₂ and comparisons with satellite data
55 demonstrate the need for high quality ground-based measurements to augment satellite observations
56 (Kim et al., 2017; Jung et al., 2017). The driving reason behind the interest is the effect of elevated levels
57 of NO₂ in Korea on human health (Kim and Song, 2017 and references therein). Measurements of N O₂
58 from aircraft have been used to obtain altitude profiles to compare with data obtained from fixed site
59 measurements and to obtain a national scale estimate of pollutant exposure (Lee et al., 2015; Kim and
60 Song, 2017).

61 In addition to NO₂, PSI measurements were used to assess the amount of Formaldehyde (HCHO)
62 present in the air. This is important because of HCHO potential impact on health (Zhang et al., 2013,)
63 and because it plays a strong role in tropospheric reactions leading to the formation of boundary layer
64 ozone. Sources of HCHO are from atmospheric reactions with volatile organic compounds (VOC) emitted
65 from ground sources and industrial activities (Lee et al., 2009). A previous paper describes HCHO
66 retrievals from a PSI located at Yonsei University in Seoul using a similar spectral fitting retrieval
67 algorithm used in the current study (Park et al., 2018), but using a different wavelength fitting range,
68 335 – 358 nm instead of 332 – 359 nm used in this study. The choice of spectral fitting window is
69 discussed in Spinei et al. (2018).



70 To give an idea of the effect of different fitting
71 windows, I am showing a graph to the left. This paper
72 used fitting window 2 (FW2 332 – 359 nm). For NO₂,
73 there is no ambiguity with fitting window. For HCHO,
74 the ambiguity comes from cross-correlation effects with
75 O₃, NO₂, and BrO

76
77
78
79 Some information about the different instruments, technique and retrieval of data should be
80 included in this work:

81
82 The instruments described in this paper are Pandora, details given in this paper, OMI satellite
83 instrument, 4-STAR, described in this paper, and CAMS.

84
85 Added Line 463: Quoting from Richter et al., 2015, “CAMS is a multi-species spectrometer configured for
86 the simultaneous detection of ethane (C₂H₆) and formaldehyde (CH₂O). The spectrometer utilizes a

87 tunable, fiber optically pumped difference frequency generation laser source in combination with a
88 Herriott type multi-pass absorption cell with an effective path length of 89.6 m”

89
90 Line 318: OMI is a polar orbiting push broom hyperspectral instrument (300 – 500 nm with resolution of
91 0.45 nm in the UV and 1 nm in the visible and a spatial resolution of 13 x 24 km²) onboard the AURA
92 satellite

93
94 I suppose that Pandora retrieval is based in a DOAS algorithm, but if not, the kind of
95 algorithm used should be, at least, mentioned and cited. If it is the case, a small mention
96 to DOAS retrieval or DOAS technique should be included in the text and cited.

97
98 The retrieval technique and error estimates for HCHO are discussed in a companion paper, Spinei et al.
99 (2018) also submitted to AMT. The PSI description is given starting on Page 4 and in included references.
100 The algorithm is a modified form of DOAS. The big difference is that there is no attempt to flatten the
101 spectral shape (important for ozone) , but not for NO₂ or HCHO.

102
103 Regarding to OMI, characteristic of the data used would be welcome in order to sustain
104 some statements about the differences between GB and satellite measurements
105 mentioned along the text. I will revisit this point later on in the proper section.

106
107 For the interpretation of CNO₂, it would be interesting to mention what is the
108 contribution to CNO₂ of stratospheric column, if stratospheric and tropospheric
109 contribution can separated and what is the sensitivity to troposphere of Pandora
110 instrument.

111
112 For polluted regions, such as Seoul or Olympic Park, the stratospheric amount of NO₂ (0.1±0.05 DU) is
113 negligible compared to the total column amount 0.5 to 3 DU. The stratospheric column cannot be
114 separated, but is small compared to the tropospheric amount.

115
116 On Page 4 I have added

117 Figures 3 and 4 summarize all of the Pandora C(NO₂) data obtained during the KORUS-AQ
118 campaign. Figure 3 presents histograms in percent frequency of occurrence for all nine sites. All of the
119 sites located within or downwind of major cities have production of NO_x mainly from transportation and
120 power generation as its major sources. The ratio of transportation NO_x production compared to all
121 other sources is estimated as up to a factor of three (Kim et al., 2013). Of these sites, Anmyeondo
122 frequently (40%) retrieves values of C(NO₂) that are close to the typical stratospheric values of 0.1±0.05
123 DU. Other sites occasionally have clean days with similar low values.

124
125
126 NO₂ during KORUS-AQ campaign.

127
128
129 For the interpretation of CNO₂, it would be interesting to mention what is the contribution to
130 CNO₂ of stratospheric column and for AQ purposes to what extent tropospheric column resides
131 below boundary layer. Also would be important to state what the sensitivity to troposphere of
132 Pandora instrument is.

133 The sensitivity to stratospheric and tropospheric NO₂ are approximately the same as long as direct-sun
134 measurements are possible. The estimated retrieval error is ±0.05 DU with a precision of ±0.01 DU. This
135 has been mentioned on Page 5 line 147. Figure 4 demonstrates this accuracy and precision.

136

137 Later on, in this same section you consider that measured CNO₂ at Anmyeondo is mainly
138 stratospheric. How can you differentiate this stratospheric contribution? See above

139

140 In order to have a reference, which level of CNO₂ is typical of polluted places?

141 In the US, a value of 0.3 DU would be typical

142 In Korea a value of 0.5 DU is common.

143 Line 173: I added, "Typical C(NO₂) amounts are 0.3 to 0.5 DU in polluted regions."

144

145 A previous intercomparison of two of the GB instruments used in this work has been done with
146 a very good agreement. But, to what extent is this good agreement extensive to the remaining
147 GB instruments?

148 Of the new instruments installed during KORUS-AQ (not the older instruments Seoul and Busan), they
149 were run side by side at Goddard Space Flight Center with similar results. Our experience is that shipping
150 does not alter the calibration.

151

152 From figure 2a, lower panel, it seem that there is a level of cloud or aerosol coverage that limits
153 the agreement between the two GB compared instruments. It can be seen that between 17 and
154 18h where the difference between instruments is greater than 0.05 DU. Has been carried out
155 any study in which this level has been delimited in order to exclude these data for this work? Or
156 this situation only is observed when high coverage (due to cloud or aerosol) and low CNO₂ are
157 coincident? Is this situation contemplated by applying the filter of CNO₂ error >0.1 DU?

158

159 All data with error estimates > 0.1 DU were eliminated. The purpose of Figure 2 is to demonstrate that
160 good retrievals do not require perfectly clear skies.

161

162 In page 8, L185, it is said that figure 3 and 4 are consistent with a large NO₂ pollution source in
163 the Seoul metropolitan area that tends to transport eastward to the eastern stations near Seoul.
164 This is not totally clear for me since there must be sources in all the cities, as traffic. It is also
165 difficult to see from the different axis for different stations in figure 3. Please, explain this point
166 with more detail. In figure 4 it is difficult to see.

167

168 The highest pollution sources are close to the Seoul metropolitan area. This includes Olympic Park just
169 to the east of Seoul. As one proceeds eastward from Seoul to Taewha, the traffic level and population
170 density diminishes from extremely heavy to moderate. All of the sites have their own local sources
171 augmented by transport. Since I do not model the transport of NO₂, I have removed the speculation
172 about transport.

173

174 The sentence now reads, ". Figures 3 and 4 show that sites near Seoul metropolitan area (Olympic Park)
175 have larger amounts of pollution compared to those further away (Taehwa, Songchon, and Yeosu)."

176

177

178

179 In line 189, are you referring figure 4 instead figure 5?

180 It should be (Figs. 4 and 5)

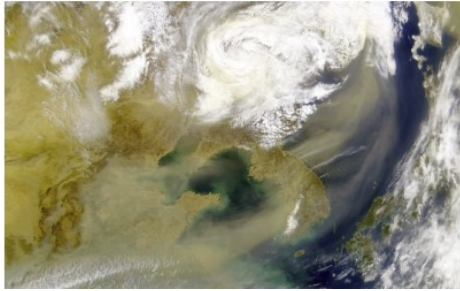
181
182 Busan is located in the eastern coast, maybe NO₂ is transported from Busan to the Ocean but
183 attending to the eastward transport proposed for Seoul and eastern stations surrounding Seoul,
184 the amounts of NO₂ in Busan shouldn't be given by transport from western locations? But
185 considering that the mechanism of transport to the Ocean is the cause for CNO₂ dissipation in
186 Busan, why are there some days that this mechanism doesn't work and concentrations over 3
187 DU are observed? Just in case, this situation is observed only 3 days. Is there any common
188 pattern for them?

189
190 NO₂ from Busan certainly reaches the ocean areas just to the east of the city and probably dilutes the
191 total amount over the city. I changed the sentence to read some in place of much, "Busan is located on
192 the southeastern coastline, so that some of its NO₂ pollution dissipates over the ocean, except for
193 occasional days when very high amounts (3 DU) occur."

194
195 Busan, while smaller than Seoul, has a very high density of people located near the city center and quite
196 heavy traffic. On days when there is little wind, NO₂ will accumulate in the lower troposphere.

197
198 Occasional plumes observed at Anmyeondo, are supposed to come from Northwards or China,
199 is there any evidence of this? Maybe a retro trajectory for these days? Literature?

200
201 Satellite pictures showing dust transport are common. These also carry NO₂ when the wind levels are
202 reasonably high.



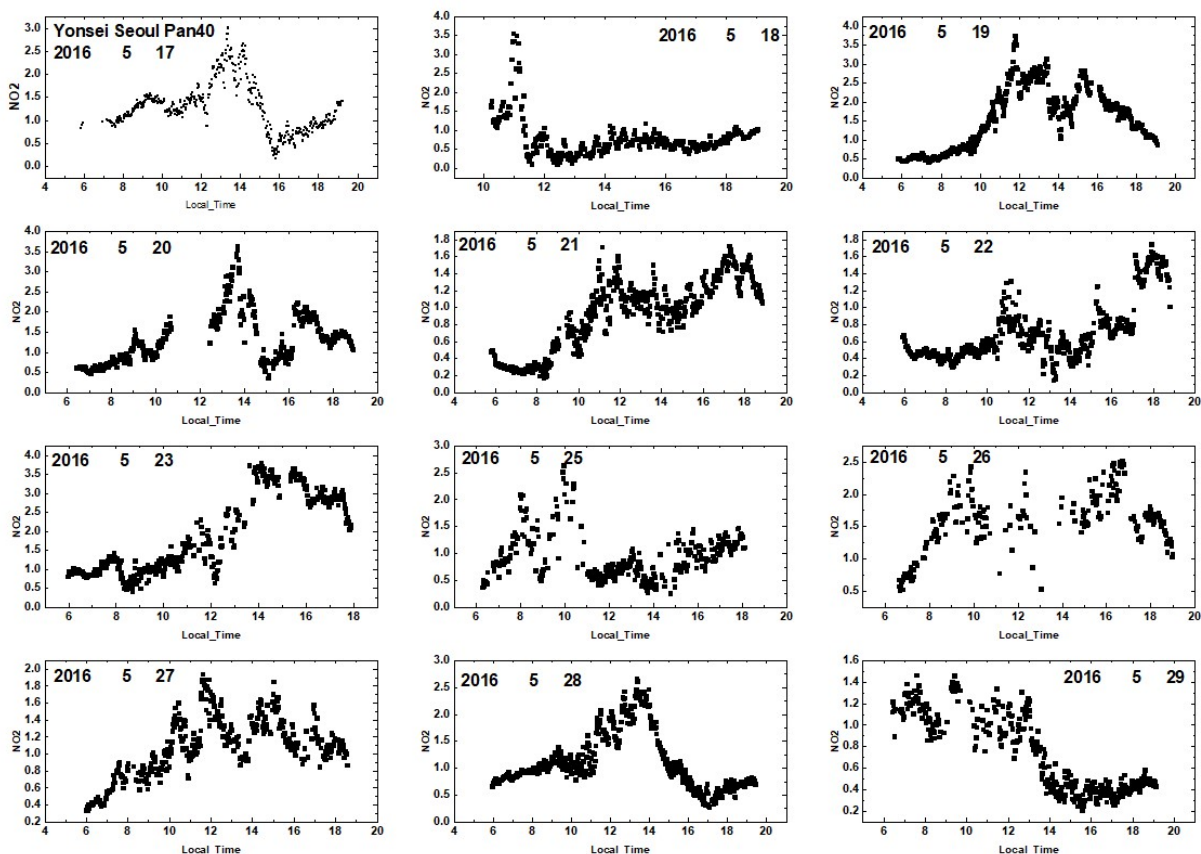
203
204
205 I changed the sentence to be more speculative, since I have no direct evidence of the source. The island
206 region Anmyeondo during the KORUS-AQ campaign had little traffic and a low population density.

207
208 "The most frequently occurring C(NO₂) value at Anmyeondo is 0.15 – 0.2 DU, which means that the
209 measured NO₂ amount are partly from the stratosphere with very little tropospheric or boundary layer
210 NO₂. There are occasional C(NO₂) plumes that could be from industrial activity to the north, and,
211 perhaps, from China. Transport of NO₂ from China occurs episodically in significant amounts (Lee et al.,
212 2014)."

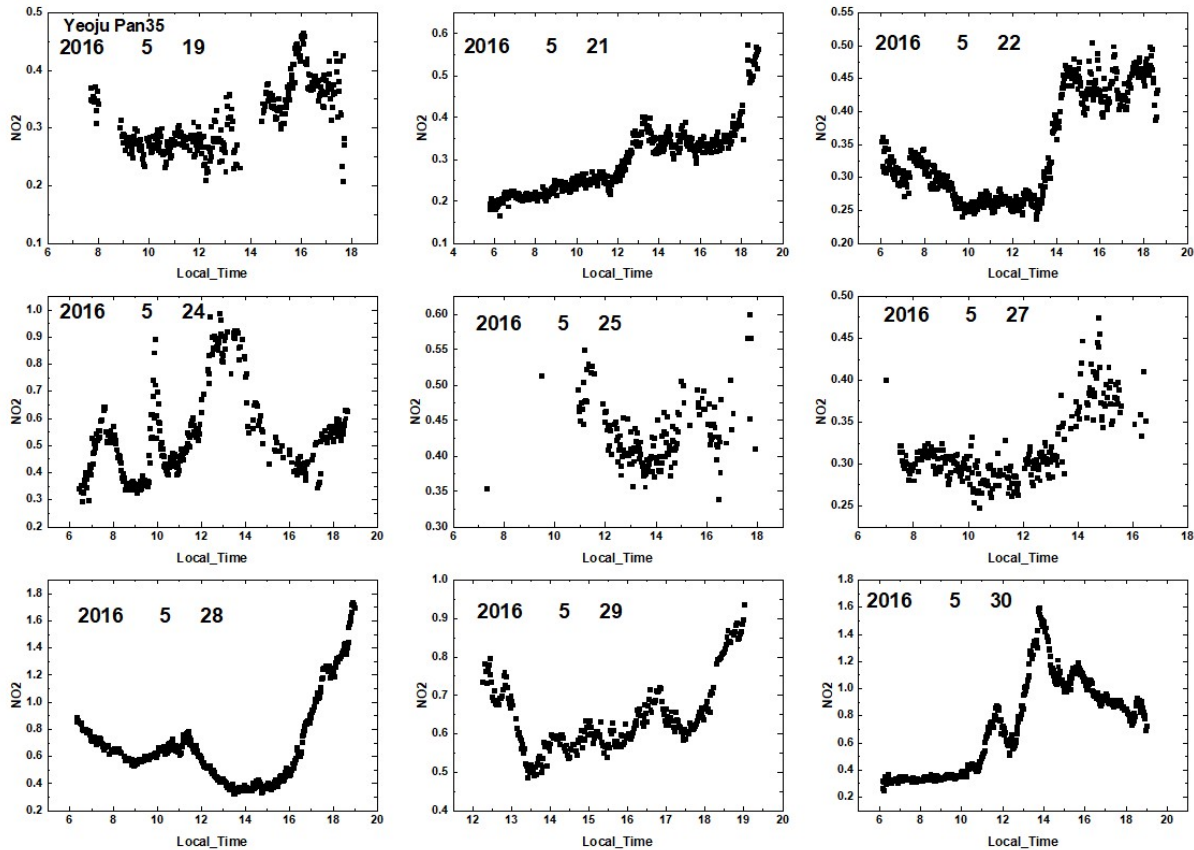
213
214
215 Diurnal variation of CNO₂
216 Is there any explanation for the increasing of CNO₂ at the late afternoon? The high amounts of
217 CNO₂ observed at Seoul even in the morning are associated with an anticyclonic situation when
218 high pressures confine pollutants in the boundary layer? Or it is always the same, no matter the
219 meteorological situation is? The evolution from days 130 to 150 could indicate an anticyclonic
220 situation followed by a low pressure system (rain or wind) because the following days seems to
221 be less polluted. This meteorological situation could also explain the increase along the day of

222 CNO2. Regarding the eastern stations around Seoul, they have not only the transported air
223 masses from Seoul but also their own sources. This is not easy to interpret without a chemical
224 model but do you think it could explained the two maxima observed at midday and at late
225 afternoon at Olympic Park and Taehwa Mt? It is a pity that the series for these last stations stops
226 at day 150, maybe the same behavior than at Seoul could be observed.
227

228 The weather during the KORUS-AQ days was frequently partly cloudy with some days of rain. Not the
229 best measuring weather. However, I do not know what the wind conditions were relative to the rooftop
230 of the physics building at Yonsei. The building is substantially elevated over the main city streets. I am
231 showing here a series of individual plots for 12 days for Seoul and 9 days for Yeosu. The patterns are not
232 clear. Most of the time, the amount increases in the afternoon, but there are morning peaks (25th). I
233 have also included some daily plots from Yeosu. The pattern is irregular. The 3-D plots give the general
234 idea of the diurnal variation. The plots below are not in the paper



235



236

237

238 Could you cite instead the source for automobile emission from which the brochure of Thermo

239 Sci is taken? I cannot find a journal reference to the measurements made by the company. However, I
 240 added a reference related to NO/NO2 ratios (Walters et al., 2015)

241

242 To compare to Boersma et al. and extract any conclusion it would be necessary to know if the
 243 meteorological situation considered in Boersma et al., is the same than in this work. Is it the
 244 same? This is not clear enough in the text. The situation observed by Boersma et al. is in the
 245 same kind of environment? I removed the reference to Boersma et al.

246

247 Longer-term changes in CNO2

248

249 Figure 6 and text would be gain in clarity if L(t), M(t) and ZM(t) would be identified in the figure
 250 6.

251 ZM(t) and L(t) are not shown in Figure 6. As it says in the text, The “zero slope functions” are obtained
 252 by subtracting a linear least squares fit L(t) to monthly running average curves M(t) in panels C and F to
 253 form zero slope functions $ZM(t) = M(t) - L(t)$.” However, M(t) is shown in panels C and F. I have not
 254 labelled panels C and F.

255

256 It is difficult to see any monthly variation in the black line of panels B and E in that scale. Please,

257 change the scale from 0 to 1.5.

258
259 There is almost no monthly variation in the deseasonalized time series. I am attaching two plots with the
260 original and with an expanded inset scale for Gwangju. The first is the original NO₂ data monthly running
261 average. The second is the same plot after removing the seasonal behavior. These plots are now in an
262 appendix.

263

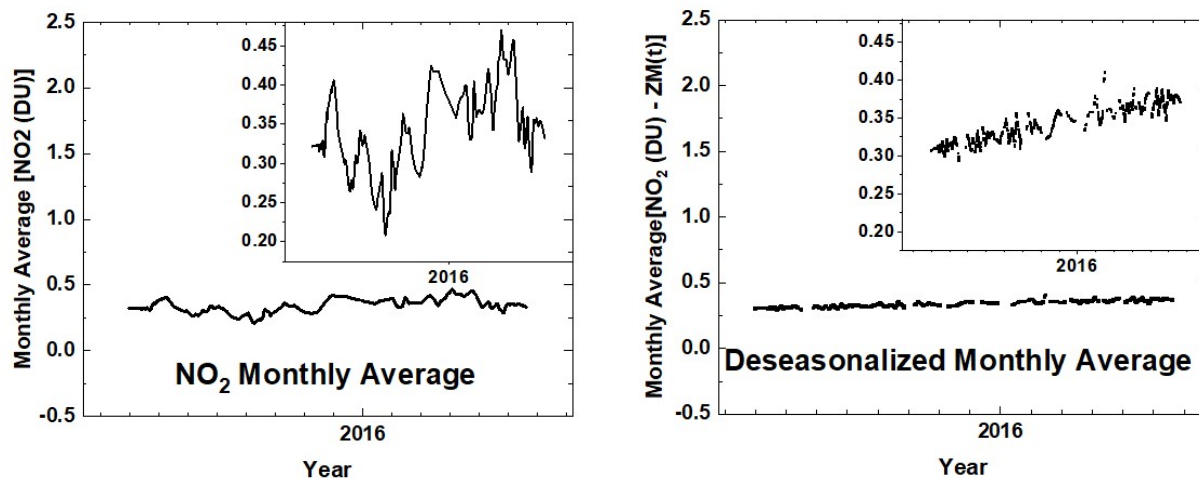


Fig. A1 An illustration of the deseasonalization (right panel) of the monthly running average of NO₂ for the Gwangju site (left panel) shown in Fig. 6. The insets are magnifications of the main plots.

264
265 Less polluted stations, Gwangju and Anmyeondo show a positive trend in CNO2 whereas the
266 remaining stations that are more polluted show a negative CNO2 trend. This is difficult to
267 understand. Could you explain it a little?

268
269 For Gwangju and Anmyeondo, the time series are too short (13 Months) to infer that the changes
270 represent increasing or decreasing long-term changes in pollution levels. The data from the two long
271 term sites (Seoul and Busan) does suggest that clean-up efforts have occurred in spite of increasing
272 population during the period of observation. Automobile exhaust has cleaned up considerably based on
273 US data. I do not have access to Korean automobile exhaust data.

274
275 Short time series are a universal problem with acquiring “campaign” data instead of locating
276 instruments permanently at fixed sites. The Pandora program is now implementing the long-term site
277 approach. It is possible that Korean efforts at lowering pollution in larger cities are having an effect, but
278 this data series is too short to support the hypothesis.

279
280 Comparison with OMI satellite Overpass Data.

281
282 Differences observed between OMI and GB instruments are surely due to the different observed
283 air masses by OMI and GB, part of it would be due to the OMI FOV as it is stated in the text. In
284 fact a better coincidence observed in Gwangju support this fact. This could be stated in the text
285 since if differences are only due to OMI FOV, comparison would be more coincident in western
286 stations.

287
288 To discuss this point a brief description of how have OMI data been calculated is important to

289 include. OMI overpass is only one point per day. But how has this point been calculated? By
290 using the closest orbit to the station, as a averaging of some measurements? In this case a plot
291 where the different points used by a OMI overpass could support the FOV as a cause of the
292 observed differences. Small discussion about sensitivity of OMI to lower tropospheric NO₂ and
293 a discussion comparing it to Pandora sensitivity in troposphere or boundary layer is missed out
294 in the text as well.

295

296 But the differences are also due to the hour of the overpassing. It is not possible for OMI to
297 capture the elevated CNO₂ observed at late afternoon, but you can check if the comparison
298 improves when you don't consider late afternoon GB data.

299

300 The OMI data are acquired from the station overpass time series up to a maximum of 3 points per day
301 (90 minutes apart), but usually 1 point per day. The distance from the central location does vary. The
302 Pandora data are selected to be within 8 minutes of the overpass time, that is, up to an average of 16
303 Pandora points per OMI point. This is stated clearly in the opening paragraph of section 5. The OMI
304 overpass data link is given in the paragraph. The data link contains the distance from the target site for
305 every point in the time series. The overpass data does have varying distances. For most of the overpass
306 data, the average distance is 20±20 km with a few points further away.

307

308 The 0 – 40 km variation plus the OMI field of view, which is quite large, 13 x 24 km², compared to city
309 center dimensions. The result is that there is spatial averaging that reduces the high levels of NO₂ seen
310 in PSI measurements near the center of a highly polluted metropolitan area. For cleaner sites, the
311 averaging does not produce as large an effect. Other OMI retrieval effects, such as uncertainty in the
312 surface reflectivity and the size of the averaging kernel near the surface (sensitivity), produce errors that
313 are much smaller than the differences seen against PSI.

314

315 Figure 9b is difficult to see. As you are using 3 month average data, it would be useful to see
316 line+symbol instead only line. In that case it would be possible to see if there is not a
317 displacement of minima, it is not clear for me if they are coincident.

318

319 The data are 3 month running averages. There are approximately 1500 data points. I have added a
320 comment to the figure caption about running averages. There is no displacement of the minima

321

322 The data are derived from 3- month running averages of the daily data. Interpolation has been used
323 where there are missing data points.

324

325 Please make minor grid lines darker for this figure and enlarge the plot in order that details can
326 be seen. Done

327

328

329 Figure 9b shows the 1500 data points that are approximately a 3-month running average and the
330 interpolation for missing data. These are just the solid curves in Figure 9b on an expanded scale.

331

332 It is very interesting that seasonal evolution is captured by OMI and GB the first two years in
333 both stations and in the last two years for Seoul. But there is a double maxima in spring captured
334 by GB in 2013 and 2014. Although it is not exactly in the scope of this paper, is there any
335 explanation for this apparently unusual seasonal behaviour, especially for year 2014?

336

337 I do not know why there are differences in the seasonal cycle

338

339

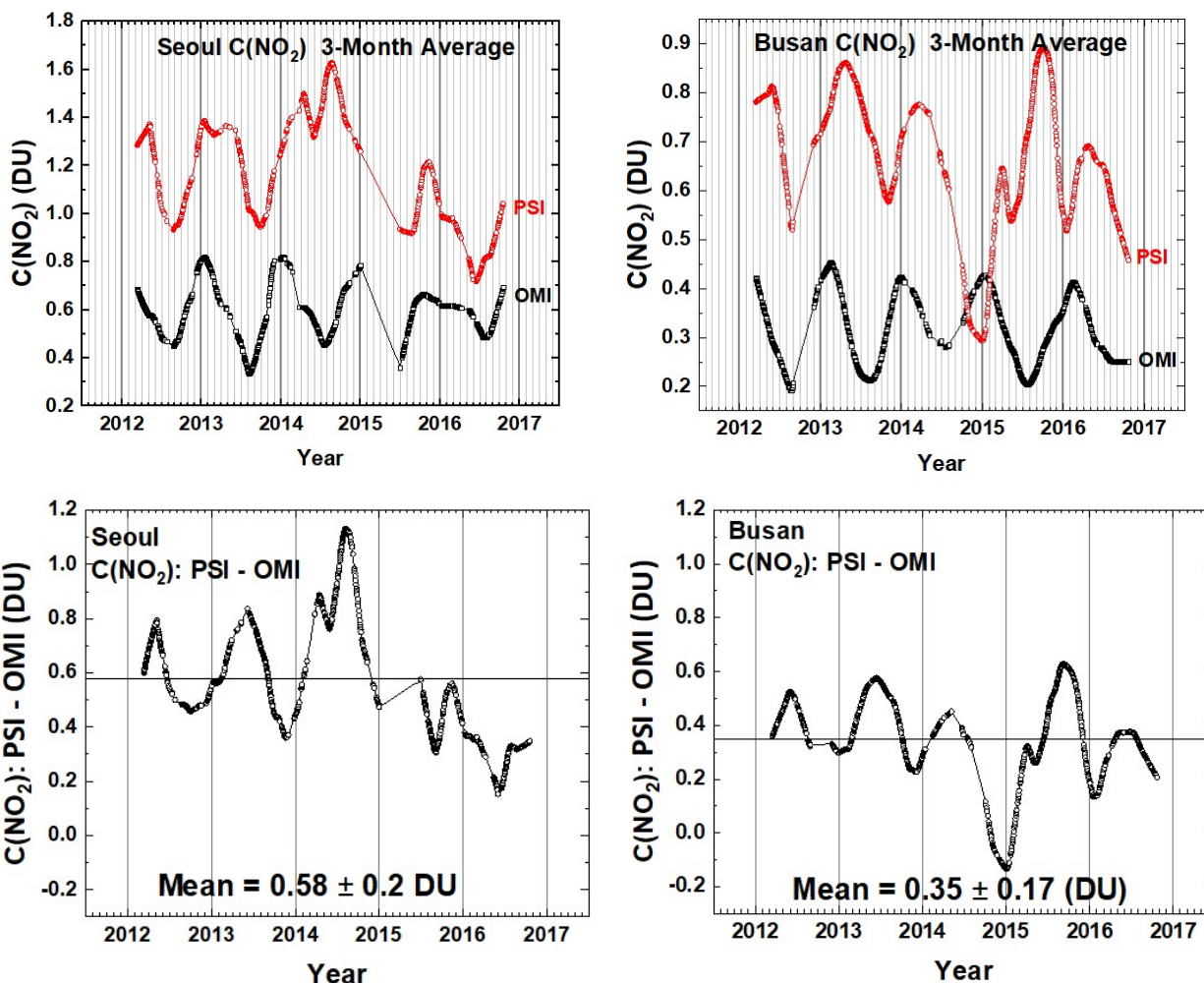


Fig. 9b Comparisons between the seasonal averages for C(NO₂) from OMI (black) and PSI (red) at Seoul and Busan for a 5-year period. The lower panels show the seasonal difference between the PSI and OMI. The individual data points are shown derived from a Lowess(0.1) smoothing, approximately a 3-month running averages of the daily data. Interpolation has been used where there are missing data points.

340

341 The minimum in CNO2 observed by GB in Busan at the end of 2014 is really surprising, is there
342 any explanation for such behaviour?

343

344 This could be a local effect during winter months at the university in Busan. The PSI appears to have
345 been operating normally. There is no periodic maintenance or recalibration of the PSI.

346

347 I don't think that the objective of OMI were to stated AQ in big cities, it is clear that continuous
348 monitoring is a better technique to know the evolution of pollutants along the day in order to
349 control the impact of pollutants on public health.

350

351 I agree. Polar orbiting satellites only give a midday snapshot of the pollution levels.

352
353 I have added: "The results from PSI suggest that local ground-based monitoring of pollution is important
354 for estimating their impact on human health, particularly since amounts of C(NO₂) occurring later in the
355 afternoon exceed the amounts at the time of the satellite overpass."
356

357
358 Formaldehyde from five Korus-AQ sites
359

360 I don't know if this is even possible, but in order to investigate differences observed in CHCHO
361 from PSI and aircraft instrument, it would be interesting to have both instrument measuring
362 together a couple of days from GB in the same location. In this way it would be possible to
363 estimate whether the differences are due to different retrieval or observation technique more
364 than to the approximations made to correct the observed column from aircraft to compare to
365 GB instrument.

366
367 The aircraft did operate on more than 1 day. I picked a sample from May and June to show typical
368 results. Measurements from other days were very similar.

369
370 In figure 18, most of plotted days don't show the expected diurnal evolution, but an increase of
371 HCHO along the day with greater amount observed at late afternoon, is there any explanation
372 about this? The same behaviour is observed in figure 19a for the same station, it seems to be
373 the habitual diurnal variation of HCHO for this site.

374
375 I'm not sure what the "expected" diurnal variation should be. Not enough measurements have been
376 made to date.

377
378 Technical corrections.

379
380 Page 5, L 136. 2.0 should be 2 OK

381
382 Figure 2 has been changed to

383

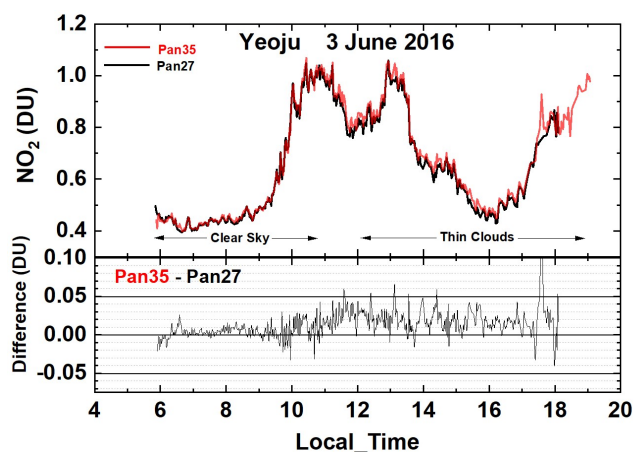


Fig. 2a C(NO₂) amounts from Pandora 27 and 35 in

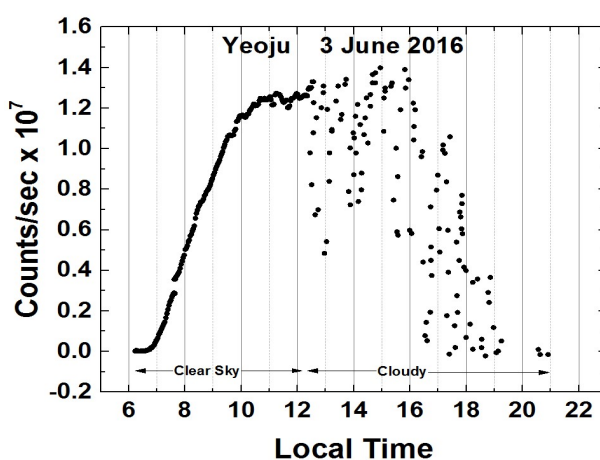


Fig. 2b Pandora 35 estimate of cloud or aerosol

Yeosu, Korea during 3 June 2016 and their difference $|\text{Pan35} - \text{Pan27}| < 0.05 \text{ DU}$. cover from measured counts/second at approximately 500 nm.

384 Figure 2a. Please include a grid in the lower panel that permits to see the level of $\pm 0.05 \text{ DU}$.

385 OK

386 Figure 2a. Please remove last sentence of the caption. OK

387

388 Figure 2b. Please do not include an explanation in the caption but in the text. OK

389

390 The text now reads: "Figure 2b shows the effect of thin clouds in terms of reduced measured count rates
391 for a single spectrometer pixel near 500 nm showing a near noon count rate of 1.26×10^7 counts/second
392 followed by a reduced count rate as clouds move in front of the sun. The cloud plus aerosol cover
393 estimate is from the same date 3 June 2016 as the $C(\text{NO}_2)$ amounts shown in Fig.2a."

394

395

396 Page 10 line 237 4.0 should be 4 OK

397

398 Figure 6. Dots are extremely difficult to see, please make them darker. Missing labels in x axis of
399 panel A, B and E. I tried making them darker. Except for a few high-value points, it makes no difference
400 in being able to see the individual dots. There are 5400 dots, most of which are near the black curve.
401 There are no missing axis labels. Instead, panels A, B, D, and E have the same labels and same scale
402 (Years) broken down by Month.

403

404 Figure 6. Please explain in the caption what is the dark line in panel B and E. Re-organize the text
405 in the caption, it is very confusing. OK

406

407 The figure 6 caption is now: "Approximately 1 year of daily column $C(\text{NO}_2)$ amount data (Panels A and D)
408 and the monthly running average amount (dark plot in Panels A and D). The data are from GIST at
409 Gwangju and Amnyeondo. Panels A and D are the original time series with one data point every 80
410 seconds, panels B and E are the deseasonalized time series. Panels C and F are an expanded scale of the
411 monthly running averages $M(t)$ of $C(\text{NO}_2)$ that are identical to the solid lines in panels A and D. The
412 vertical extent (panels A, B, D, and E) on a given day is the range of diurnal variation from early morning
413 to late afternoon"

414

415 Also, see the graphs near line 247 of this reply. The insets show the results of deseasonalization.

416

417 Figure 6. Greater plots and vertical grid would be also very useful. I added the vertical grid

418

419 Figures 17 and 18. Please include vertical grids. Put greater tick labels. OK

420

421 Figures 19a and 19b, please darken the dot, they are difficult to see. Add vertical grids to the left
422 panels. There are over 11000 points for each site. Darkening the points will not make them visible
423 except for outliers.

424

425 Figure 19b panel B, correct typo for Anmyeondo OK

1 **NO₂ and HCHO measurements in Korea from 2012 to 2016 from Pandora Spectrometer Instruments**
2 **compared with OMI retrievals and with aircraft measurements during the KORUS-AQ campaign**

3 **Jay Herman¹, Elena Spinei², Alan Fried³, Jhoon Kim⁴, Jae Kim⁵, Woogyung Kim³, Alexander Cede⁶, Nader**
4 **Abuhassan¹, Michal Segal-Rozenhaimer^{7,8}**

5

6

7

8

9

10

11

12

13

14

15

16

17

18 **Correspondence email: jay.r.herman@nasa.gov**

19 **¹University of Maryland Baltimore County JCET**

20 **²Virginia Polytechnic Institute and State University, Blacksburg, VA 24061, USA**

21 **³Institute of Arctic & Alpine Research, University of Colorado, Boulder, Colorado**

22 **⁴Dept. of Atmospheric Sciences, Yonsei University, Seoul Korea**

23 **⁵Department of Atmospheric Science, Pusan University, Busan, Korea**

24 **⁶Goddard Earth Sciences Technology & Research (GESTAR) Columbia, Columbia, MD 21046, USA**

25 **⁷Earth Science Division, NASA Ames, Mountain View, California**

26 **⁸Bay Area Environmental Research Institute, Petaluma, California**

27

28

29 **NO₂ and HCHO measurements in Korea from 2012 to 2016 from Pandora Spectrometer Instruments**
30 **compared with OMI retrievals and with aircraft measurements during the KORUS-AQ campaign**

31
32 **Abstract**

33
34 Nine Pandora Spectrometer Instruments (PSI) were installed at 8 sites in South Korea as part of
35 the KORUS-AQ (Korea U.S.-Air Quality) field study integrating information from ground, aircraft,
36 and satellite measurements for validation of remote sensing air-quality studies. The PSI made
37 direct-sun measurements of total vertical column NO₂, C(NO₂), with high precision (0.05 DU,
38 where 1DU = 2.69x10¹⁶ molecules/cm²) and accuracy (0.1 DU) that were retrieved using
39 spectral fitting techniques. Retrieval of Formaldehyde (HCHO) total column amounts were also
40 obtained at five sites using the recently improved PSI optics. The HCHO retrievals have with
41 high precision, but possibly lower accuracy than for NO₂ because of uncertainty about the
42 optimum spectral window for all ground-based and satellite instruments. PSI direct-sun
43 retrieved values of C(NO₂) and C(HCHO) are always significantly larger than OMI (AURA satellite
44 Ozone Monitoring Instrument) retrieved C(NO₂) and C(HCHO) for the OMI overpass times (13.5
45 ± 0.5 hours). In urban areas, PSI C(NO₂) averages are at least a factor of two larger than OMI
46 averages. Similar differences are seen for C(HCHO) in Seoul and nearby surrounding areas. Late
47 afternoon values of C(HCHO) measured by PSI are even larger, implying that OMI early
48 afternoon measurements underestimate the effect of poor air quality on human health. The
49 primary cause of the OMI underestimate is the large OMI field of view FOV that includes
50 regions containing low values of pollutants. In relatively clean areas, PSI and OMI are more
51 closely in agreement. C(HCHO) amounts were obtained for five sites, Yonsei University in Seoul,
52 Olympic Park, Taehwa Mtn., Amnyeondo, and Yeosu. Of these the largest amounts of C(HCHO)
53 were observed at Olympic Park and Taehwa Mountain, surrounded by significant amounts of
54 vegetation. Comparisons of PSI C(HCHO) results were made with the Compact Atmospheric
55 Multispecies Spectrometer CAMS during overflights on the DC-8 aircraft for Taehwa Mtn and
56 Olympic Park. In all cases, PSI measured substantially more C(HCHO) than obtained from
57 integrating the CAMS altitude profiles. PSI C(HCHO) at Yonsei University in Seoul frequently
58 reached 0.6 DU and occasionally exceeded 1.5DU. The semi-rural site, Mt. Taehwa, frequently
59 reached 0.9 DU and occasionally exceeded 1.5DU. Even at the cleanest site, Amnyeondo, HCHO
60 occasionally exceeded 1 DU.

61
62 Keywords: Pandora, KORUS-AQ, NO₂, HCHO, Formaldehyde, Korea

63

64 **1 Introduction**

65 The purpose of this paper is to present the retrieved amounts of nitrogen dioxide and
66 formaldehyde, NO₂ and HCHO, obtained from Pandora Spectrometer instruments (PSI) during the
67 KORUS-AQ campaign (Korea US Air Quality: May – June 2016). Quoting from a NASA website: “Korea
68 U.S.-Air Quality (KORUS-AQ) is a joint field study between NASA and the Republic of Korea to advance
69 the ability to monitor air pollution from space. The campaign will assess air quality across urban, rural
70 and coastal South Korea using observations from aircraft, ground sites, ships and satellites to test air
71 quality models and remote sensing methods. Findings will help develop observing systems using models
72 and data to improve air quality assessments for decision makers.” A thorough description of the KORUS-
73 AQ campaign and its motivations is given in a pre-campaign white paper, [https://espo.nasa.gov/korus-
74 aq/content/KORUS-AQ_White_Paper](https://espo.nasa.gov/korus-aq/content/KORUS-AQ_White_Paper).

75 Assessing air quality in South Korea is of interest because of the levels of pollution arising from
76 high densities of population and intense industrial activity associated with the production of NO₂.
77 Recent measurements of surface concentrations of NO₂ and comparisons with satellite data
78 demonstrate the need for high quality ground-based measurements to augment satellite observations
79 (Kim et al., 2017; Jung et al., 2017). The driving reason behind the interest is the effect of elevated levels
80 of NO₂ in Korea on human health (Kim and Song, 2017 and references therein). Measurements of N O₂
81 from aircraft have been used to obtain altitude profiles to compare with data obtained from fixed site
82 measurements and to obtain a national scale
83 estimate of pollutant exposure (Lee et al., 2015;
84 Kim and Song, 2017).

85 In addition to NO₂, PSI measurements
86 were used to assess the amount of Formaldehyde
87 (HCHO) present in the air. This is important
88 because of HCHO potential impact on health
89 (Zhang et al., 2013,) and because it plays a strong
90 role in tropospheric reactions leading to the
91 formation of boundary layer ozone. Sources of
92 HCHO are from atmospheric reactions with
93 volatile organic compounds (VOC) emitted from
94 ground sources and industrial activities (Lee et al.,
95 2009). A previous paper describes HCHO
96 retrievals from a PSI located at Yonsei University
97 in Seoul using a similar spectral fitting retrieval
98 algorithm used in the current study (Park et al.,
99 2018), but using a different wavelength fitting
100 range, 335 – 358 nm instead of 332 – 359 nm
101 used in this study. The choice of spectral fitting
102 window is discussed in Spinei et al. (2018).



Fig. 1 KORUS-AQ sites for 9 Pandora instruments at 8 sites.

103 As part of the KORUS-AQ campaign, a network of nine PSI was installed in Korea at 8 locations
 104 (Fig. 1 and Table 1). Five of the sites were selected to be “down-wind” from Seoul, an extremely NO₂
 105 polluted area. The intent of the network was to integrate column density observations of NO₂ and
 106 HCHO into a multi-perspective framework of observations including ground-based, satellite, and
 107 airborne measurements of air quality. Viewing air quality through these multiple perspectives is
 108 important for connecting observations from future geostationary satellites to air quality networks such
 109 that conditions both at the surface and aloft can be better understood and represented across
 110 unmonitored areas. The data are especially important for computer models used for forecasts and
 111 decision making. Five of the KORUS-AQ PSI had recently improved optics that permitted retrieval of total
 112 vertical column formaldehyde (C(HCHO)). Part of the network was installed in April 2015, a year before
 113 the start of the campaign. Three PSI continue to operate in Korea, one each, in Busan and Seoul since
 114 2012, and one in Gwangju operating since April 2015.

115
 116 Measurements of daytime total columns in Dobson Units, where 1 DU = 2.69 x 10¹⁶
 117 molecules/cm², C(NO₂), C(O₃) and C(HCHO) are obtained every 80 seconds, which enables the PSI to
 118 show rapid short term (minutes to hours) variations in most locations with significant pollution (e.g.,
 119 C(NO₂) > 0.2 DU). PSI measurements of the visible and UV wavelengths are obtained separately (40
 120 seconds each). A visible wavelength blocking filter, U340, reduces stray light for UV measurements.

121

Table 1 KORUS-AQ Locations (South to North)

Locations	Alt(m)	Latitude	Longitude
Gwangju	33	35.2260 N	126.8430 W
Busan	228	35.2353 N	129.0825 W
Anmyeondo	41	36.5380 N	126.3300 W
Taehwa Mtn	160	37.3123 N	127.3106 W
Yeoju-1 & 2	90	37.3385 N	127.4895 W
Songchon	49	37.4100 N	127.5600 W
Olympic Park	26	37.5232 N	127.1260 W
Seoul	181	37.5644 N	126.9340 W

122
 123 Details on the Pandora spectrometer instrument can be found in Herman et al., (2009 and 2015)
 124 as well as a NASA Pandora website
 125 https://avdc.gsfc.nasa.gov/pub/DSCOVER/Pandora/Web_Pandora/index.html and the data used are
 126 available from <https://avdc.gsfc.nasa.gov/pub/DSCOVER/Pandora/DATA/KORUS-AQ/>

127
 128 The PSI consists of a small Avantes low stray light spectrometer (280 – 525 nm with 0.6 nm
 129 spectral resolution with 4 times oversampling) connected to an optical head by a 400 micron single
 130 strand fiber optic cable. The spectrometer is temperature stabilized at 20°C (68°F) inside of a weather
 131 resistant container. The optical head consists of a collimator and lens giving rise to a 1.6° FOV (field of
 132 view) FWHM (Full Width Half Maximum) with light passing through two filter wheels containing
 133 diffusers, a UV340 filter (blocks visible light), neutral density filters, and an opaque position (dark
 134 current measurement). When the diffuser is used, the FOV is increased to over 2°. The optical head is

135 connected to a small suntracker capable of accurately following the sun's center using software running
136 on a small computer-data logger contained in a weatherproof outer box along with the spectrometer in
137 a second inner temperature controlled box. The PSI is capable of obtaining C(NO₂), C(HCHO) and C(O₃)
138 amounts sequentially over a period of 80 seconds including two dark current determinations. The
139 integration time for NO₂ in bright sun is about 4 milli-seconds that is repeated and averaged for 20
140 seconds (up to 4000 measurements) to obtain very high signal to noise ratios and very high precision
141 (precision < 0.01 DU). Similar comments apply to C(O₃), but not to C(HCHO), since formaldehyde
142 absorption spectrum is mixed in with absorption from NO₂ and O₃. This causes cross-correlation effects
143 in the retrieval algorithm that make C(HCHO) retrievals sensitive to the selection of the wavelength
144 range. The main source of noise in the measurement comes from the presence of clouds or haze in the
145 FOV, which increases the exposure time and reduces the number of measurements in 20 seconds.
146 Accuracy in the DOAS-type retrieval is obtained using careful measurements of the spectrometer's slit
147 function, wavelength calibration, knowledge of atmospheric absorption cross sections, and the solar
148 spectrum at the top of the atmosphere. Accuracy for C(NO₂) has been estimated to be ±0.05 DU. A
149 recent addition of anti-reflection coatings to the PSI optics has improved accuracy and precision by
150 reducing the residuals associated with spectral fitting using trace gas absorption cross sections. The
151 reduced residuals are necessary for the retrieval of formaldehyde and bromine oxide that absorb in
152 spectral regions dominated by ozone and NO₂.

153
154 This paper discusses the distribution of C(NO₂) and C(HCHO) over Korea at the sites where the
155 PSI were located (Fig. 1). Section 2 shows the amounts of NO₂ observed by PSIs at the 8 KORUS-AQ
156 sites. Section 3 discusses the diurnal variation of NO₂. Section 4 looks at longer term changes in NO₂
157 obtained from PSIs that were deployed before the beginning of the KORUS-AQ campaign. Section 5
158 evaluates the disagreement with **Ozone Monitoring Instrument** (OMI) satellite C(NO₂) retrievals (Kramer
159 et al., 2008). Section 6 compared PSI C(NO₂) retrievals with the aircraft overpass retrievals from the
160 4STAR instrument (Segal-Rozenhaimer et al., 2014). Section 6 discusses retrievals of C(HCHO) amounts
161 for five PSI sites, the diurnal variation of C(HCHO), and comparisons with the Compact Atmospheric
162 Multispecies Spectrometer CAMS (Richter et al., 2015) from DC-8 aircraft overflights of 5 PSI sites.

163

164 **2 NO₂ during the KORUS-AQ Campaign (May – June 2016)**

165 An example of NO₂ retrieval from two independently calibrated Pandoras that were initially
166 located at the same site (Yeoju, Korea, 37.3385°N, 127.4895°W) are compared in Fig. 2a showing that
167 the difference in C(NO₂) amount is less than 0.05 DU even in the presence of thin afternoon clouds (Fig.
168 2b) that decrease the measured solar irradiance by more than a factor of 2. Though Yeoju is a relatively
169 clean site in Korea (located to the southeast of Seoul Lat=37.5644°N, Long=126.934°W), C(NO₂) amounts
170 frequently reach moderately high values (e.g., 1 DU on 3 June 2016), and occasionally even higher (2-3
171 DU). However, Yeoju has much less C(NO₂) compared to Seoul, less than 30 km distant, where PSI
172 measurements were found to reach over 3 DU (Fig. 3) during the campaign period from mid-April to
173 early June, 2016. **Typical C(NO₂) amounts are 0.3 to 0.5 DU in polluted regions.**

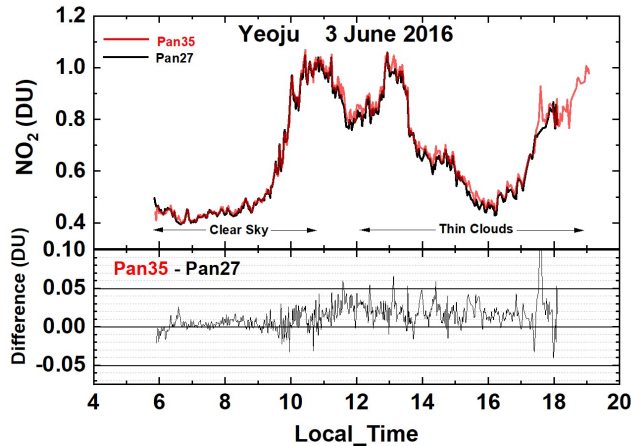


Fig. 2a C(NO₂) amounts from Pandora 27 and 35 in Yeosu, Korea during 3 June 2016 and their difference $|\text{Pan35} - \text{Pan27}| < 0.05$ DU.

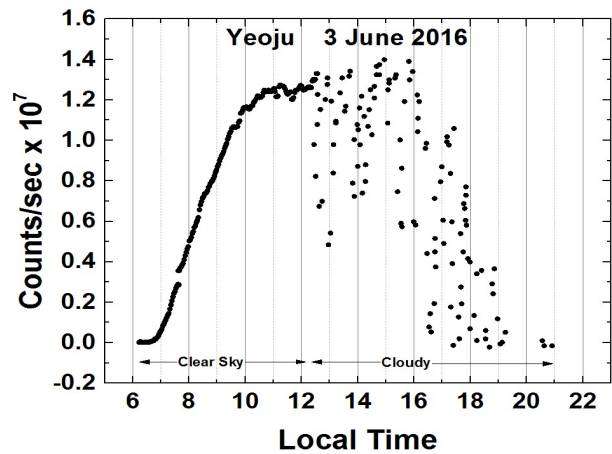


Fig. 2b Pandora 35 estimate of cloud or aerosol reduced measured counts/second at approximately 500 nm.

174 In a manner similar to Fig. 2a, C(NO₂) amounts can show large variability from day-to-day and
 175 intraday, as well as between different sites. The largest amounts of C(NO₂) are in the north (Seoul and
 176 Olympic Park) associated with the largest population and industry concentrations, while the southern
 177 cities of Busan and Gwangju have smaller amounts of C(NO₂). The smallest C(NO₂) amounts are at
 178 Anmyeondo (an island on west coast of Korea 42 km south of Seoul, usually not downwind of Seoul),
 179 and Songchon to the east of Seoul.

180
 181 Figure 2b shows the effect of thin clouds in terms of reduced measured count rates for a single
 182 spectrometer pixel near 500 nm showing a near noon count rate of 1.26×10^7 counts/second followed
 183 by a reduced count rate as clouds move in front of the sun. The cloud plus aerosol cover estimate is
 184 from the same date 3 June 2016 as the C(NO₂) amounts shown in Fig.2a. The effect of thin clouds for
 185 C(NO₂) retrieval (Fig. 2a) is increased noise (reduced precision) with a very small impact on accuracy.
 186 There are two effects on PSI observations to consider in association with thin clouds. First, is multiple
 187 scattering within the cloud affecting the optical path and effective air mass factor AMF. This has a very
 188 small effect on AMF, since most of the NO₂ is near the surface well below the clouds. Second, is the
 189 reduction in the number of measurements during a fixed 20 second measuring period causing a
 190 decrease in the signal to noise ratio. The weather during the campaign was occasionally very cloudy,
 191 which caused some missing NO₂ and O₃ data. However, most of the cloudy days were light to moderate
 192 cloud cover, which permitted C(NO₂) amounts to be determined, but with lower precision compared to
 193 clear-sky direct sun measurements (e.g., Figs 2a and b). When the cloud cover becomes sufficiently
 194 thick, precision is reduced (increased point-to-point scatter) and the spectral fitting error increases. A
 195 small percentage of data points with high retrieval error, C(NO₂ Error) > 0.1 DU, have been removed
 196 from the data set.

197

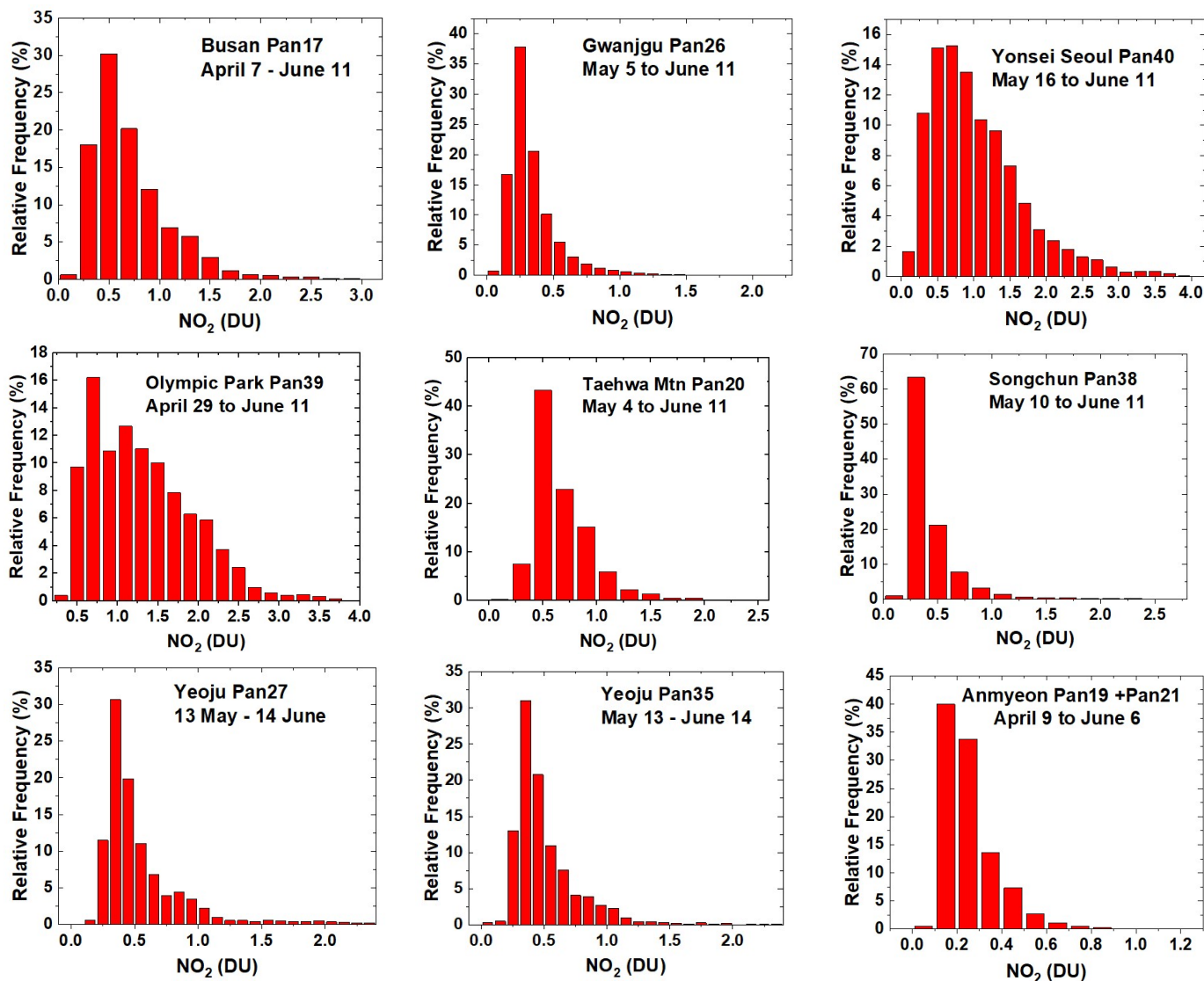


Fig. 3. Frequency distributions of $C(\text{NO}_2)$ across the KORUS-AQ PSI network: April 20 to Jun 6 2016, except as labelled. The axes vary for different sites.

198
199
200
201
202
203
204
205
206

Figures 3 and 4 summarize all of the Pandora $C(\text{NO}_2)$ data obtained during the KORUS-AQ campaign. Figure 3 presents histograms in percent frequency of occurrence for all nine sites. All of the sites located within or downwind of major cities have production of NO_x mainly from transportation and power generation as its major sources. The ratio of transportation NO_x production compared to all other sources is estimated as up to a factor of three (Kim et al., 2013). Of these sites, Anmyeondo frequently (40%) retrieves values of $C(\text{NO}_2)$ that are close to the typical stratospheric values of 0.1 ± 0.05 DU. Other sites occasionally have clean days with similar low values.

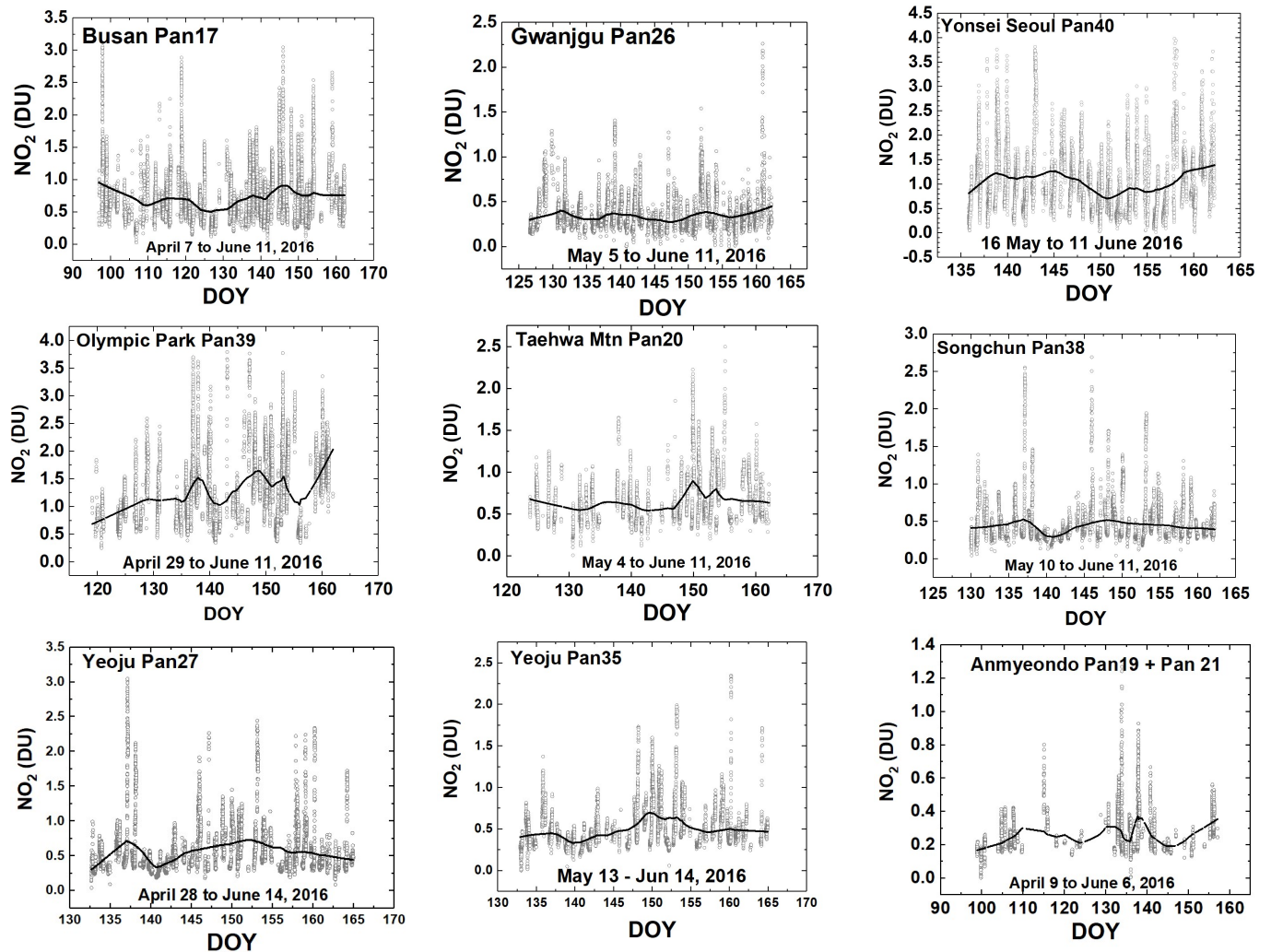


Fig. 4 NO₂ time series vs day of the year (DOY) and diurnal variability (daily vertical extent) at 9 Pandora sites. Notice the very high NO₂ amounts in Seoul and nearby Olympic Park. The black curves are approximately weekly least squares running averages. The daily vertical extent corresponds to diurnal variation (Fig. 2). Note: the vertical scales are different for each site to show the daily variability relative to the running average.

207
208
209
210
211
212
213
214
215

The Seoul site frequently has amounts of C(NO₂) greater than 2 DU. The same is true of Olympic Park, located in the eastern part of the Seoul metropolitan area. For locations increasingly distant from Seoul, the amount of C(NO₂) decreases in response to smaller local emissions, since the short chemical lifetime of NO₂ normally precludes long distance transport. Compared to Seoul, the two smaller southern cities, Gwangju and Busan, have relatively low levels of C(NO₂) on most days, with the most typical values ranging from 0.3 to 0.5 DU, although high values exceeding 2 DU can occur on rare occasion.

216
217
218
219

Figure 4 shows the same data as Fig. 3, but in the form of a time series covering the KORUS-AQ period. The daily variation (at least one point every two minutes) is shown in the vertical extent corresponding to each day's data. Figures 3 and 4 show that sites near Seoul metropolitan (Olympic Park) area have larger amounts of pollution compared to those further away (Taehwa, Songchon, and

220 **Yeosu**. Even though average $C(\text{NO}_2)$ amounts are much lower at Songchon and Yeosu, there are times
221 when the pollution levels are quite high ($C(\text{NO}_2) > 2$ DU, **Figs. 4 and 5**). There are days when the amount
222 of $C(\text{NO}_2)$ gets close to 4 DU in Seoul, 3 DU in Olympic Park and Busan, and 4 DU for one day in Yeosu
223 (April 27). The southern cities, Busan and Gwangju are much less polluted on average, which results in a
224 much smaller effect on adjacent regions. **Busan is located on the southeastern coastline, so that some of
225 its NO_2 pollution dissipates over the ocean, except for occasional days when very high amounts (3 DU)
226 occur.** Anmyeondo is quite clean, since it is located on the western coast well south of Seoul. **The most
227 frequently occurring $C(\text{NO}_2)$ value at Anmyeondo is 0.15 – 0.2 DU, which means that the measured NO_2
228 amount are partly from the stratosphere with very little tropospheric or boundary layer NO_2 . There are
229 occasional $C(\text{NO}_2)$ plumes that could be from industrial activity to the north, and, perhaps, from China.
230 Transport of NO_2 from China occurs episodically in significant amounts (Lee et al., 2014).**

231

232 **3 Diurnal Variation of $C(\text{NO}_2)$**

233

234 Grouping the diurnal variation together from multiple days (Fig. 5) reveals a pattern to NO_2
235 emissions and accumulation related to the main NO_2 emission sources (automobiles and power
236 generation) for the 3 largest cities in Korea: Seoul (Pan40), Busan (Pan17), and Gwangju (Pan26). For
237 Seoul, the amounts of $C(\text{NO}_2)$ during the morning (1 DU at 10:00) are much less than later in the
238 afternoon (over 2 -3 DU at 16:00) on almost every day with values occasionally reaching as high as 6 DU.
239 Even the relatively low morning values of $C(\text{NO}_2)$ represent a significant amount of pollution. The 6 DU
240 $C(\text{NO}_2)$ amount in Seoul is unusual, but coincides with the peak values frequently occurring in the late
241 afternoon. $C(\text{NO}_2)$ behavior at nearby Olympic Park to the east of Seoul is very similar to Yonsei
242 University in the heart of Seoul, even though Olympic Park's traffic density is lower than Seoul. Olympic
243 Park is close enough to the metropolitan Seoul area for the transport of NO_2 combined with local
244 production from traffic to produce a very similar diurnal pattern. The moderately large city of Busan also
245 has high values of NO_2 , occasionally reaching 3 DU in the afternoon. Busan has relatively low values of
246 NO_2 in the morning, having peaks in the mid-afternoon and declining in the late afternoon. Gwangju,
247 located in the southwest, is a smaller city with less pollution (peak values = 1.6 DU) and does not have as
248 distinct an afternoon maximum.

249

250

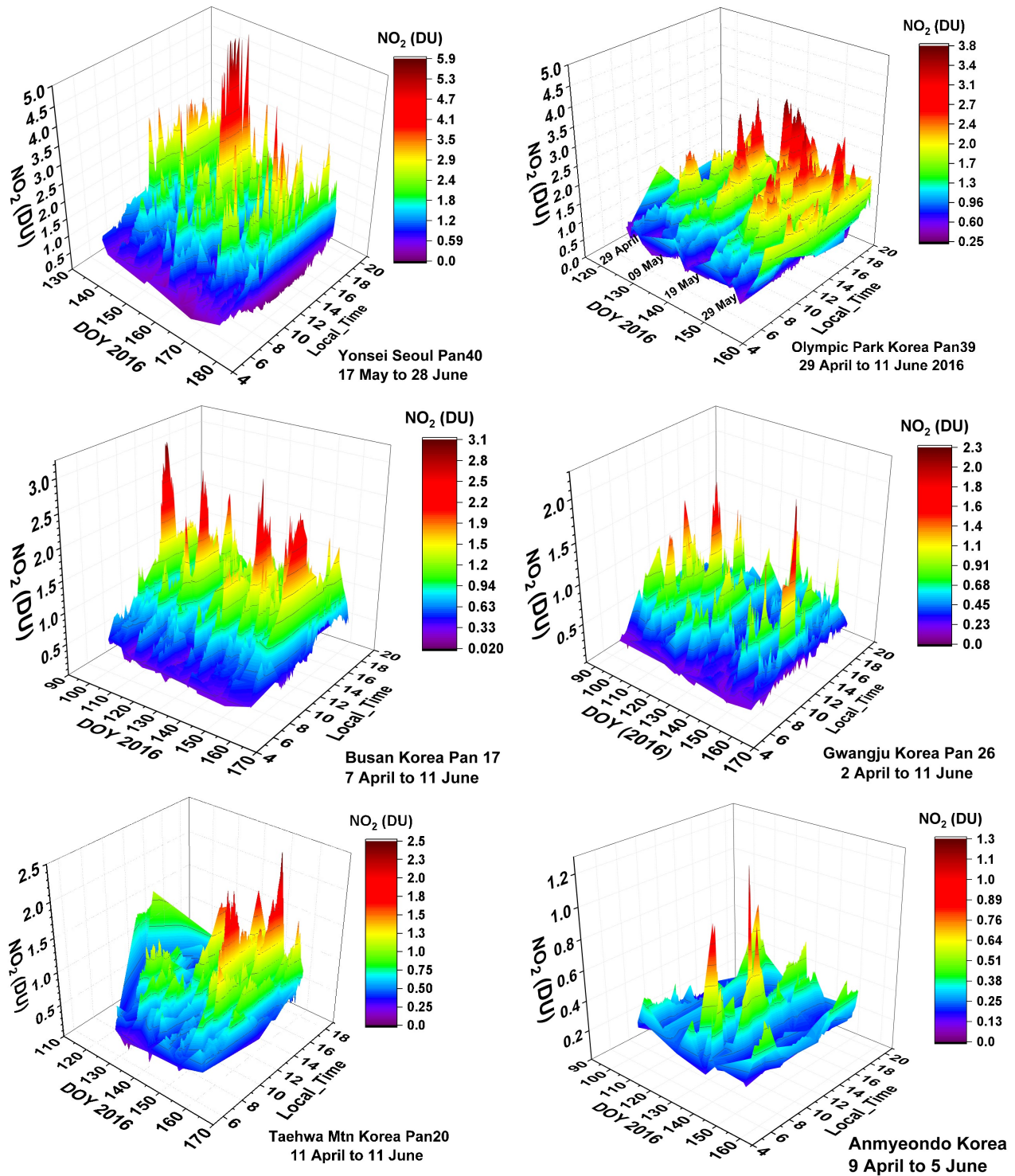


Fig. 5 NO₂ amounts vs Day of the Year (DOY) and Local Time for six sites as labeled in each panel. Day 120=April 29, Day 130=May 9, Day 140=May 19, Day 150=May 29, Day 160=June 8, Day 170 =June18.

252 The panels in Fig. 5 for Taehwa Mtn. and Anmyeondo show regions outside the Seoul
253 metropolitan area that still show substantial amounts of NO₂. Compared to Seoul, the Taehwa site is a
254 semi-rural location with only a small amount of car traffic in the immediate area. However, there are
255 major highways about 6 km from the site that are close enough to permit transport of NO₂ to the
256 Taehwa Mountain site. All of the sites showed a tendency to have peak NO₂ occur in the late afternoon.
257 Anmyeondo on the west central coast of Korea shows C(NO₂) amounts that are quite low with
258 occasional plumes arriving from the north or the west (China).

259 The basic daily pattern of C(NO₂) in urban Korea arises from large amounts of automobile traffic
260 and power plants emitting NO_x (for modern automobiles, roughly 99 % NO and 1 % NO₂). An FTIR
261 analysis of automobile exhaust shows that NO is emitted at 127 ppm, NO₂ at 1.6 ppm, HCHO at 39 ppm,
262 and CH₃OH at 139 ppm as part of the main emissions containing H₂O (143577 ppm) and CO₂ (122191
263 ppm). (<https://tools.thermofisher.com/content/sfs/brochures/D10248~.pdf>); see also Walters et al.,
264 2015).

265 NO quickly converts into NO₂ in the presence of ozone and volatile organic compounds VOCs in
266 the atmosphere and can convert back to NO by solar photolysis. KORUS-AQ results frequently show
267 increasing NO₂ during the day with peaks in the afternoon. For these days the measurements imply that
268 the amount of locally produced NO_x and conversion into NO₂ dominates the losses of NO₂ by photolysis
269 and transport out of the region. Other days occasionally show a different behavior, with NO₂ peaks in
270 the morning and a decline thereafter suggesting transport out of the region.

271 **4 Longer-Term Changes in C(NO₂)**

272 Some of the sites used for the KORUS-AQ campaign (Gwangju and Anmyeondo) had PSIs set up
273 in April 2015, about one year before the start of the campaign. Two other sites (Seoul and Busan) have
274 PSI C(NO₂) data starting in 2012. The extended data sets for Seoul and Busan provide the opportunity to
275 estimate 5-year changes in C(NO₂) amount and seasonal dependence.

276 In Fig. 6, the daily variation over one year at Gwangju and Anmyeondo are evaluated to estimate
277 one year secular trends. The vertical extent in the time series is not noise or uncertainty, but rather the
278 80 second per data point variability throughout each day (e.g., see Fig. 2). Before calculating linear least
279 squares slopes, the unadjusted time series (grey data points in Panels A and D) were deseasonalized
280 (grey data points in Panels B and E) by subtracting a function with zero slope derived from a 30 day
281 running average (dark line in panels A and D or the identical curves in C and F). The running average
282 curves in panels A and D are shown with expanded scale in panels C and F to clearly show the seasonal
283 variation. The “zero slope functions” ZM(t) are obtained by subtracting a linear least squares fit L(t) to
284 monthly running average curves M(t) in panels C and F to form zero slope functions ZM(t) = M(t) – L(t).
285 The results ZM(t) are functions that look similar to the M(t) plots in panels C and F, but with zero slopes.
286 The resulting ZM(t) are then subtracted from the respective original time series (grey circles) in panels A
287 and D. The results are the grey circles in Panels B and E. Similar monthly running means are shown in
288 Panels B and E that have almost no monthly variations (see appendix Fig. A1).

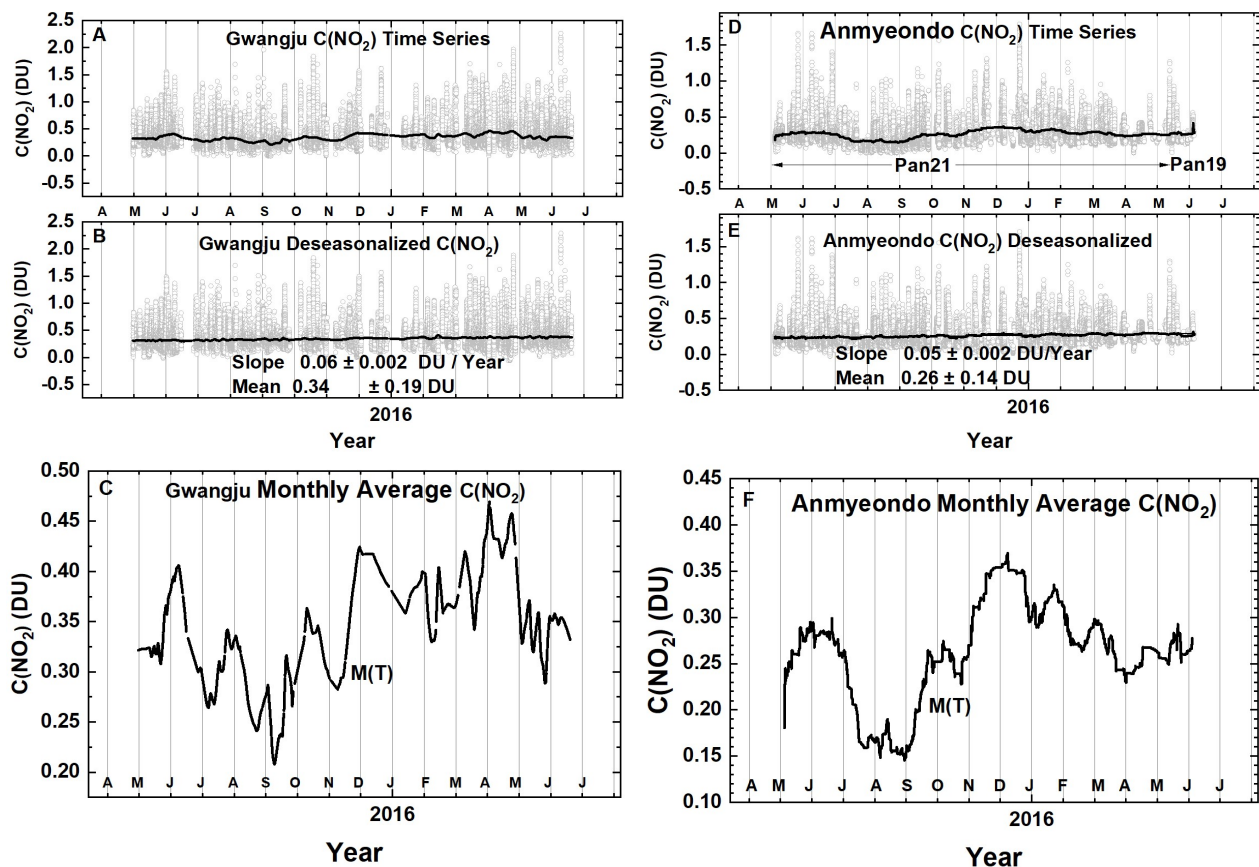


Fig. 6 Approximately 1 year of daily column $C(\text{NO}_2)$ amount data (Panels A and D) and the monthly running average amount (dark plot in Panels A and D). The data are from GIST at Gwangju and Anmyeondo. Panels A and D are the original time series with one data point every 80 seconds, panels B and E are the deseasonalized time series. Panels C and F are an expanded scale of the monthly running averages $M(t)$ of $C(\text{NO}_2)$ that are identical to the solid lines in panels A and D. The vertical extent (panels A, B, D, and E) on a given day is the range of diurnal variation from early morning to late afternoon.

289 The linear trends in Figs. 6B and 6E suggest that there was an increase in pollution levels in
 290 Gwangju and Anmeondo over the period of observation. The southern city of Gwangju (Pan 26) has
 291 higher average $C(\text{NO}_2)$ amounts, 0.34 ± 0.19 DU, compared to the relatively clean coastal site
 292 Anmyeondo, 0.26 ± 0.14 DU. Gwangju seasonal cycle has a minimum in $C(\text{NO}_2)$ amount in September-
 293 October and a very broad maximum from December to May. The Gwangju PSI is located away from
 294 major city traffic on a university campus (Gwangju Institute of Science and Technology, GIST) so that the
 295 average amount of NO_2 (about 0.34 DU) is moderate with some days reaching 1.5 DU. The slopes are
 296 statistically significant at the 2-standard deviation level ($p < 0.05$) and imply that $C(\text{NO}_2)$ was increasing
 297 at a substantial rate. However, the period of observation was too short to estimate multi-year long-term
 298 trends. Additional long-term monitoring of these sites would be desirable for air quality purposes.

299 The PSI on Anmyeondo was located away from a commercial area with moderate traffic and
 300 very near the shore of the Yellow Sea at a regional Global Atmosphere Watch (GAW) station. For
 301 Anmyeondo there is a clear seasonal cycle similar to that in Gwangju with a minimum in September-

302 October and a broad maximum during the winter-spring months. Amnyeondo had an average amount
 303 of 0.25 DU, which is lower than observed at Gwanjgu.

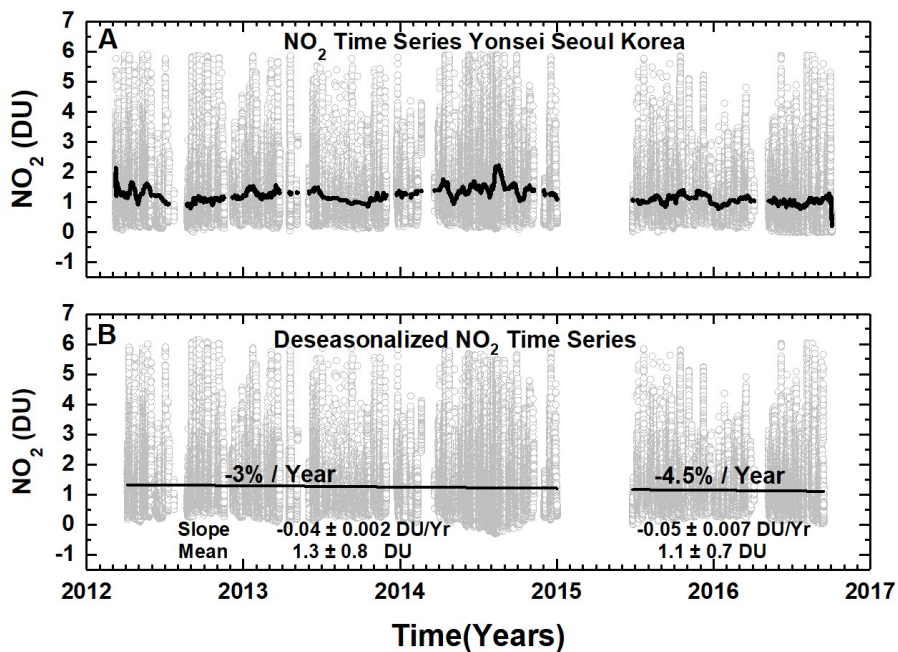


Fig. 7 (A) NO₂ time series at Yonsei University in Seoul NO₂(grey) and (B) deseasonalized time series. Combined slope = -0.05 ± 0.001 DU/Year and Mean = 1.2 ± 0.8 DU or the decrease is -4 ± 0.08 % / Year. Seoul has no clear seasonal cycle.

304

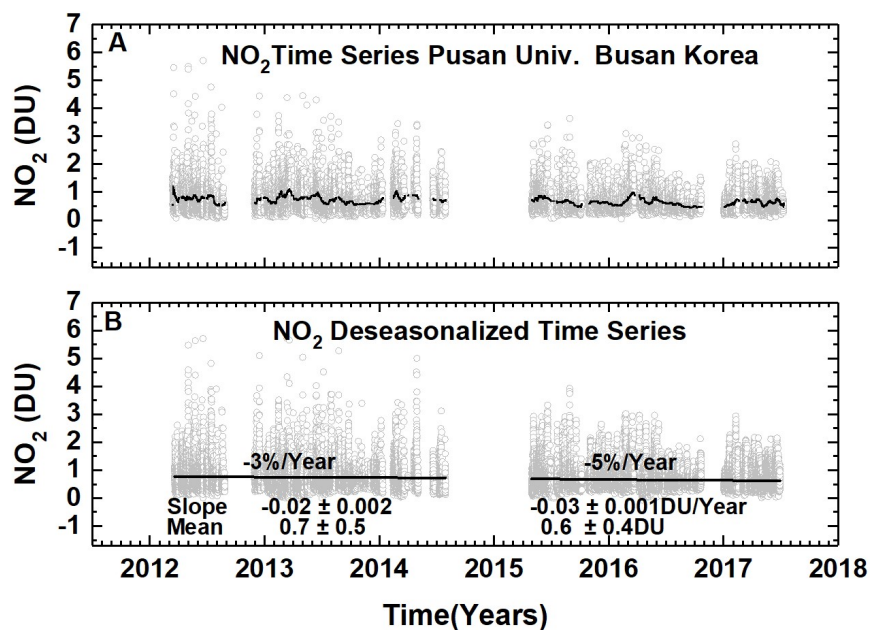


Fig. 8 (A) Pusan University in Busan NO₂ daily time series (grey) and (B) deseasonalized time series with linear trends.

305 Figures 7 and 8 each contain an approximately 5-year daily time series (grey) for Seoul (Yonsei
306 University) and Busan (Pusan University) and a linear fit to a deseasonalized version of the time series.
307 Since the observations at both sites had an extended period of missing data, the slopes were estimated
308 separately for each segment and for the combined time series. Both Seoul and Busan show a steady
309 reduction in NO₂ air pollution with an average reduction of about -4 % per year. A recent paper by
310 Duncan et al., (2016) estimated a decrease in C(NO₂) for Seoul in about a 10 x 10 km box of about 1.6 ±
311 1.4 % per year over the 2004 to 2013 period based on a 2014 average C(NO₂) amount of 0.6 DU, or
312 about half of the average value 1.3 ± 0.8 DU observed by the PSI. The larger reduction in C(NO₂)
313 measured by the PSI is caused by a reduction in higher than average afternoon C(NO₂) amounts that are
314 rarely observed by OMI overpass at 13:30 local time. OMI is a polar orbiting push broom hyperspectral
315 instrument (300 – 500 nm with resolution of 0.45 nm in the UV and 1 nm in the visible and a spatial
316 resolution of 13 x 24 km²) onboard the AURA satellite. The high observed late afternoon values are not
317 restricted to Seoul, but occur for all of the urban areas where the PSI has been deployed. The high late
318 afternoon values do not regularly occur in remote rural areas such as Amnyeondo.

319 Seoul and Busan C(NO₂) measurements are remarkable for the large peak amounts that are seen
320 on most days compared to the 1.5 to 2 DU peak values for Gwangju and Amnyeondo. For Yonsei, the
321 peak values range above 5 to 6 DU in the years 2012 to 2015, but decrease somewhat in 2015 to 2016.
322 In 2015 - 2016, the decrease appears to be large, but is only 0.2 DU relative to a mean of about 1.2 DU.
323 A smaller decrease appears for Busan (Fig. 8) relative to a mean of about 0.6 DU. All of the PSI
324 measurements show very high values of NO₂ during almost every day when measurements were
325 possible. Since the NO₂ concentrations represented by these large column amounts are probably in the
326 boundary layer near the sources of NO₂, there is a strong effect on local air quality.

327

328 5 Comparison with OMI Satellite Overpass Data

329

330 Seoul and Busan have 5-year PSI data records (Figs. 9a and 9b), and Gwangju has a 1-year data
331 record (Figs. 6 and 10) spanning the KORUS-AQ campaign. The PSI C(NO₂) can be matched in time (± 8
332 minutes) with the overpass time from OMI (Ozone Monitoring Instrument) onboard the AURA satellite
333 (mid-day overpass times 13:30 ± 90 minutes). Figure 9a shows the C(NO₂) daily variation at the OMI
334 overpass time with far more high values of C(NO₂) from the PSI than observed by OMI. The solid lines
335 represent the seasonal dependence, which are shown separately in Fig. 9b along with the C(NO₂)
336 differences, PSI - OMI. The result is that the average PSI values are double those observed by OMI's
337 large FOV. (OMI Version 03: <https://avdc.gsfc.nasa.gov/index.php?site=666843934&id=13>)

338

339 The seasonal dependence (Fig. 9b) of C(NO₂) from OMI for both Seoul and Busan is fairly
340 regular, with maxima in January of each year and minima in July-August. The seasonal behavior of
341 C(NO₂) obtained from the PSI for Seoul varies with high values extending from January into the summer
342 months and with minima varying from August in 2012, September-October in 2013, missing in 2014, July
343 in 2015, and June in 2016. For Busan, the maxima occur in the Spring for 2013 and 2014, October for
344 2015, and in the Spring for 2016. The minima are also variable. The difference between OMI and PSI
345 retrievals depends on local conditions for PSI and on an area average for OMI.

346
347

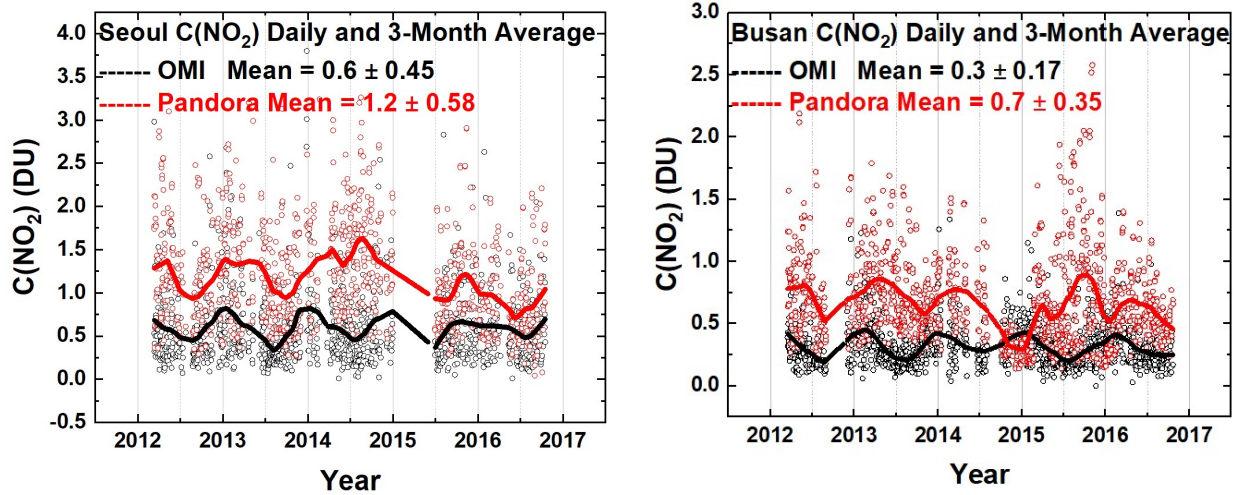
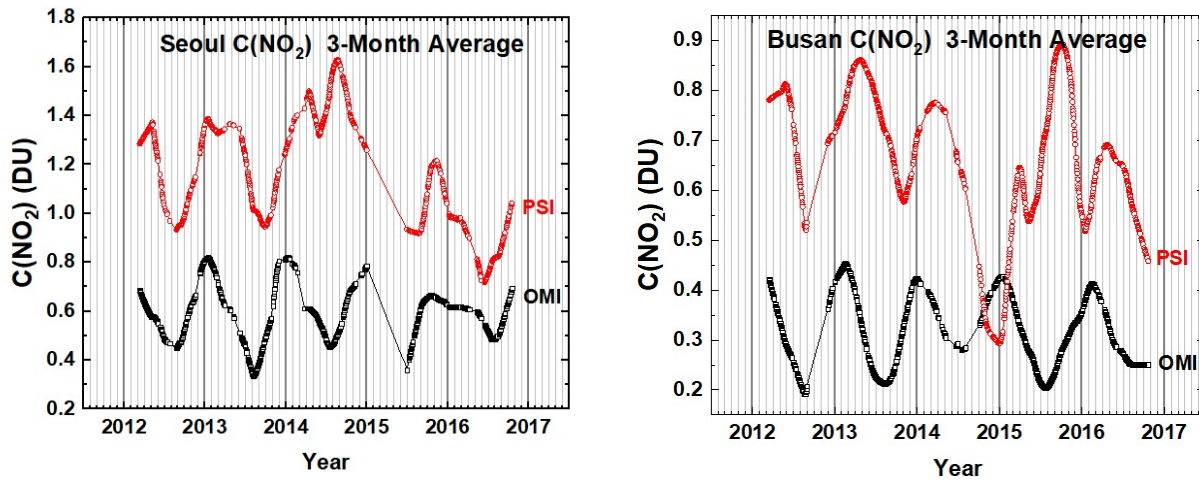


Fig. 9a Comparisons between the daily values of C(NO₂) for OMI (black) and PSI (red) at Seoul and Busan for a 5-year period. Solid lines show the average seasonal variation (Lowess(0.1)), see also Fig. 9b. Linear interpolation is used where there are missing data points.

348



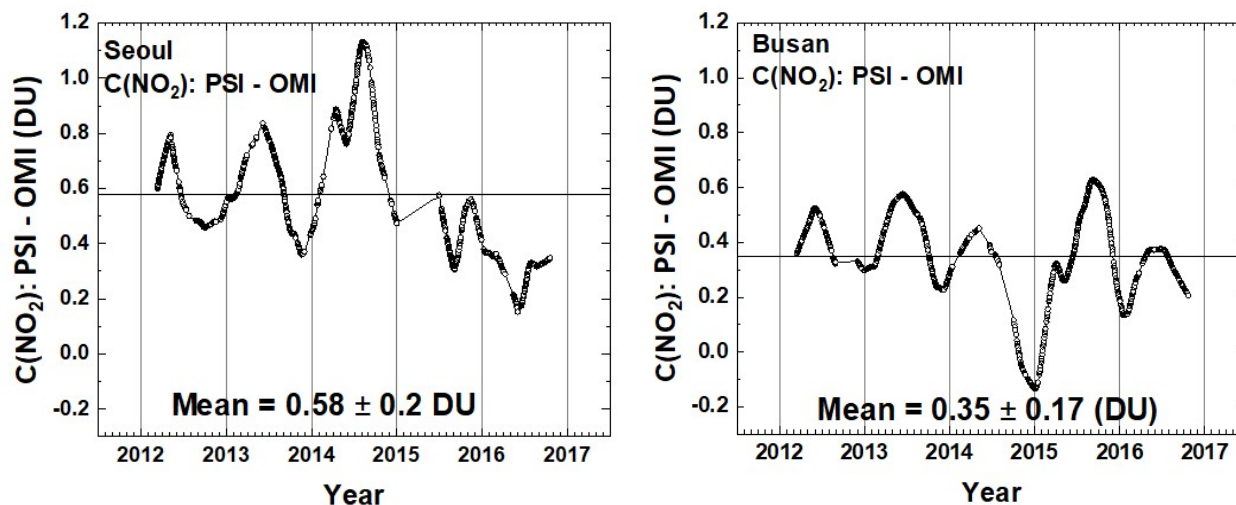


Fig. 9b Comparisons between the seasonal averages for $C(\text{NO}_2)$ from OMI (black) and PSI (red) at Seoul and Busan for a 5-year period. The lower panels show the seasonal difference between the PSI and OMI. The individual data points are shown derived from a Lowess(0.1) smoothing, approximately a 3-month running averages of the daily data. Interpolation has been used where there are missing data points.

349
350
351
352
353
354
355
356
357

Figure 9b shows that the PSI has a mean difference compared to OMI in Busan of 0.35 DU and peak values (up to 2.5 DU at 13:30 and 4 DU in the late afternoon). The differences are important when considering pollution effects on human health (Krafta et al., 2005; Latza et al., 2009). Even larger differences are observed in Seoul, where the mean difference is 0.58 DU between Pandora and OMI at the satellite overpass time. The results from PSI suggest that local ground-based monitoring of pollution is important for estimating their impact on human health, particularly since amounts of $C(\text{NO}_2)$ occurring later in the afternoon exceed the amounts at the time of the satellite overpass.

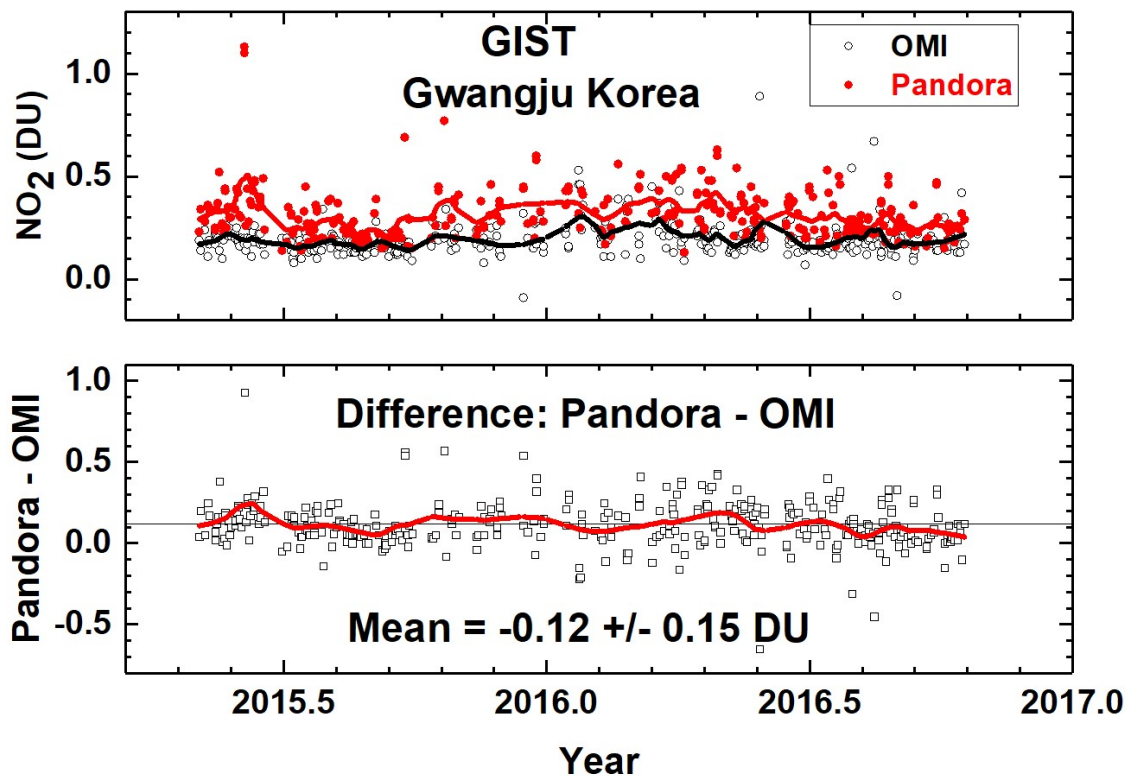


Fig. 10 C(NO₂) time series from Pandora (red) and OMI (black) for GIST University in Gwangju Korea and their differences. The comparison is formed from time coincidences between Pandora and OMI.

358 A comparison with Lowess(0.1) fits (Locally Weighted least squares fit to 0.1 of the data points,
 359 (Cleveland, 1981)) to the matched Pandora vs OMI overpass data (about 3-month averages) shows that
 360 PSI C(NO₂) is larger than OMI measured C(NO₂) mostly because of its much smaller 2^o field of view (a
 361 circle of 35 meters diameter at 1 km altitude) compared to OMI's FOV of 13 x 24 km² at nadir, which
 362 may encompass areas outside of the city or the adjacent ocean areas. For example, the center of Seoul
 363 is about 48 km from the Yellow Sea, while the OMI overpass file lists FOV center distances of over 60 km
 364 from Seoul. Another possible reason for the differences is that OMI C(NO₂) retrievals use NO₂ vertical
 365 profile shape factors from the low resolution (~110 x 110 km) Global Model Initiative (GMI) model
 366 simulation to calculate air mass factors that are used to determine observed tropospheric NO₂ vertical
 367 columns, while much finer resolution profiles are needed to more accurately represent highly polluted
 368 urban areas such as Seoul. Increases in OMI retrieved tropospheric column NO₂ up to 160 % are found
 369 when using model derived 1.33 x 1.33 km² profile shape factors (Goldberg et al., 2017). The effect of
 370 moderate amounts of cloud or aerosol have little effect on the PSI direct -sun spectral fitting retrieval of
 371 C(NO₂) as shown in Fig. 2. OMI and MAXDOAS retrievals are sensitive to the presence of aerosols and
 372 clouds (Kanaya et al., 2014), which may contribute to the underestimate of C(NO₂) by OMI even after
 373 corrections are made for retrieved aerosol and cloud amounts (Chimot, et al. 2016).

374
 375 The implications for assessing clean air indices suggest that OMI underestimates the human
 376 health effect from trace gases such as NO₂, especially in highly populated urban areas. Figure 5 gives a

377 much clearer picture of the degree of pollution than is possible with just the 13:30 OMI comparison
378 measurements, since the late afternoon is the time of maximum pollution.

379
380 The city of Gwangju is much smaller than Busan, with less industrial activity, especially
381 automobiles. PSI observations at GIST show much closer agreement with OMI (Fig. 10), especially since
382 GIST is located within the city boundaries, but in an area with much less concentrated industrial activity
383 compared to the center of Gwangju. The large OMI FOV over a relatively clean area reduce the OMI
384 difference in measured NO₂ amount compared to the PSI C(NO₂) amounts. OMI still measures less than
385 the PSI (0.12 ± 0.15 DU), but the mean difference is not statistically significant. However, OMI clearly
386 misses the high values of C(NO₂) that are present in the PSI observations.

387
388

389 **5.1 Comparison with 4STAR DC-8 Overpass Data**

390

391 C(NO₂) results were obtained by the Spectrometer for Sun-tracking Sky-Scanning Atmospheric
392 Research (4STAR) flown on-board the DC-8 during KORUS-AQ and compared with the PSI (Fig. 11). The
393 4STAR is an airborne sunphotometer, capable of measuring total C(NO₂), C(O₃), water vapor and AOD
394 columns in its direct-sun mode (Segal-Rozenhaimer et al., 2014; Shinozuka et al., 2013), which is similar
395 to the mode used by the PSI network.

396

397 A detailed description of 4STAR is given in Dunagan et al., (2013). In brief, the instrument has
398 two structurally rigid grating array spectrometers that are combined to yield continuous spectra
399 between 300-1700 nm. The instrument sampling rate is 1 Hz, and the nominal integration time used for
400 C(NO₂) retrievals is 50 ms (with six spectra averaged per one sampling period). Dark counts are
401 measured every 20 min using a shutter mechanism. The 4STAR light collection system has fiber optic
402 bundle foreoptics that is connected to the spectrometers. A two-axis motion control system with analog
403 feedback provides active tracking of the solar disk. The instrument full field of view (FOV) is ~1.25°.
404 C(NO₂) is retrieved following a method described in Segal-Rozenhaimer et al. (2014), but using the 460-
405 490 nm spectral range. A series of 4STAR columnar NO₂ values above aircraft (for legs below 300 m)
406 taken from DC8 “missed approach” maneuvers overflying Olympic Park PSI station, within a radius of 5
407 km, are shown in Fig. 11. There is a relatively good correlation (R²=0.7), with a slight positive bias of
408 4STAR compared with the PSI values. This might result from higher noise effects (i.e. small amount of
409 spectra averages) for 4STAR during the fast change of altitude when the aircraft performs its “missed
410 approach” overpasses over the PSI stations. Relaxing the altitude constraint to include legs below 500 m
411 showed good agreement with the PSI station at Taewha Mountain, but with an overall lower correlation
412 coefficient (R²=0.54), which is expected due to averaging of larger vertical range. As with PSI, 4STAR
413 shows better agreement with OMI C(NO₂) for low values of C(NO₂), but considerable differences over
414 polluted areas (Segal-Rozenhaimer et al., *in prep.*), when 4STAR C(NO₂) values are averaged within each
415 of the OMI pixels corresponding to the flight path for each of the days.

416
417

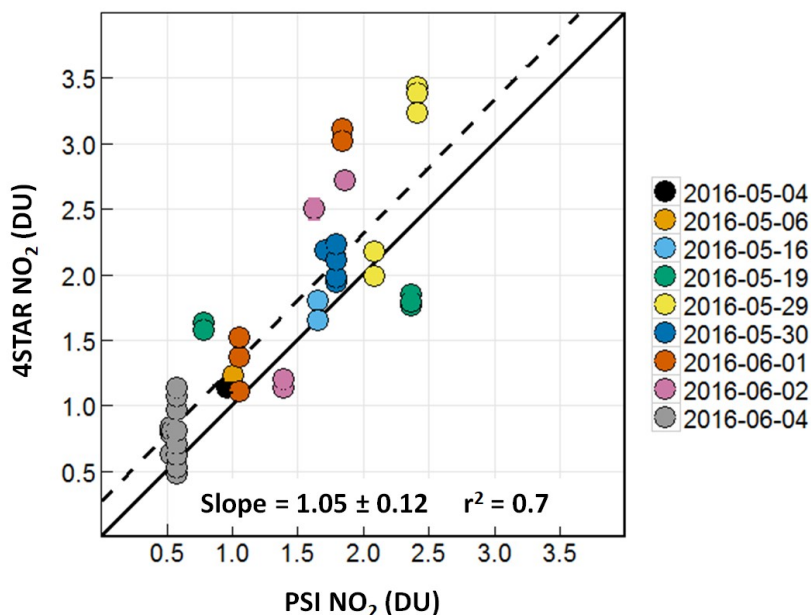


Fig. 11 A correlation plot of C(NO₂) from 4STAR onboard the DC-8 compared to the C(NO₂) amount measured by the PSI at Olympic Park on nine different days. The solid black line is the 1:1 line drawn for reference. The dashed line represents the data linear fit, with a slope of 1.05, and a correlation coefficient $r^2 = 0.7$, as shown on the plot.

418

419 **6 Formaldehyde from Five Korus-AQ Sites**

420

421 PSI makes two sets of direct-sun measurements every 80 seconds. One set is for measurements
 422 in the visible range (380 – 525 nm used for NO₂) and the other is for the UV range (290 – 380 nm with a
 423 filter, U340, which blocks visible light). Formaldehyde is derived from the same set of spectral
 424 measurements used for ozone (i.e., with a U340 blocking filter), but using the spectral range 332 - 359
 425 nm. Sources of error in the C(HCHO) retrieval arise from the selection of the fitting window and the
 426 amount of C(HCHO) remaining in the reference spectrum after application of the modified Langley
 427 estimation (MLE) method of calibration (Herman et al., 2009, Spinei et al., 2018). The MLE extrapolation
 428 to zero C(HCHO) could have an offset error of 0.1 to 0.2 DU. Selecting different fitting windows can also
 429 cause the C(HCHO) retrievals to differ. For example, a wider alternate fitting window, 324 -360 nm,
 430 retrieves HCHO values that are about 8 % higher because of different amounts of interference from
 431 overlapping absorption by O₃, NO₂, and BrO at the spectral resolution of 0.5 to 0.6 nm currently in use.
 432 Absolute offset errors do not affect the retrieval precision (relative column amounts), which is
 433 approximately 0.1 DU. **A detailed analysis of the algorithms and uncertainties is discussed by Spinei et**
 434 **al., 2018.**

435

436 The Olympic Park area has much more vegetation than central Seoul for the production of
 437 isoprene (<http://www.olympicpark.co.kr>), which is a significant source of the chemicals needed for
 438 formaldehyde production in the atmosphere (Luecken et al., 2012). Observations from PSI show that
 439 C(HCHO) starts out every day at low levels 0.6 DU at about 08:00 and increases to over 2 DU until 18:00
 440 (Fig.s 12 and 13). Most HCHO arises from photochemical production, while a significant fraction is

441 chemically derived from automotive emissions in densely populated urban areas (Friedfeld et al., 2002;
 442 Garcia et al., 2006; Lei et al., 2009; Liteplo et al., 2010). Regardless of the precursor source, HCHO forms
 443 in the atmosphere primarily by photochemistry, which causes HCHO to usually be a minimum early in
 444 the day, increase into the afternoon, and decline towards evening. The PSI C(HCHO) observations (Figs.
 445 12 and 13) support this pattern of daily variation.
 446

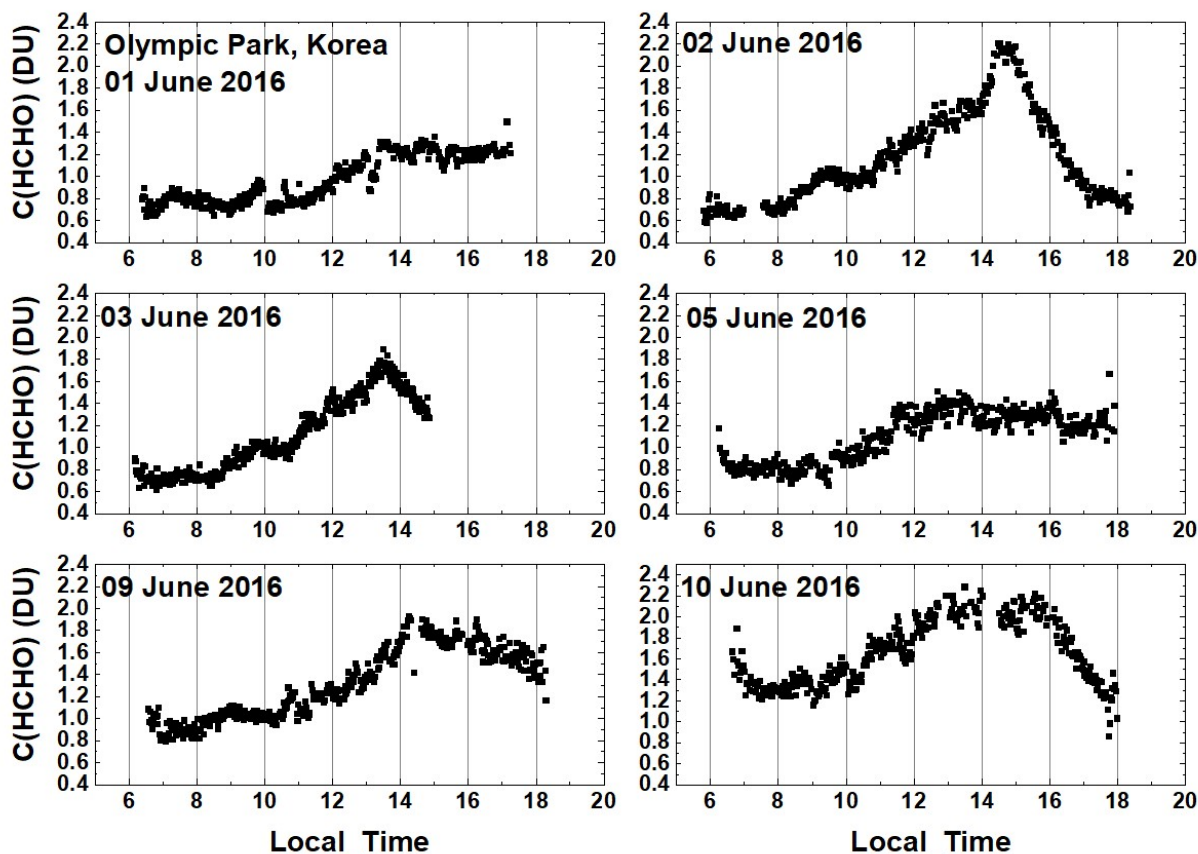


Fig. 12 C(HCHO) from PSI at Olympic Park for 6 days in June 2016. C(HCHO) on 2 June 2016 has a peak value of 2.3 DU at 14:30 hours.

447
 448 A summary of the daily time dependence of C(HCHO) at Olympic Park during the entire
 449 KORUS-AQ campaign is shown in Fig. 13. As in Fig. 12, minimum values are observed in the
 450 morning (06:00 – 08:00) before the chemical and direct sources of HCHO are significant. There
 451 is strong buildup during the day that reached a maximum between 15:00 to 16:00, and then
 452 diminished towards sunset. As with NO₂, the daily pattern of late afternoon peaking of HCHO
 453 amounts presents a problem for polar orbiting satellite observations (e.g., OMI observations at
 454 13:30) assessing air quality.

455
 456
 457

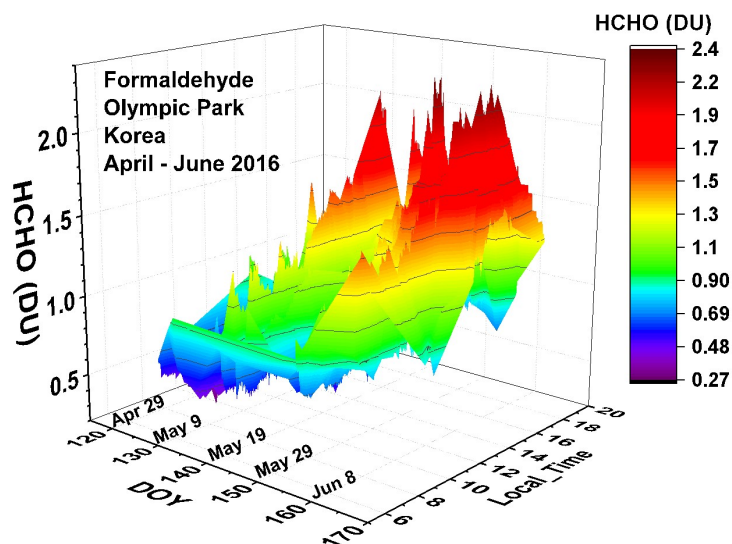


Fig. 13 Pandora measured formaldehyde amounts vs day of the year and local time for 29 April 2016 to 11 June 2016 in Olympic Park.

458

459 Figure 14 shows two altitude profiles acquired by the Compact Atmospheric Multispecies
 460 Spectrometer (CAMS) (Richter et al., 2015) onboard the DC-8 aircraft as it spiraled over the
 461 Olympic Park area on 4 May 2016 in the morning and at midday. Quoting from Richter et al.,
 462 (2015), "CAMS is a multi-species spectrometer configured for the simultaneous detection of ethane
 463 (C₂H₆) and formaldehyde (CH₂O). The spectrometer utilizes a tunable, fiber optically pumped difference
 464 frequency generation laser source in combination with a Herriott type multi-pass absorption cell with an
 465 effective path length of 89.6 m"

466

467 The morning integrated amount on 4 May was 1.02×10^{16} molecules cm^{-2} (0.38 DU) and the
 468 afternoon amount was 6.95×10^{15} molecules cm^{-2} (0.26 DU), both substantially less than the PSI
 469 measured values of 0.48 DU and 0.42 DU, respectively. There were no surface measurements of HCHO
 470 mixing ratio on 4 May at Olympic Park. On 2 June at 11:40 there was a surface measurement 3.94 ppb.
 471 Including the surface measurement in the profile integral yields $\text{Integ}(0.026, 7.2) = 0.55$ DU, while PSI
 472 measured 1.2 DU, which is consistent with the differences shown in Fig. 14. The notation in Fig 14 is

473
$$\text{Integ}(z_1, z_2) = \int_{z_1}^{z_2} \text{HCHO}(z) dz$$
 for the altitudes z_1 to z_2 .

474

475

476

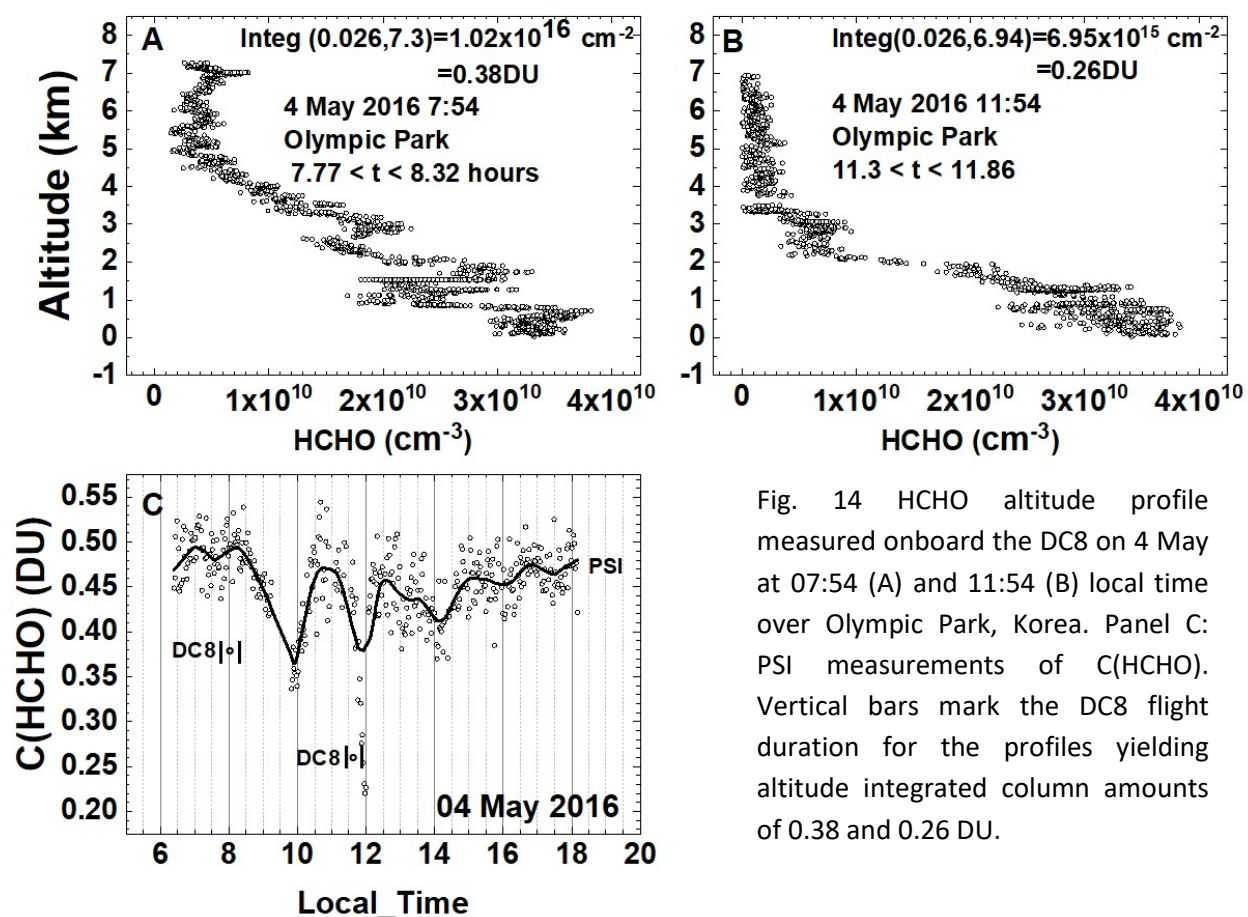


Fig. 14 HCHO altitude profile measured onboard the DC8 on 4 May at 07:54 (A) and 11:54 (B) local time over Olympic Park, Korea. Panel C: PSI measurements of C(HCHO). Vertical bars mark the DC8 flight duration for the profiles yielding altitude integrated column amounts of 0.38 and 0.26 DU.

477 The profiles used data for lower altitudes obtained from aircraft “missed approach”
 478 maneuvers at a nearby Seoul Airbase, 8.5 km from Olympic Park, (Fig. 15). When available, a
 479 single surface altitude point was added using ground-based volume mixing ratio measurements
 480 obtained from US Environmental Protection Agency measurements using quantum cascade
 481 laser instruments (Hottle et al., 2009, Spinei et al., 2018 and references therein). The DC-8 minimum
 482 altitude exactly over Olympic Park was typically around 0.4 km above the surface (black circles
 483 Fig. 15). Large vertical DC-8 HCHO gradients were observed as the DC8 descended to lower
 484 altitudes over Seoul Airbase. A comparison of 10-second DC-8 HCHO averages at the points of
 485 closest spatial approach to the Olympic Park (black circles) site on June 4, for example, to peak
 486 HCHO measurements during missed approaches at the nearby Seoul Airbase (20 – 40 meters
 487 above the ground) revealed ratios in the observed HCHO (black circles) ranging between 75 % to
 488 83 % of the maximum values near the surface. Since Olympic Park DC-8 overpasses miss
 489 significant near surface HCHO amounts, the profiles shown in Figs. 14 and 16 incorporate the
 490 HCHO amounts down to the surface at an altitude of 0.026 km asl derived from the “missed
 491 approach” at Seoul airbase. HCHO measurements above the maximum altitude over Olympic
 492 Park (see Fig. 14 and 16) were taken from the closest time over the Taewha Mtn. site, 28 km

493 from Olympic Park. The assumption is that the horizontal gradients above 2.2 km (Fig. 15) can
494 be neglected,
495

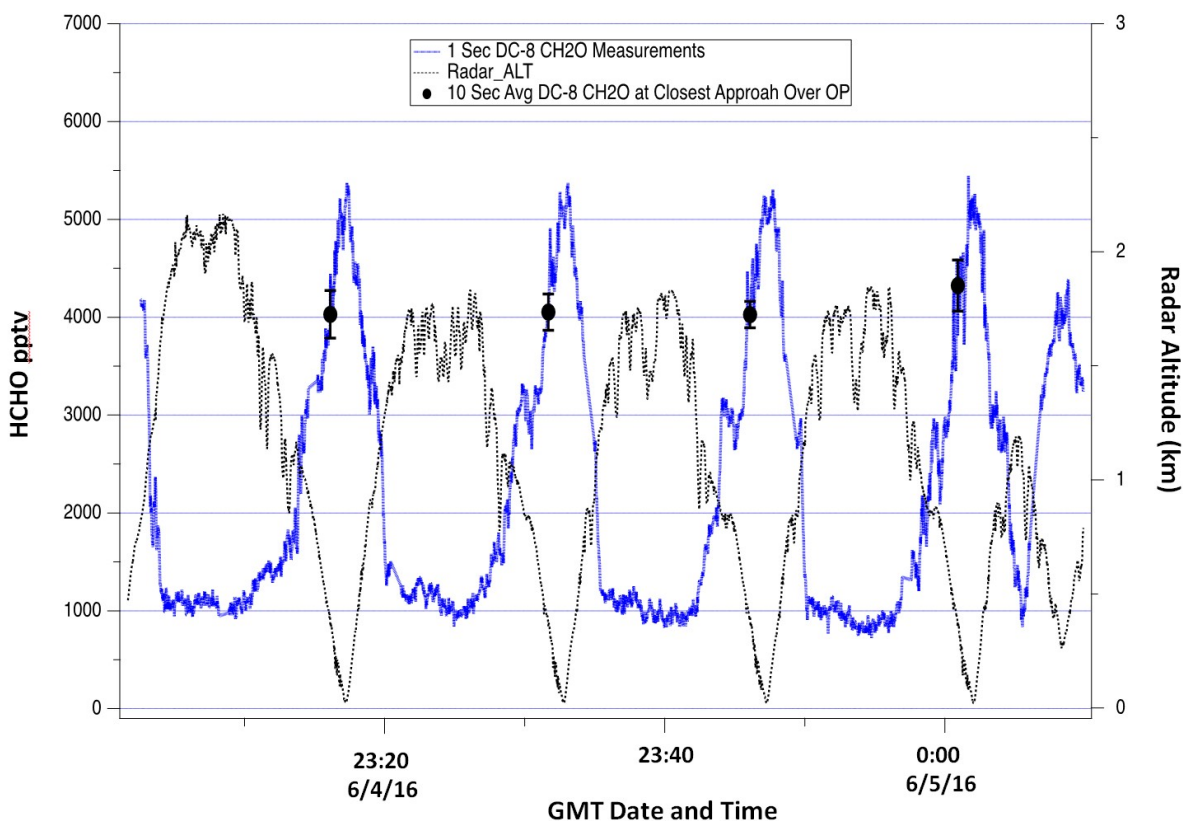


Fig. 15 DC-8 HCHO measurements over Olympic Park on June 4. The continuous blue profiles show the 1-second HCHO data while the black points with error bars show the 10-second average and standard deviation of this data at points of closest approach above the Olympic Park site.

496
497 After conversion from mixing ratio to molecules/cm³ using the measured atmospheric
498 density, the resulting profile data were integrated from the minimum (0.026 km asl, Table 1) to
499 the maximum heights indicated in Fig. 14. The result is 0.38 DU at 07:54 and 0.26 DU at 11:54
500 compared to the measurements from the Pandora instrument 0.48 and 0.38 DU. The derived
501 vertical HCHO columns from the DC8 data in Fig. 14 A and B are 79 % of PSI measured C(HCHO) in the
502 morning and 68 % of PCI C(HCHO) at midday (Fig 14 C).

503
504 A similar comparison is shown in Fig. 16 for 5 June 2016 where the amount of C(HCHO)
505 is much larger than on 4 May. Integration of the measured profiles yields column densities of
506 0.60 and 0.82 DU at 08:30 and 15:21 hours. For this case, at both times the DC8 values are
507 about 77 % and 63 % of the PSI measured column amounts, 0.78 and 1.3 DU. For both cases in

508 Figs. 14 and 15 the 23 % to 37 % differences are outside of the expected error from PSI fitting
 509 window selection and from residual HCHO included in the MLE calibration method.
 510

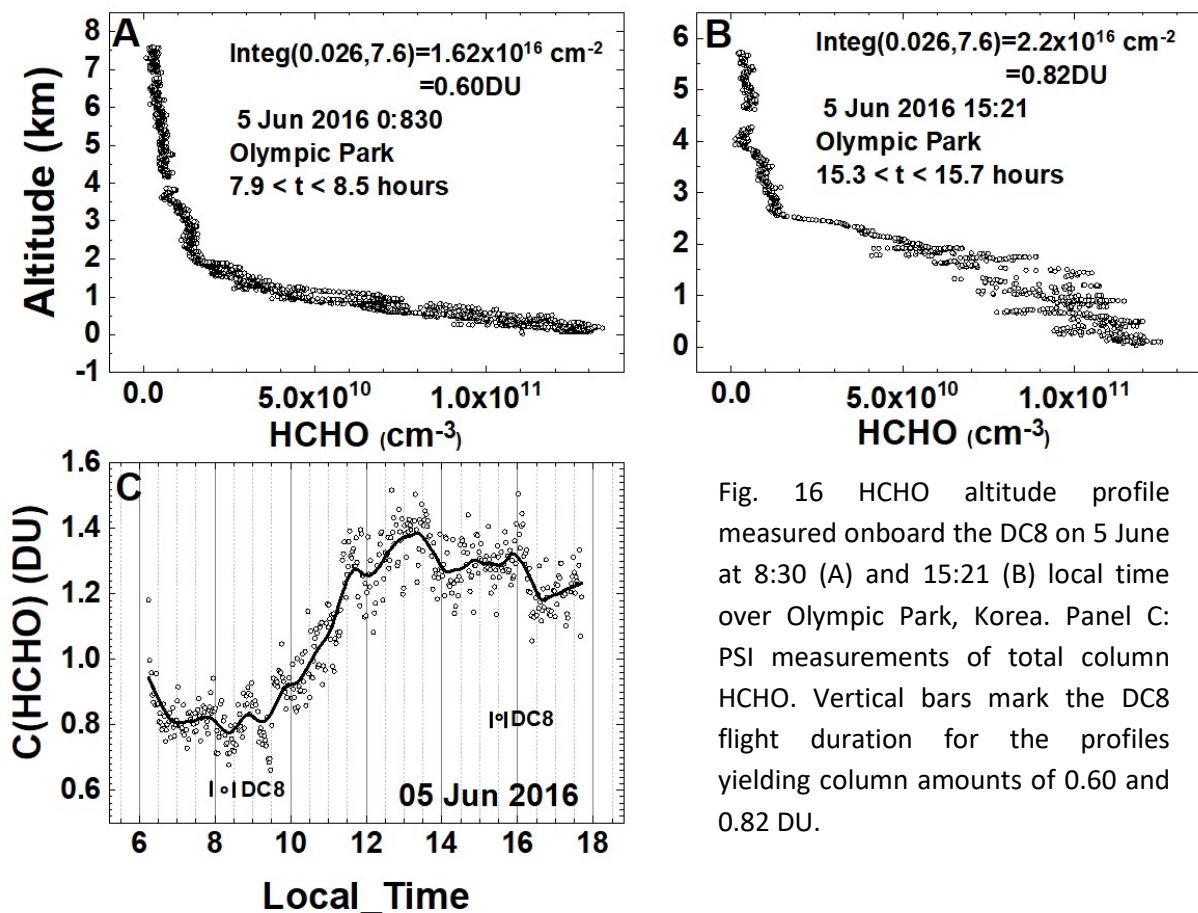


Fig. 16 HCHO altitude profile measured onboard the DC8 on 5 June at 8:30 (A) and 15:21 (B) local time over Olympic Park, Korea. Panel C: PSI measurements of total column HCHO. Vertical bars mark the DC8 flight duration for the profiles yielding column amounts of 0.60 and 0.82 DU.

511
 512 Another Olympic Park case on 9 June 2016 shows DC8=0.79 vs PSI=1 DU at 08:06,
 513 DC8=0.74 vs PSI=1.3 DU at 12:12, and DC8=1.13 vs PSI=1.9DU, or the DC8 measurements are 79
 514 % and 57 % less than the PSI total column HCHO. All of the remaining comparisons of DC8
 515 profile results with PSI C(HCHO) show similar results. The reasons for the disagreement between
 516 C(HCHO) measured by direct sun observations (PSI) and the integrated column density from aircraft
 517 measurements of HCHO VMR are not known. Contributions to the differences include the selection of
 518 the PSI wavelength window (332 - 359 nm) and possible interference from overlapping NO₂ and O₃
 519 absorption that are not properly included, and, more likely, the use of CAMS measured volume mixing
 520 ratios at the lowest altitudes from the nearby Seoul airbase, 8.5 km from Olympic Park, where spatial
 521 variation may affect the calculation of C(HCHO). The use of Taehwa Mtn. data for higher altitudes over
 522 Olympic Park contributes 25 % for 3 of the above cases and 50 % for 4 May 2016 at 07:54 (Fig.
 523 14A). This is probably not the reason for the disagreement between CAMS and PSI, since the percent
 524 underestimate for CAMS over Taehwa is about the same magnitude (Table 2) as over Olympic Park.

525
526
527
528
529
530
531
532
533
534
535
536

PSI measurements show that Olympic Park produces more HCHO almost every day than observed at the Yonsei University in Seoul and Taehwa Mountain sites (Figs. 12, 17, 18). The hourly variations observed during the KORUS-AQ campaign at the Yonsei University in Seoul and at Taehwa Mountain sites are similar to Olympic Park even though most of the HCHO is locally produced by photochemistry, but has a relatively short lifetime of a few hours in polluted air where there is significant ozone and OH. However, at typical wind speeds of 10 -20 km/hour and a chemical lifetime of 2.5 hours (Dufour et al., 2009), HCHO can be transported about 25 – 50 km, which is far enough for some transport of HCHO between the PSI sites at Yonsei, Olympic Park, and Taehwa Mtn. DC8 CAMS results over the Taehwa Mtn. site compared to PSI are given in Table 2 with differences similar to Olympic Park

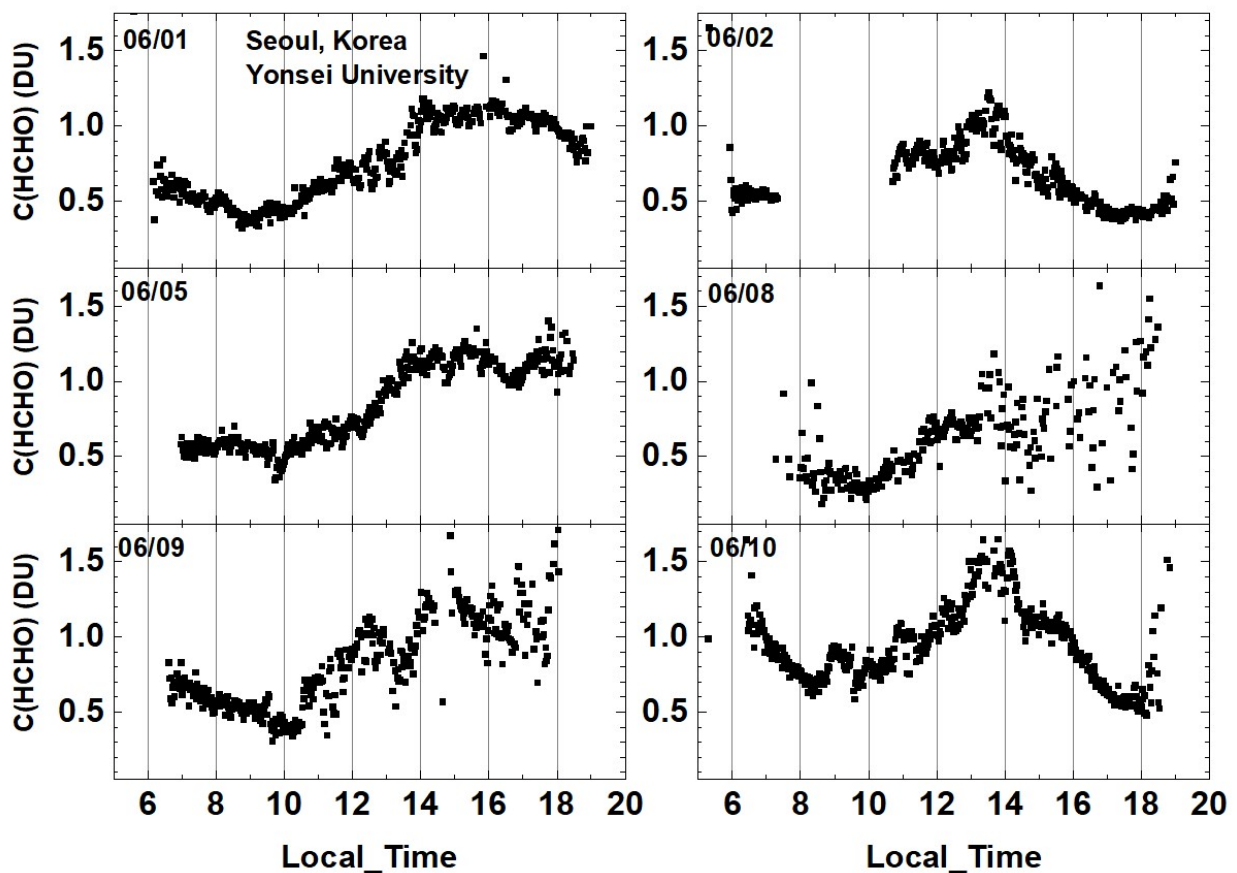


Fig. 17 Total column HCHO from Pandora Yonsei University, Seoul for 6 days in June 2016. C(HCHO) on 2 June 2016 has a peak value of 1.2 DU at 13:30 hours.

537
538
539
540

541

Table 2 Taehwa Mtn DC8 compared to PSI measurements (see 10 Jun in Fig. 18)

Date	LT	DC8 HCHO DU	PSI HCHO	Percent
11 May	08:25:19	0.4	0.6	67
18 May	08:34:26	0.4	0.5	80
30 May	12:05:00	0.5	0.9	56
10 Jun	08:22:45	1	1.16	86
10 Jun	12:22:53	1	1.5	67
10 Jun	15:46:03	1	1.3	77

542

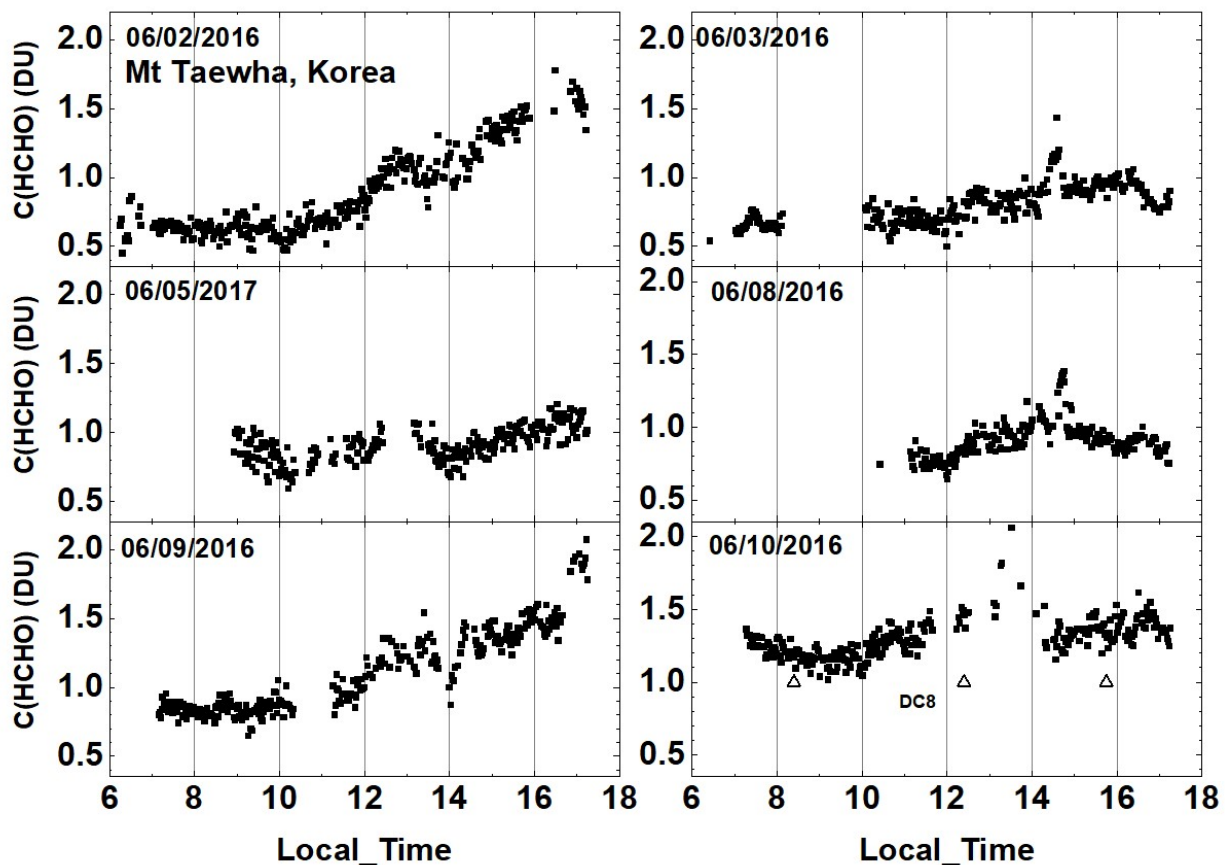


Fig. 18 Total column HCHO from Pandora at Taehwa Mountain for 6 days in June 2016. C(HCHO) on 2 June 2016 has a peak value of 1.7 DU at 16:20. △ are DC8 measurements on 10 June

543

544 Figure 19a and 19b summarizes all of the C(HCHO) data obtained during KORUS-AQ at
 545 the five sites. The graphs on the left show all of the data points (light gray circles) as a function
 546 of the local time and a Lowess(0.1) fit to the data showing the average hourly behavior. The
 547 spread of the data about the Lowess(0.1) fit represents the day-to-day variation at a given local
 548 time. On average, Mt. Taehwa tends to increase throughout each day, while Yonsei and
 549 Olympic Park show maxima at 14:00 and 15:30, respectively. Similarly, in Fig. 18b Yeogju

550 increases during the day having a maximum at 17:42 while Anmyeondo has a broad peak with
 551 maxima at 12:00 and 13:42.
 552

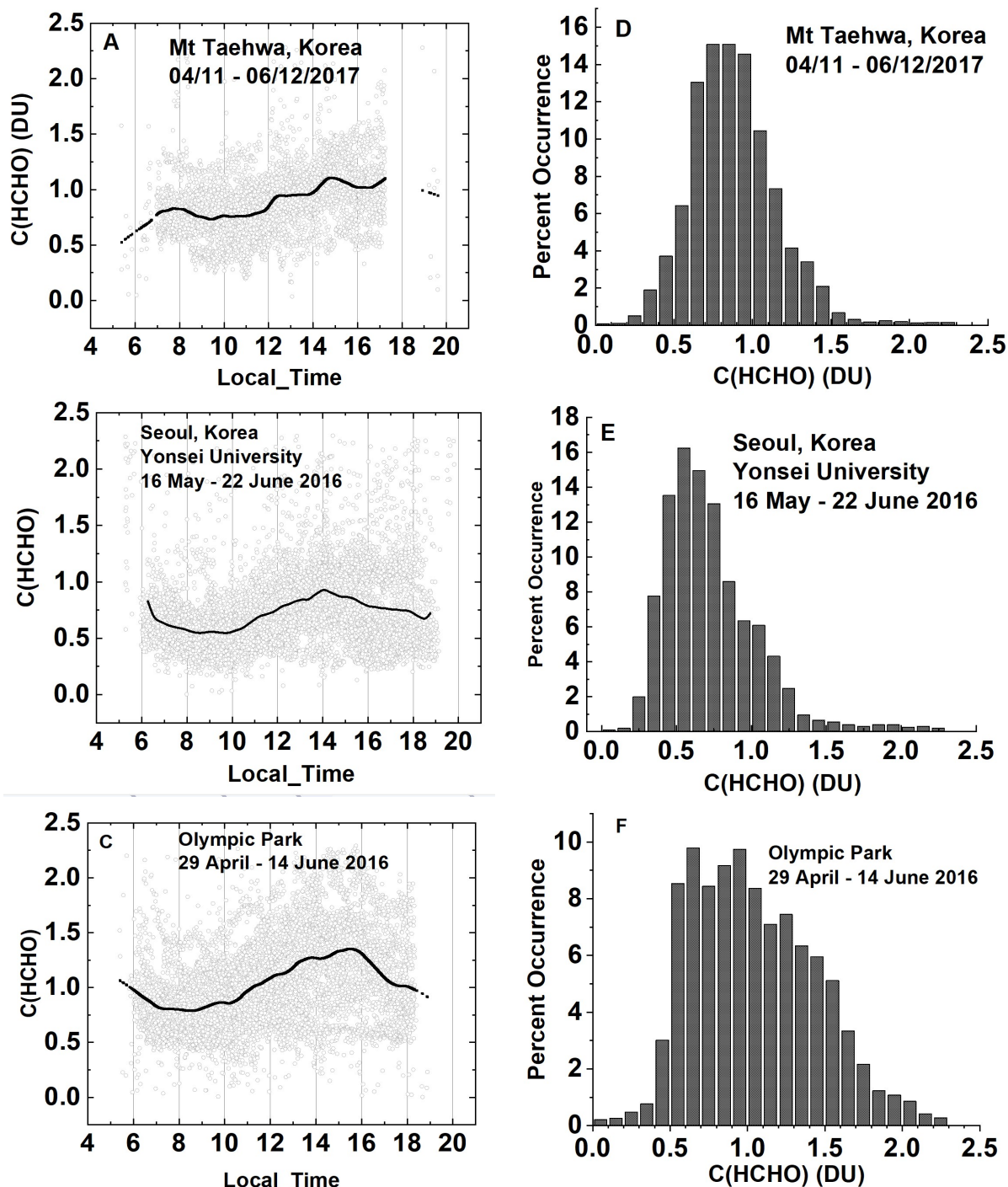


Fig. 19a Summary of total column HCHO for the stated dates during the KORUS-AQ campaign. The solid line is a Lowess(0.1) fit to the data. The sharp cutoffs in panel A, B, and C were caused by obstructions of the direct sun from the PSI FOV in the afternoon.

553

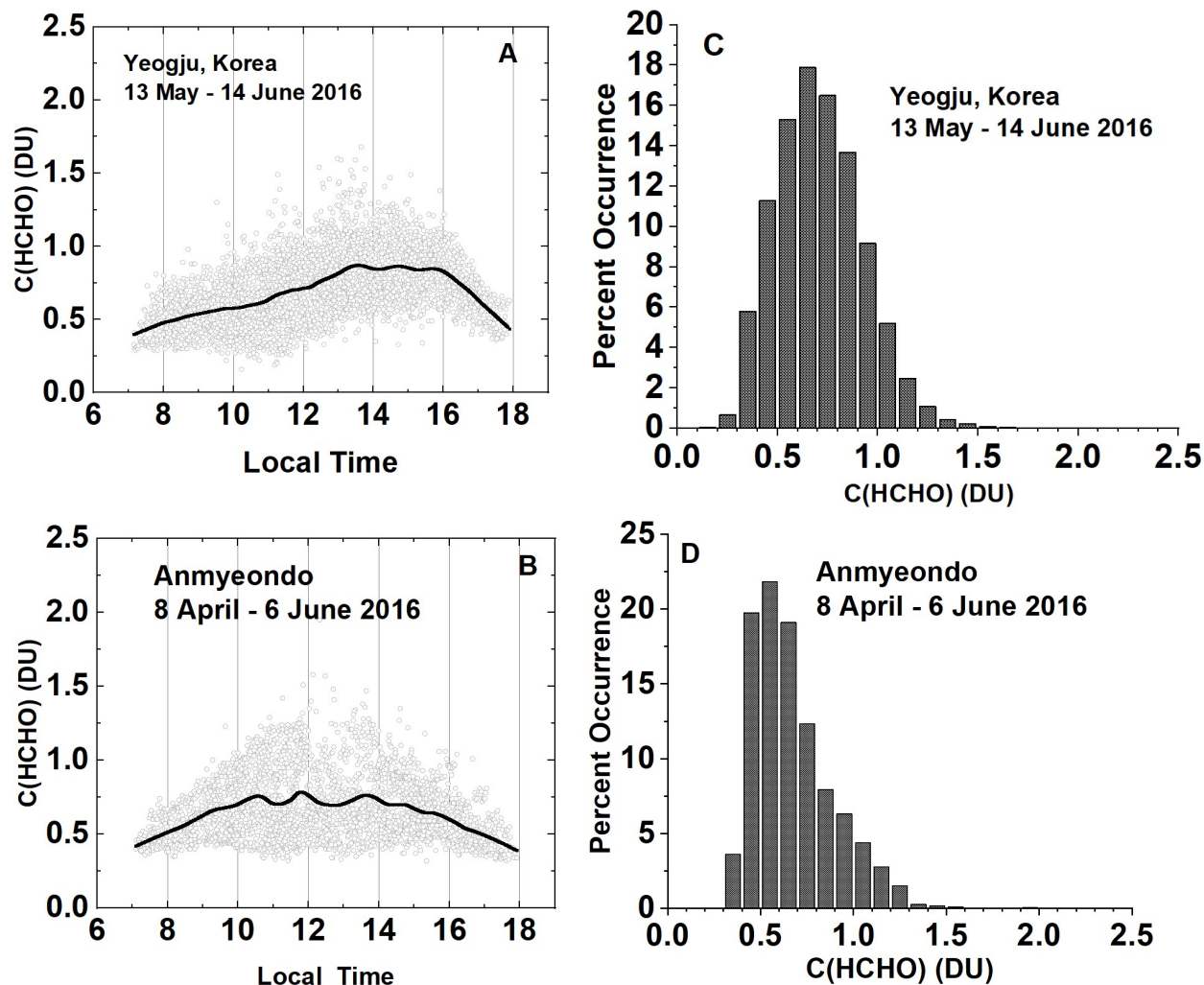


Fig. 19b Summary of total column HCHO for the stated dates during the KORUS-AQ campaign. Panels A and B represent the daily variation at a given local time. The solid line is a Lowess(0.1) fit to the data. Panels C and D show the frequency of occurrence (%) for different amounts of HCHO.

554

555 The histograms on the right side of Fig. 19 represent the percent frequency of
 556 occurrence of $C(\text{HCHO})$ in 0.1 DU bins. $C(\text{HCHO})$ at Mt. Taehwa and Seoul rarely exceeds 1.5 DU
 557 compared to Olympic Park where $C(\text{HCHO}) > 2$ DU for a significant fraction of time. The most
 558 frequent values are 0.6 DU for Seoul, 0.9 DU for Mt Taehwa, and over 1 DU for Olympic Park.
 559 Olympic Park also has a broader distribution towards higher values of $C(\text{HCHO})$ than other sites.
 560

561 The general intra-day $C(\text{HCHO})$ time dependence and $C(\text{HCHO})$ percent occurrence are
 562 shown for two additional sites (Fig. 19b), Yeogju and Anmyeondo. Yeogju shows an increase in
 563 $C(\text{HCHO})$ from morning to a peak value of 0.85 DU at 14:42, which then declines after 16:00. In

564 contrast, Amnyeondo is almost symmetric with the sun position, having a maximum of about
 565 0.77 DU near 12:00 and 13:42 hours.

566 The average change in C(HCHO) during the spring campaign at the five sites is
 567 summarized in Fig. 20. Of the sites, Olympic Park showed the largest change rate, 58 %/Month
 568 followed by Amnyeondo at 50 %/Month, then Taehwa (33 %/Month), Yonsei Seoul (25
 569 %/Month), and Yeogju (-13 %/Month). Amnyeondo tends to have lower C(HCHO) amounts
 570 because of its relatively isolated coastal location. These 2-month trends include seasonal
 571 increases during the campaign months May and June, 2016.

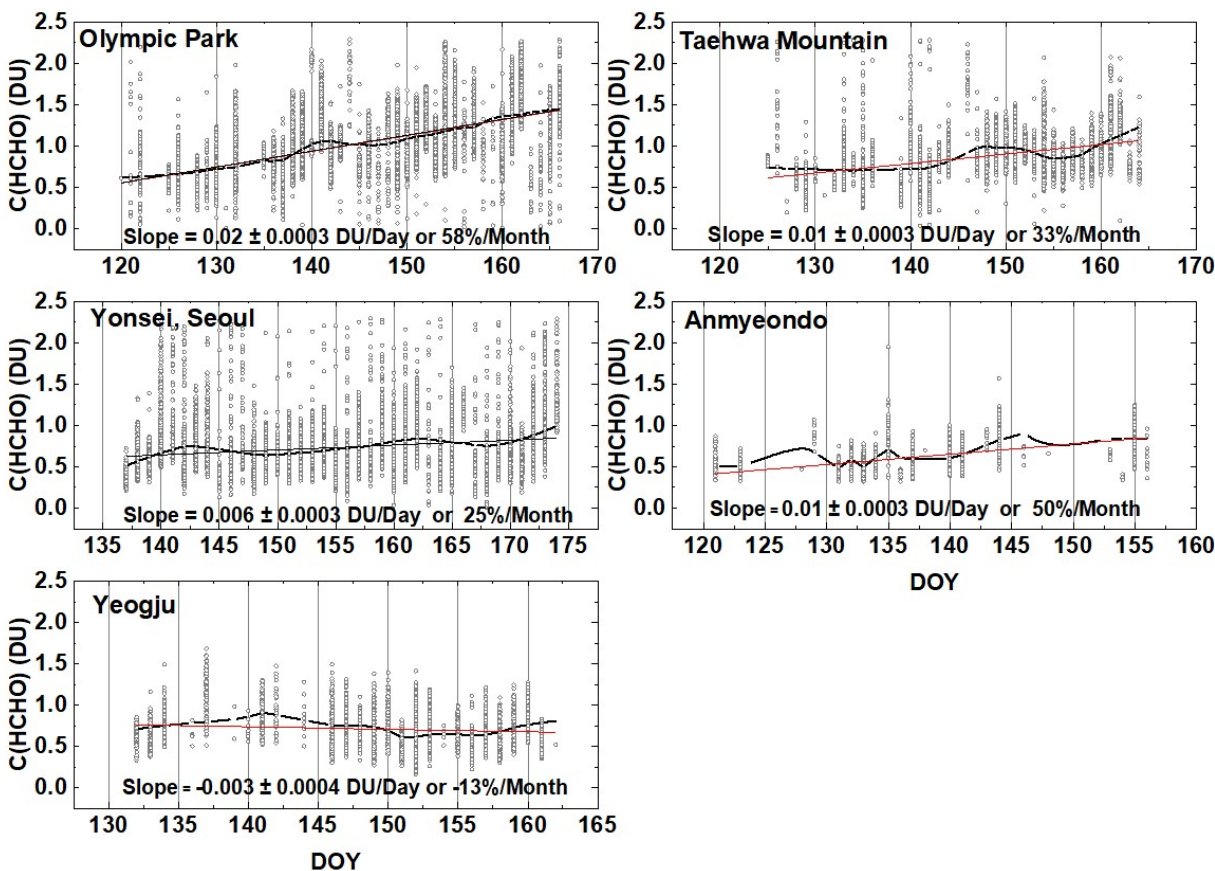


Fig. 20 The springtime change in C(HCHO) over about a 40 day period depending on the site. The “vertical bars” are the diurnal variation within each day of data. The thicker red curve is a Lowess(0.3) fit to the data, while the thin red line is a linear least squares fit. The Lowess(0.3) fit is approximately a 10-day local least-squares average.

572 It is difficult to compare PSI C(HCHO) with OMI for the KORUS-AQ period, since OMI
 573 overpass C(HCHO) data for 2016 have some missing days (Fig. 21). For days with matching
 574 data points over Seoul, PSI C(HCHO) (approximately 0.8 DU) is almost always larger than the
 575 OMI values (0.2 DU) plus a few very high PSI values and two high OMI values. The general
 576 day-to-day variations are similar.
 577

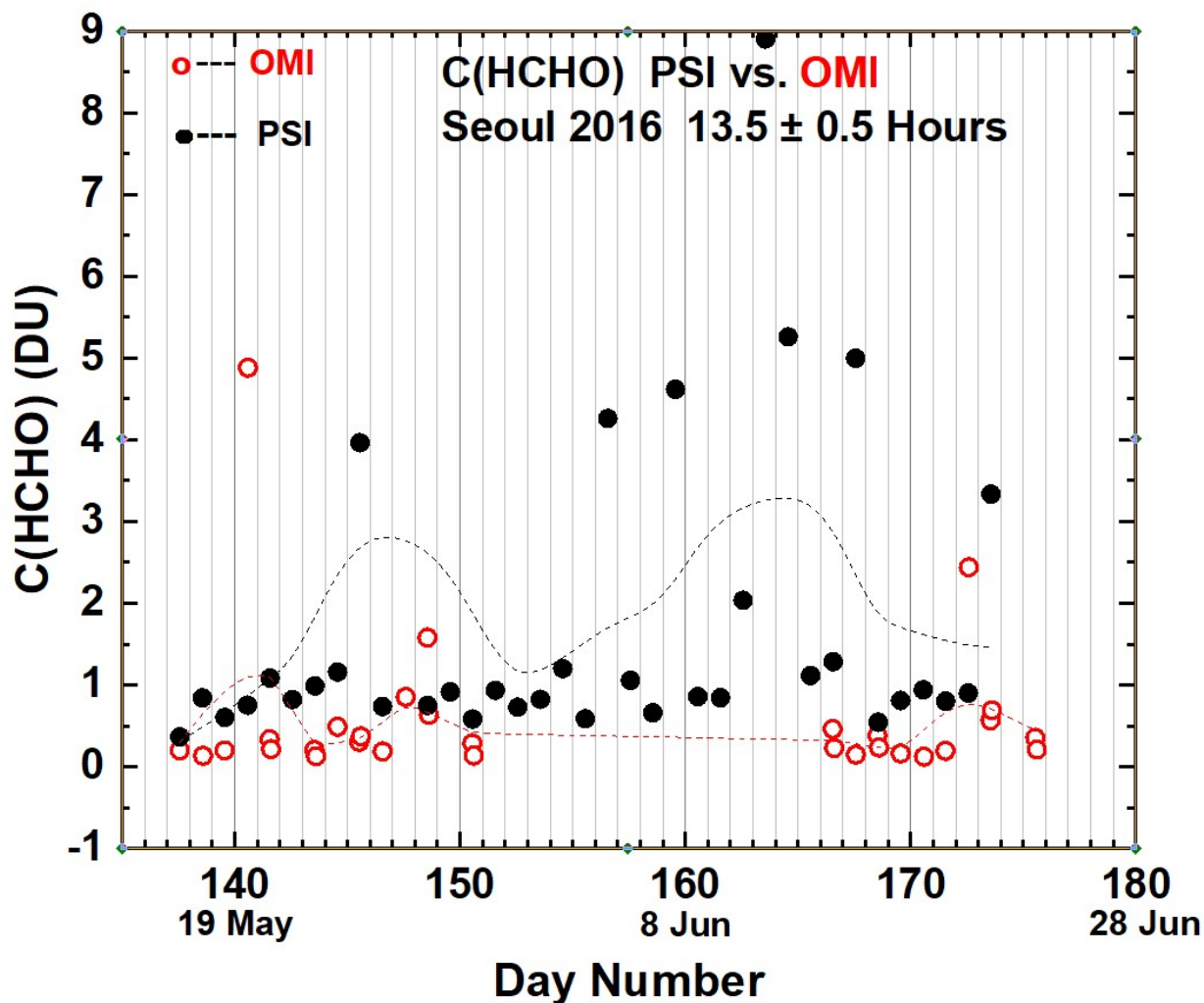


Fig. 21 Compare PSI • and OMI ◊ retrievals of C(HCHO) at 13.5 ± 0.5 hours. OMI overpass data, V03, are from <https://avdc.gsfc.nasa.gov/index.php?site=1113974256&id=81>

578
 579
 580
 581

582 **7 Summary**

583

584 Nine Pandora Spectrometer Instruments, PSI, were installed at 8 sites in South Korea as part of
585 the KORUS-AQ ground, aircraft, and satellite measurements for air-quality studies. The measurements
586 made during the months of April to June by PSI showed that are very high amounts of urban pollution
587 from NO₂ and HCHO, and more moderate, but still high values, away from the urban centers. An
588 exception was Amnyeondo, which is located on a west-coastal island adjacent to the Yellow Sea about
589 100 km south of Seoul. The urban areas show minimum values in the morning that rise rapidly
590 throughout the day, peaking in the late afternoon for both C(NO₂) and C(HCHO).

591

592 PSI direct-sun retrieved values of C(NO₂) and C(HCHO) are always larger than OMI retrieved
593 C(NO₂) and C(HCHO) for the OMI overpass times (13.5 ± 0.5 hours). In urban areas, PSI C(NO₂) averages
594 are at least a factor of two larger than OMI averages. Similar differences are seen for C(HCHO) in Seoul.
595 However, late afternoon values measured by PSI are even larger, implying that OMI measurements
596 underestimate the effect of poor air quality on human health. The primary cause of the OMI
597 underestimate is the large OMI FOV that includes regions containing low values of pollutants. In
598 relatively clean areas, PSI and OMI are more closely in agreement.

599

600 PSI retrieved C(NO₂) amounts for Seoul frequently exceed 2 DU and occasionally reach 6 DU.
601 Other urban centers in the south, Busan and Gwangju, have smaller C(NO₂) amounts, but exhibit a
602 similar strong diurnal pattern, namely low values in the morning and high values later during midday.
603 This behavior is expected because of the large number of urban automobiles and concentrated industry.
604 Urban areas downwind from Seoul show high C(NO₂) amounts, but also show daily minimum amounts in
605 the morning that increase later in the day. Two of the sites, Seoul and Busan, have long-term C(NO₂)
606 data records, 2012 – 2016, that suggest a gradual decrease in C(NO₂) amounts in Korea. When
607 compared with OMI, both ground-based PSI's and the 4STAR aircraft instrument onboard the DC8 show
608 that the correlation is best for small values of C(NO₂), most often seen in the troposphere and
609 stratosphere and worst for high values that are usually in the boundary layer near their local sources. In
610 Olympic Park, the measurements of significant values of C(HCHO) and high values of C(NO₂) in the
611 afternoon suggest that there are increased boundary layer amounts of ozone.

612

613 C(HCHO) amounts were obtained for five sites, Yonsei University in Seoul, Olympic Park, Taehwa
614 Mtn., Amnyeondo, and Yeosu. Of these the largest amounts of C(HCHO) were observed at Olympic Park,
615 and Taehwa Mountain, both surrounded by significant amounts of vegetation. Comparisons of PSI
616 results were made with overflights on the DC8 aircraft for Taehwa Mtn and Olympic Park showing a
617 significant difference in total column HCHO. In all cases, PSI measured substantially more C(HCHO) than
618 obtained from integrating the altitude profiles measured from the DC8 overflights.

619

620 Appendix

621
622 Figure A1 illustrates the deseasonalization of the time series in Fig.6. The left panel reproduces
623 the solid black curve in Fig. 6A or 6C in the inset. The right panel reproduces the solid curve in Fig. 6B
624 and is magnified in the inset. The seasonal dependence in the left panel inset is almost non-existent in
625 the right panel inset
626

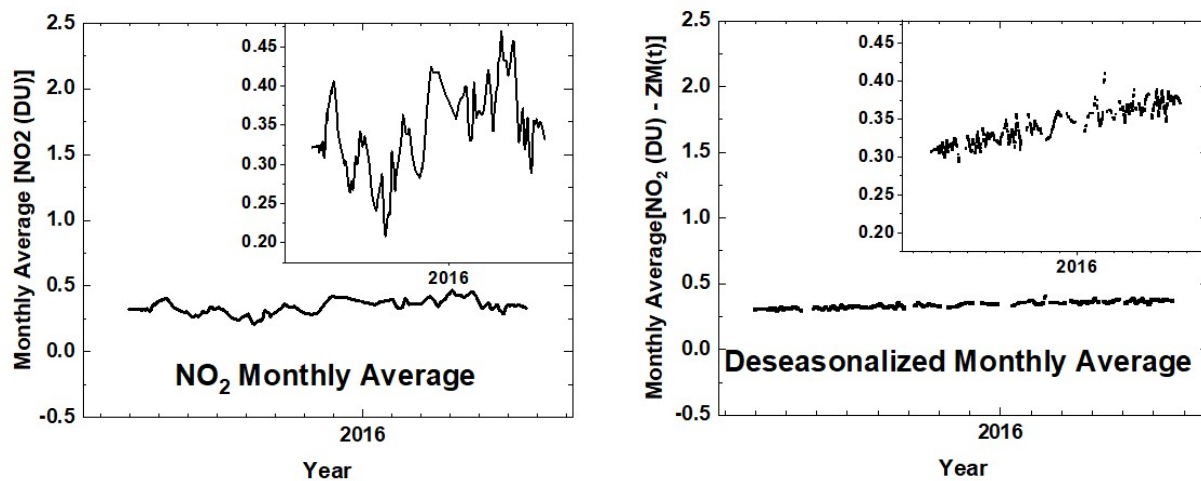


Fig. A1 An illustration of the deseasonalization (right panel) of the monthly running average of NO₂ for the Gwangju site (left panel) shown in Fig. 6. The insets are magnifications of the main plots.

627
628

629

630

631 **Data Sources**

632 **OMI Formaldehyde HCHO Version 03:** <https://avdc.gsfc.nasa.gov/index.php?site=1113974256&id=81>

633 **OMI Nitrogen Dioxide NO₂ Version 03** <https://avdc.gsfc.nasa.gov/index.php?site=666843934&id=13>

634 **Pandora KORUS-AQ** <https://avdc.gsfc.nasa.gov/pub/DSCOVr/Pandora/DATA/KORUS-AQ/>

635

636 **Author Contributions**

637

638 Jay Herman: Wrote most of the paper and performed the analysis and comparisons with the DC-8
639 aircraft measurements

640 Elena Spinei: Derived the formaldehyde altitude profiles suitable for comparison with Pandora data

641 Alan Fried: Obtained the HCHO profile data from the DC-8 CAMS instrument

642 Jhoon Kim: Provided support for the installation of Pandora instruments in Korea.

643 Jae Kim: Provided support for the Pandora located in Busan .

644 Woogyung Kim: Provided support in installing the Pandoras and analyzing the raw data

645 Alexander Cede: Provided calibration and data analysis support

646 Nader Abuhassan: Provided Pandora setup in Korea and provided the maintenance of calibration

647 Michal Segal-Rozenhaimer: Provided the 4STAR NO₂ data from the DC-8 flights and the comparison with
648 Pandora

649

650 The authors declare that they have no conflict of interest.

651 **8 References**

- 652 Boersma, K. F., D. J. Jacob, M. Trainic, Y. Rudich, I. DeSmedt, R. Dirksen, and H. J. Eskes, Validation of
653 urban NO₂ concentrations and their diurnal and seasonal variations observed from the SCIAMACHY and
654 OMI sensors using in situ surface measurements in Israeli cities, *Atmos. Chem. Phys.*, 9, 3867–3879,
655 2009.
- 656 Chimot, J., Vlemmix, T., Veeffkind, J. P., de Haan, J. F., and Levelt, P. F.: Impact of aerosols on the OMI
657 tropospheric NO₂ retrievals over industrialized regions: how accurate is the aerosol correction of cloud-
658 free scenes via a simple cloud model?, *Atmos. Meas. Tech.*, 9, 359-382, [https://doi.org/10.5194/amt-9-](https://doi.org/10.5194/amt-9-359-2016)
659 359-2016, 2016.
- 660 Cleveland, William S., LOWESS: A program for smoothing scatterplots by robust locally weighted
661 regression. *The American Statistician*. **35** (1): 54. [JSTOR 2683591](https://www.jstor.org/stable/2683591). [doi:10.2307/2683591](https://doi.org/10.2307/2683591), 1981.
662
- 663 Dufour, G., F. Wittrock, M. Camredon, M. Beekmann, A. Richter, B. Aumont, and J. P. Burrows,
664 SCIAMACHY formaldehyde observations: constraint for isoprene emission estimates over Europe?,
665 *Atmos. Chem. Phys.*, 9, 1647–1664, 2009
666
- 667 Dunagan, S. E., R. Johnson, J. Zavaleta, P. B. Russell, B. Schmid, C. Flynn, J. Redemann, Y. Shinozuka, J.
668 Livingston, and M. Segal-Rosenhaimer, 4STAR spectrometer for sky-scanning Sun-tracking atmospheric
669 research: Instrument technology, *Remote Sens. (Special Issue*
670 "Optical Remote Sensing of the Atmosphere"), 5, 3872–3895, doi:10.3390/rs5083872, 2013.
- 671 Fried, A., Walega, J. G., Olson, J. R., Crawford, J. H., Chen, G., Weibring, P., ... Millet, D. B. (2008).
672 Formaldehyde over North America and the North Atlantic during the summer 2004 INTEX campaign:
673 Methods, observed distributions, and measurement-model comparisons. *Journal of Geophysical*
674 *Research*, 113(D10). <https://doi.org/10.1029/2007JD009185>, 2008.
- 675 Friedfeld, S., M. Fraser, K. Ensor, S. Tribble, D. Rehle, D. Leleux, F. Tittel Statistical analysis of primary and
676 secondary atmospheric formaldehyde, *Atmospheric Environment*, 36, 4767-4775, 2002.
- 677 Garcia, A.R., R. Volkamer, L.T. Molina, M.J. Molina, J. Samuelson, J. Mellqvist, B. Galle, S.C. Herndon, C.E.
678 Kolb, Separation of emitted and photochemical formaldehyde in Mexico City using a statistical analysis
679 and a new pair of gas-phase tracers *Atmospheric Chemistry Physics*, 6, 4545-4557, 2006.
- 680 Goldberg D. et al., (2017), A High-Resolution And Observationally Constrained Omi NO₂ Satellite
681 Retrieval, *Atmos. Chem. Phys. Discuss.*, doi:10.5194/acp-2017-219, 2017.
- 682 Herman, Jay, Alexander Cede, Elena Spinei, George Mount, Maria Tzortziou, Nader Abuhassan, NO₂
683 Column Amounts from Ground-based Pandora and MFDOAS Spectrometers using the Direct-Sun DOAS
684 Technique: Intercomparisons and Application to OMI Validation, *J. Geophys. Res.*, 114, D13307,
685 doi:10.1029/2009JD011848, 2009.
- 686 Jung, Jinsang, JaeYong Lee, ByungMoon Kim, SangHyub Oh, Seasonal variations in the NO₂ artifact from
687 chemiluminescence measurements with a molybdenum converter at a suburban site in

688 Korea (downwind of the Asian continental outflow) during 2015 - 2016, *Atmospheric Environment* 165,
689 290-300, 2017.

690 Kanaya, Y., Irie, H., Takashima, H., Iwabuchi, H., Akimoto, H., Sudo, K., Gu, M., Chong, J., Kim, Y. J., Lee,
691 H., Li, A., Si, F., Xu, J., Xie, P.-H., Liu, W.-Q., Dzhola, A., Postlyakov, O., Ivanov, V., Grechko, E.,
692 Terpugova, S., and Panchenko, M.: Long-term MAX-DOAS network observations of NO₂ in Russia and
693 Asia (MADRAS) during the period 2007–2012: instrumentation, elucidation of climatology, and
694 comparisons with OMI satellite observations and global model simulations, *Atmos. Chem. Phys.*, 14,
695 7909-7927, <https://doi.org/10.5194/acp-14-7909-2014>, 2014.

696 Kim, Na Kyung, Yong Pyo Kim, Yu Morino, Jun-ichi Kurokawa, Toshimasa Ohara, Verification of NOx
697 emission inventory over South Korea using sectoral activity data and satellite observation of NO₂ vertical
698 column densities, *Atmospheric Environment* , 77, 496-508, 2013.

699 Kim, Daewon, Hanlim Lee, Hyunkee Hong, Wonei Choi, Yun Gon Lee and Junsung Park, Estimation of
700 Surface NO₂ Volume Mixing Ratio in Four Metropolitan Cities in Korea Using Multiple Regression Models
701 with OMI and AIRS Data, *Remote Sens.* 2017, 9, 627; doi:10.3390/rs9060627, 2017.

702 Krafta, Martin, Thomas Eikmannb, Andreas Kapposc, Nino Künzlid, Regula Rappe, Klaus Schneiderf,
703 Heike Seitzb, Jens-Uwe Voss, H.-Erich Wichmannh, The German view: Effects of nitrogen dioxide on
704 human health – derivation of health-related short-term and long-term values, *International Journal of*
705 *Hygiene and Environmental Health*, 208, 305–318, 2005.

706 Kramer, L.J., R. J. Leigh, J. J. Remedios, et al., “Comparison of OMI and Ground-Based in situ and
707 MAXDOAS Measurements of Tropospheric Nitrogen Dioxide in An Urban Area,” *J. Geophys. Res.* 113,
708 D16S39, 2008.

709 Latza, Ute, , Silke Gerdes, and Xaver Baur, Effects of nitrogen dioxide on human health: Systematic review
710 of experimental and epidemiological studies conducted between 2002 and 2006, *International Journal of*
711 *Hygiene and Environmental Health* 212, Pages 271 - 287, doi.org/10.1016/j.ijheh.2008.06.003, 2009.

712 Lee, Gyeem, Hye-Ryun Oh, Chang-Hoi Ho, Jinwon Kim, Chang-Keun Song, Lim-Seok Chang, Jae-Bum Lee,
713 Seungmin Lee, Airborne Measurements of High Pollutant Concentration Events in the Free Troposphere
714 over the West Coast of South Korea between 1997 and 2011, *Aerosol and Air Quality Research*, 16,
715 1118–1130, 2016.

716 Lei, W., Zavala, M., de Foy, B., Volkamer, R., Molina, M. J., and Molina, L. T.: Impact of primary
717 formaldehyde on air pollution in the Mexico City Metropolitan Area, *Atmos. Chem. Phys.*, 9, 2607–2618,
718 2009.

719 Liteplo, R.G., R. Beauchamp, M.E. Meek, and R. Chénier. Formaldehyde. Geneva: International
720 Programme on Chemical Safety; 2002. [18 May 2010]. (Concise International Chemical Assessment
721 Document 40) (<http://www.inchem.org/documents/cicads/cicads/cicad40.htm>).

722 Luecken, D.J., W.T. Hutzell, M.L. Strum, G.A. Pouliot, Regional sources of atmospheric formaldehyde and
723 acetaldehyde, and implications for atmospheric modeling, *Atmospheric Environment* 47, 477-490,
724 doi:10.1016/j.atmosenv.2011.10.005, 2012.

725 Meller, Richard, and Geert K Moortgat. Temperature dependence of the absorption cross sections of
726 formaldehyde between 223 and 323 k in the wavelength range 225-375 nm. *Journal of Geophysical*
727 *Research: Atmospheres* (19842012), 105(D6):70897101, 2000.

728
729 **Park, Junsung, Hanlim Lee, Jhoon Kim, Jay Herman, Woogyung Kim, Hyunkee Hong, Wonei Choi,**
730 **Jiwon Yang and Daewon Kim, HCHO column density retrieval using Pandora measurements in Seoul,**
731 **Korea: Temporal characteristics and comparison with OMI measurement, *Remote Sens.*, 10, 173,**
732 **doi:10.3390/rs10020173, 2018.**

733
734 Richter D., P. Weibring, J. G. Walega, A. Fried, S. M. Spuler, M. S. Taubman: Compact highly sensitive
735 multi-species airborne mid-IR spectrometer, *Appl. Phys. B*, doi: 10.1007/s00340-015-6038-8, 2015.

736 Russell, A. R., Perring, A. E., Valin, L. C., Bucseba, E. J., Browne, E. C., Wooldridge, P. J., and Cohen, R. C.: A
737 high spatial resolution retrieval of NO₂ column densities from OMI: method and evaluation, *Atmos.*
738 *Chem. Phys.*, 11, 8543-8554, 2011.

739 Segal-Rosenheimer, M., P. B. Russell, B. Schmid, J. Redemann, J. M. Livingston, C. J. Flynn, R. R. Johnson,
740 S. E. Dunagan, Y. Shinzuka¹, J. Herman, A. Cede, N. Abuhassan, J. M. Comstock, J. M. Hubbe, A.
741 Zelenyuk³, and J. Wilson, (2014) Tracking elevated pollution layers with a newly developed
742 hyperspectral Sun/Sky spectrometer(4STAR): Results from the TCAP 2012 and 2013 campaigns, *J.*
743 *Geophys. Res. Atmos.*, 119, 2611–2628, doi:10.1002/2013JD020884, 2014.

744 Shinzuka, Y., et al. , Hyperspectral aerosol optical depths from TCAP flights, *J. Geophys. Res. Atmos.*,
745 118, 12,180–12,194, doi:10.1002/2013JD020596, 2013.

746 Spinei, E., N. Abuhassan, A Cede, M. Tiefengraber, M. Mueller, J. Herman, N. Nowak, B. Poche, S. Choi⁷,
747 A. Whitehill, J. Szykman, V. Lukas, D. Williams, R. Long, Jin Liao, Jason St. Clair, Glenn Wolfe, Thomas
748 Hanisco, Changmin Cho, Alan Fried, Petter Weibring, Dirk Richter, Robert Swap, James Walega, Pandora
749 formaldehyde measurements during KORUS-AQ over Olympic Park and Taehwa (South Korea, April-June
750 2016), (submitted to AMT), 2018.

751 Walters, Wendell & Goodwin, Stanford & Michalski, Greg. (2015). The Nitrogen Stable Isotope
752 Composition ($\delta^{15}\text{N}$) of Vehicle Emitted NO_x. *Environmental science & technology*. 49.
753 10.1021/es505580v, 2015.

754 **Zhang, Hongliang, Jingyi Li, Qi Ying, Birnur Buzcu Guven, and Eduardo P. Olaguer, Source apportionment**
755 **of formaldehyde during TexAQS 2006 using a source-oriented chemical transport model, *J. Geophys.***
756 ***Res.*, 118, 1525–1535, doi:10.1002/jgrd.50197, 2013.**

757 Zhu, Lei, Daniel J. Jacob, Frank N. Keutsch, Loretta J. Mickley, Richard Scheffe, Madeleine Strum, Gonzalo
758 González Abad, Kelly Chance, Kai Yang, Bernhard Rappenglück, Dylan B. Millet, Munkhbayar Baasandorj,
759 Lyatt Jaeglé, and Viral Shah, Formaldehyde (HCHO) As a Hazardous Air Pollutant: Mapping Surface Air
760 Concentrations from Satellite and Inferring Cancer Risks in the United States, *Environmental Science &*
761 *Technology* 51 (10), 5650-5657, DOI: 10.1021/acs.est.7b01356, 2017.

762

763

764

765 Acknowledgement

766 The author would like to thank the Pandora project for support in completing this study as well
767 as financial support from the KORUS-AQ project NNH15ZDA001N-KORUS. All data is available from a
768 NASA data repository: <https://avdc.gsfc.nasa.gov/pub/DSCOVER/Pandora/DATA/KORUS-AQ/>
769

770

771 **Tables**

Table 1 KORUS-AQ Locations (South to North)

Locations	Alt(m)	Latitude	Longitude
Gwangju	33	35.2260N	126.8430W
Busan	228	35.2353N	129.0825W
Anmyeondo	41	36.5380N	126.3300W
Taehwa Mtn	160	37.3123N	127.3106W
Yeosu-1 & 2	90	37.3385N	127.4895W
Songchon	49	37.4100N	127.5600W
Olympic Park	26	37.5232N	127.1260W
Seoul	181	37.5644N	126.9340W

772

773

Table 2 Taehwa Mtn DC8 compared to PSI measurements in Fig. 18

Date	LT	DC8 HCHO DU	PSI HCHO	Percent
11 May	08:25:19	0.4	0.6	67
18 May	08:34:26	0.4	0.5	80
30 May	12:05:00	0.5	0.9	56
10 Jun	08:22:45	1	1.16	86
10 Jun	12:22:53	1	1.5	67
10 Jun	15:46:03	1	1.3	77

774

775

776 **Figure Captions**

777 **Fig. 1** KORUS-AQ sites for 9 Pandora instruments at 8 sites.

778 **Fig. 2a** $C(\text{NO}_2)$ amounts from Pandora 27 and 35 in Yeosu, Korea during 3 June 2016 and their difference
779 $|\text{Pan35} - \text{Pan27}| < 0.05 \text{ DU}$.

780 **Fig. 2b** Pandora 35 estimate of cloud or aerosol reduced measured counts/second at approximately 500
781 nm.

782 Fig. 3. Frequency distributions of $C(\text{NO}_2)$ across the KORUS-AQ PSI network: April 20 to Jun 6 2016,
783 except as labelled. The axes vary for different sites.

784 Fig. 4 NO_2 time series vs day of the year (DOY) and diurnal variability (daily vertical extent) at 9 Pandora
785 sites. Notice the very high NO_2 amounts in Seoul and nearby Olympic Park. The black curves are
786 approximately weekly least squares running averages. Note: the vertical scales are different for each site
787 to show the daily variability relative to the running average.

788 Fig. 5 NO_2 amounts vs Day of the Year (DOY) and Local Time for six sites as labeled in each panel. Day
789 120=April 29, Day 130=May 9, Day 140=May 19, Day 150=May 29, Day 160=June 8, Day 170 =June18.

Fig. 6 Approximately 1 year of daily column $C(\text{NO}_2)$ amount data (Panels A and D) and the monthly
running average amount (dark plot in Panels A and D). The data are from GIST at Gwangju and
Amnyeondo. Panels A and D are the original time series with one data point every 80 seconds, panels B
and E are the deseasonalized time series. Panels C and F are an expanded scale of the monthly running
averages $M(t)$ of $C(\text{NO}_2)$ that are identical to the solid lines in panels A and D. The vertical extent (panels
A, B, D, and E) on a given day is the range of diurnal variation from early morning to late afternoon.

790 Fig. 7 (A) NO_2 time series at Yonsei University in Seoul NO_2 (grey) and (B) deseasonalized time series.
791 Combined slope = $-0.05 \pm 0.001 \text{ DU/Year}$ and Mean = $1.2 \pm 0.8 \text{ DU}$ or the decrease is $-4 \pm 0.08 \% / \text{Year}$.
792 Seoul has no clear seasonal cycle.

793 Fig. 8 (A) Pusan University in Busan NO_2 daily time series (grey) and (B) deseasonalized time series with
794 linear trends.

795 Fig. 9a Comparisons between the daily values of $C(\text{NO}_2)$ for OMI (black) and PSI (red) at Seoul and Busan
796 for a 5-year period. Solid lines show the average seasonal variation (Lowess(0.1)), see also Fig. 9b. **Linear**
797 **interpolation is used where there are missing data points.**

798 Fig. 9b Comparisons between the seasonal averages for $C(\text{NO}_2)$ from OMI (black) and PSI (red) at Seoul
799 and Busan for a 5-year period. The lower panels show the seasonal difference between the PSI and
800 OMI. **The individual data points are shown derived from a Lowess(0.1) smoothing, approximately a 3-**
801 **month running averages of the daily data. Interpolation has been used where there are missing data**
802 **points.**

803 Fig. 10 C(NO₂) time series from Pandora (red) and OMI (black) for GIST University in Gwangju Korea and
804 their differences. The comparison is formed from time coincidences between Pandora and OMI.

805 Fig. 11 A correlation plot of C(NO₂) from 4STAR onboard the DC-8 compared to the C(NO₂) amount
806 measured by the PSI at Olympic Park on nine different days. The solid black line is the 1:1 line drawn for
807 reference. The dashed line represents the data linear fit, with a slope of 1.05, and a correlation
808 coefficient $r^2 = 0.7$, as shown on the plot.

809 Fig. 12 C(HCHO) from PSI at Olympic Park for 6 days in June 2016. C(HCHO) on 2 June 2016 has a peak
810 value of 2.3 DU at 14:30 hours.

811 Fig. 13 Pandora measured formaldehyde amounts vs day of the year and local time for 29 April 2016 to
812 11 June 2016 in Olympic Park.

813 Fig. 14 HCHO altitude profile measured onboard the DC8 on 4 May at 07:54 (A) and 11:54 (B) local time
814 over Olympic Park, Korea. Panel C: PSI measurements of total column HCHO. Vertical bars mark the DC8
815 flight duration for the profiles yielding altitude integrated column amounts of 0.38 and 0.26 DU.

816 Fig. 15 DC-8 HCHO measurements over Olympic Park on June 4. The continuous blue profiles
817 show the 1-second HCHO data while the black points with error bars show the 10-second
818 average and standard deviation of this data at points of closest approach above the Olympic
819 Park site.

820 Fig. 16 HCHO altitude profile measured onboard the DC8 on 5 June at 8:30 (A) and 15:21 (B) local time
821 over Olympic Park, Korea. Panel C: PSI measurements of total column HCHO. Vertical bars mark the DC8
822 flight duration for the profiles yielding column amounts of 0.60 and 0.82 DU.

823 Fig. 17 Total column HCHO from Pandora Yonsei University, Seoul for 6 days in June 2016. HCHO on 2
824 June 2016 has a peak value of 1.2 DU at 13:30 hours.

825 Fig. 18 Total column HCHO from Pandora Taehwa Mountain for 6 days in June 2016. HCHO on 2 June
826 2016 has a peak value of 1.2 DU at 12:45. ▲ are DC8 measurements on 10 June.

827 Fig. 19a Summary of total column HCHO for the stated dates during the KORUS-AQ campaign. The solid
828 line is a Lowess(0.1) fit to the data. The sharp cutoffs in panel A, B, and C were caused obstructions of
829 the direct sun from the PSI FOV in the afternoon.

830 Fig. 19b Summary of total column HCHO for the stated dates during the KORUS-AQ campaign. Panels A
831 and B represent the daily variation at a given local time. The solid line is a Lowess(0.1) fit to the data.
832 Panels C and D show the frequency of occurrence (%) for different amounts of HCHO.

833 Fig. 20 The springtime change in C(HCHO) over about a 40 day period depending on the site.
834 The “vertical bars” are the diurnal variation within each day of data. The thicker red curve is a
835 Lowess(0.3) fit to the data, while the thin red line is a linear least squares fit. The Lowess(0.3) fit
836 is approximately a 10-day local least-squares average.

837 Fig. 21 Compare PSI • and OMI o retrievals of C(HCHO) at 13.5 ± 0.5 hours. OMI overpass data, V03, are
838 from <https://avdc.gsfc.nasa.gov/index.php?site=1113974256&id=81>

839 Fig. A1 An illustration of the deseasonalization (right panel) of the monthly running average of NO_2 for
840 the Gwangju site (left panel) shown in Fig. 6. The insets are magnifications of the main plots.

841

842

843 Figures

844

845

846

847

848

849

850

851

852

853

854

855



856

Fig. 1 KORUS-AQ sites for 9 Pandora instruments at 8 sites.

857

858

859

860 **F01**

861

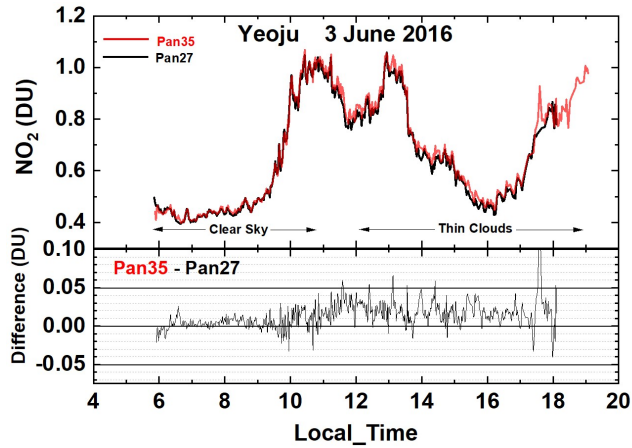


Fig. 2a $C(\text{NO}_2)$ amounts from Pandora 27 and 35 in Yeosu, Korea during 3 June 2016 and their difference $|\text{Pan35} - \text{Pan27}| < 0.05 \text{ DU}$.

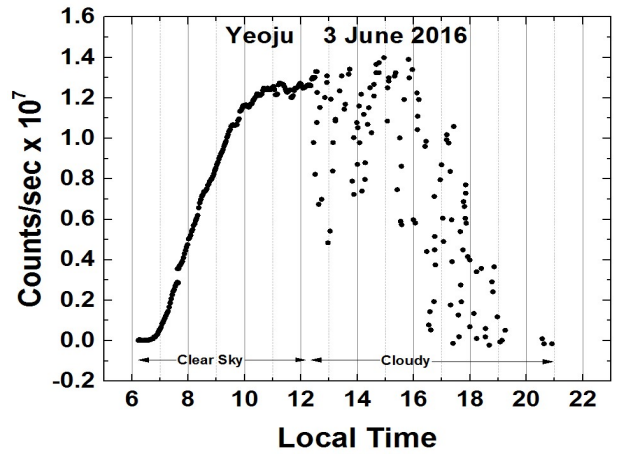


Fig. 2b Pandora 35 estimate of cloud or aerosol reduced measured counts/second at approximately 500 nm.

862

863 **F02**

864

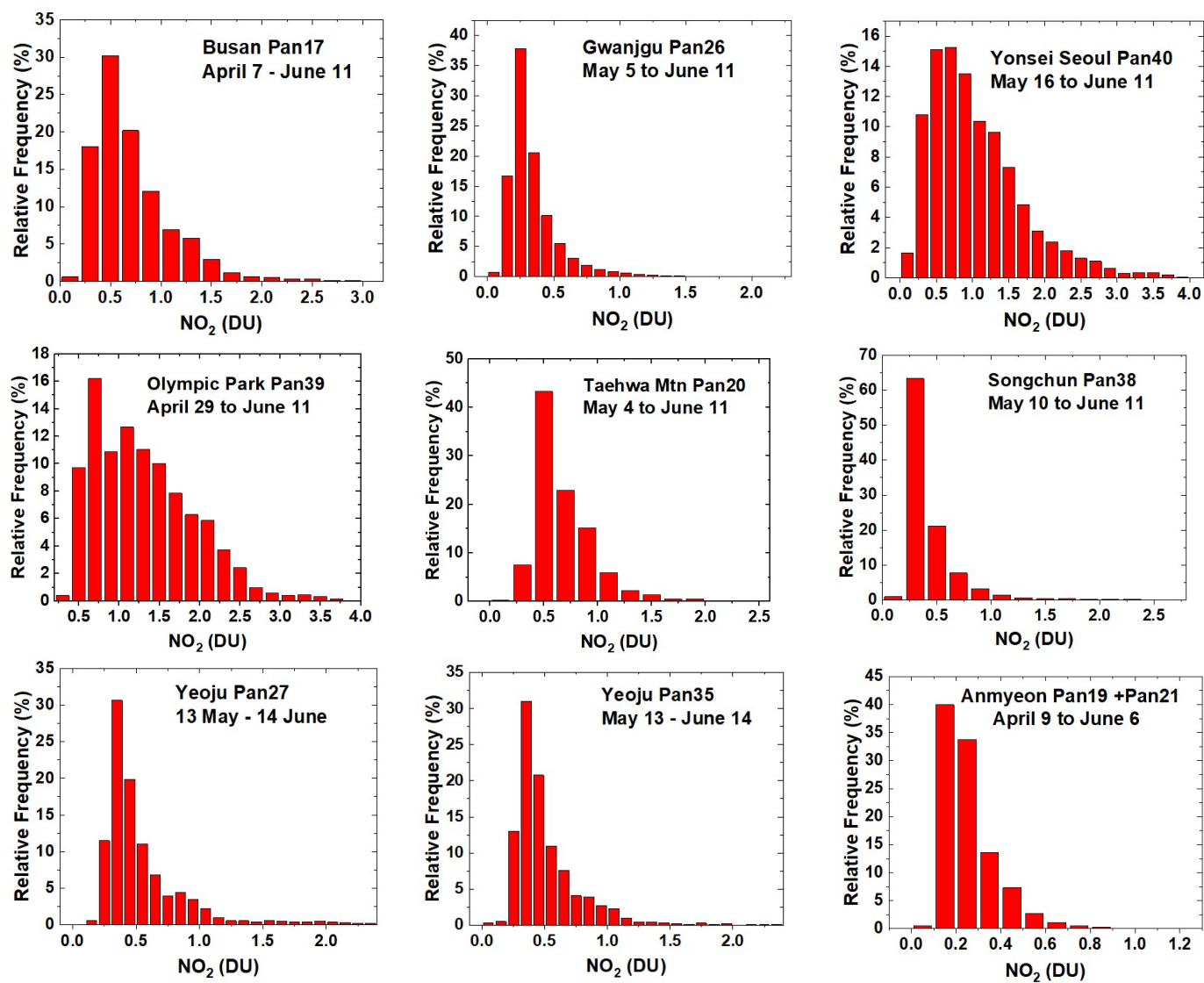


Fig. 3. Frequency distributions of $C(\text{NO}_2)$ across the KORUS-AQ PSI network: April 20 to Jun 6 2016, except as labelled. The axes vary for different sites.

865

866 **F03**

867

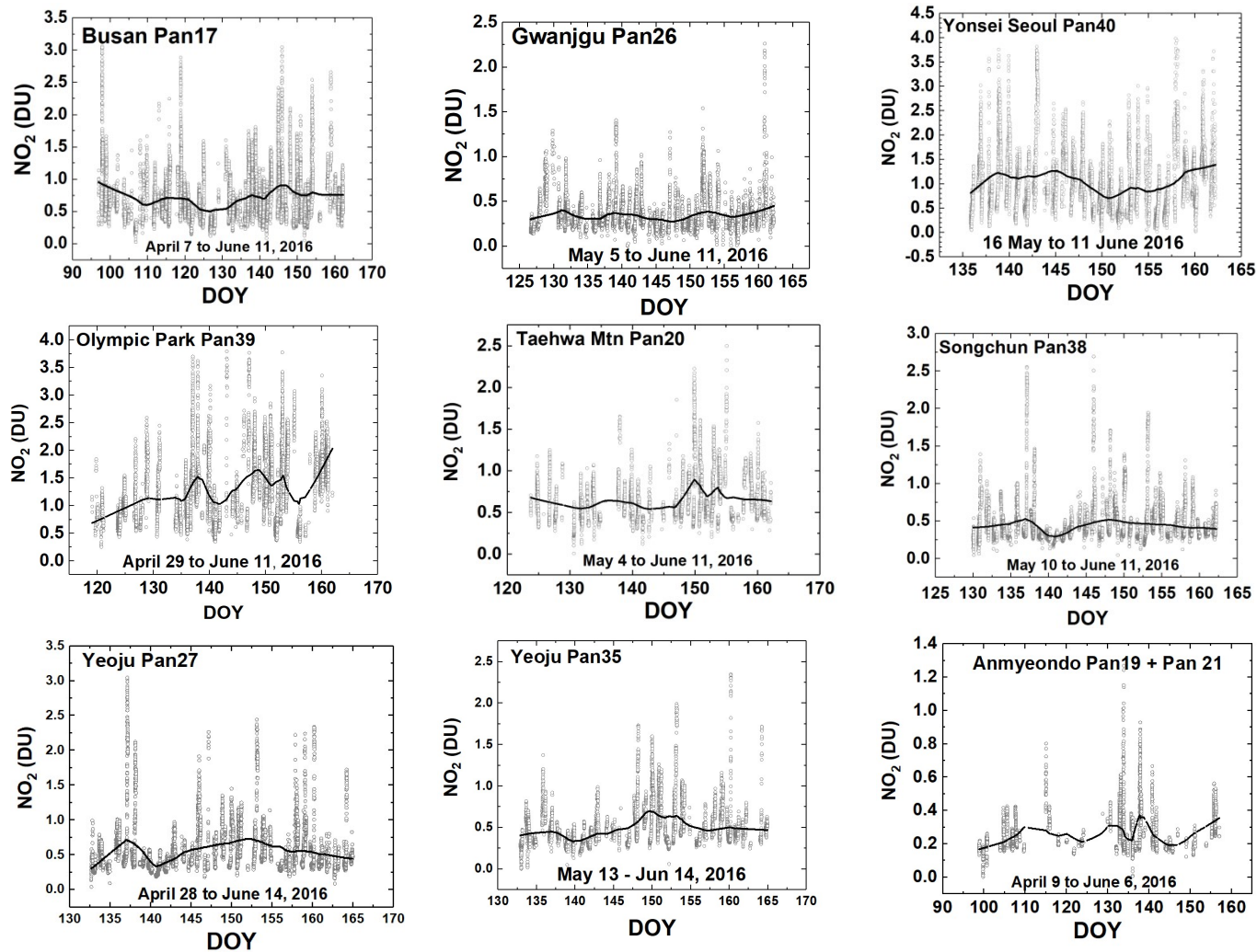


Fig. 4 NO₂ time series vs day of the year (DOY) and diurnal variability (daily vertical extent) at 9 Pandora sites. Notice the very high NO₂ amounts in Seoul and nearby Olympic Park. The black curves are approximately weekly least squares running averages. The daily vertical extent corresponds to diurnal variation (Fig. 2). Note: the vertical scales are different for each site to show the daily variability relative to the running average.

868

869 **F04**

870

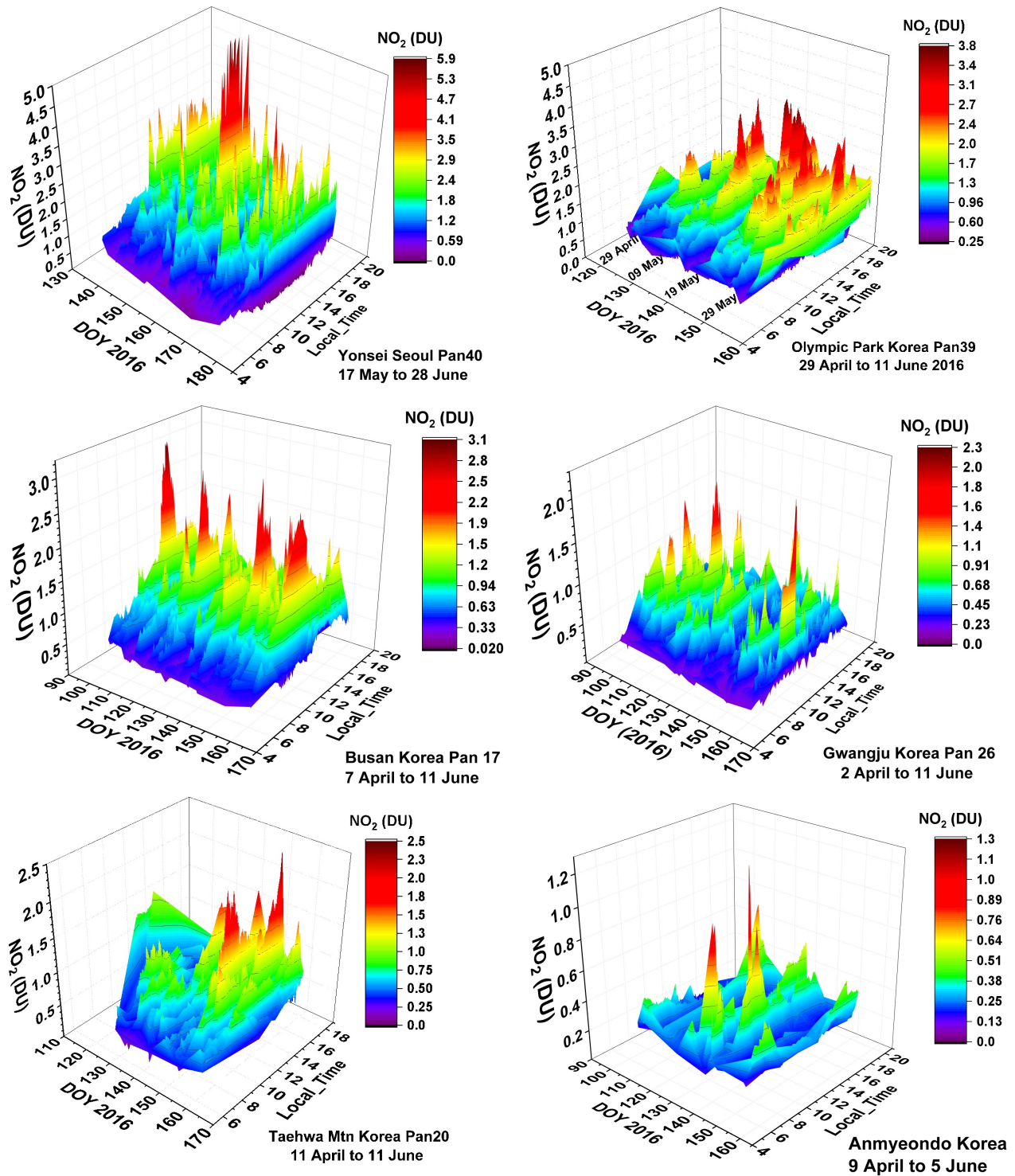


Fig. 5 NO₂ amounts vs Day of the Year (DOY) and Local Time for six sites as labeled in each panel. Day 120=April 29, Day 130=May 9, Day 140=May 19, Day 150=May 29, Day 160=June 8, Day 170 =June18.

871

872 **F05**

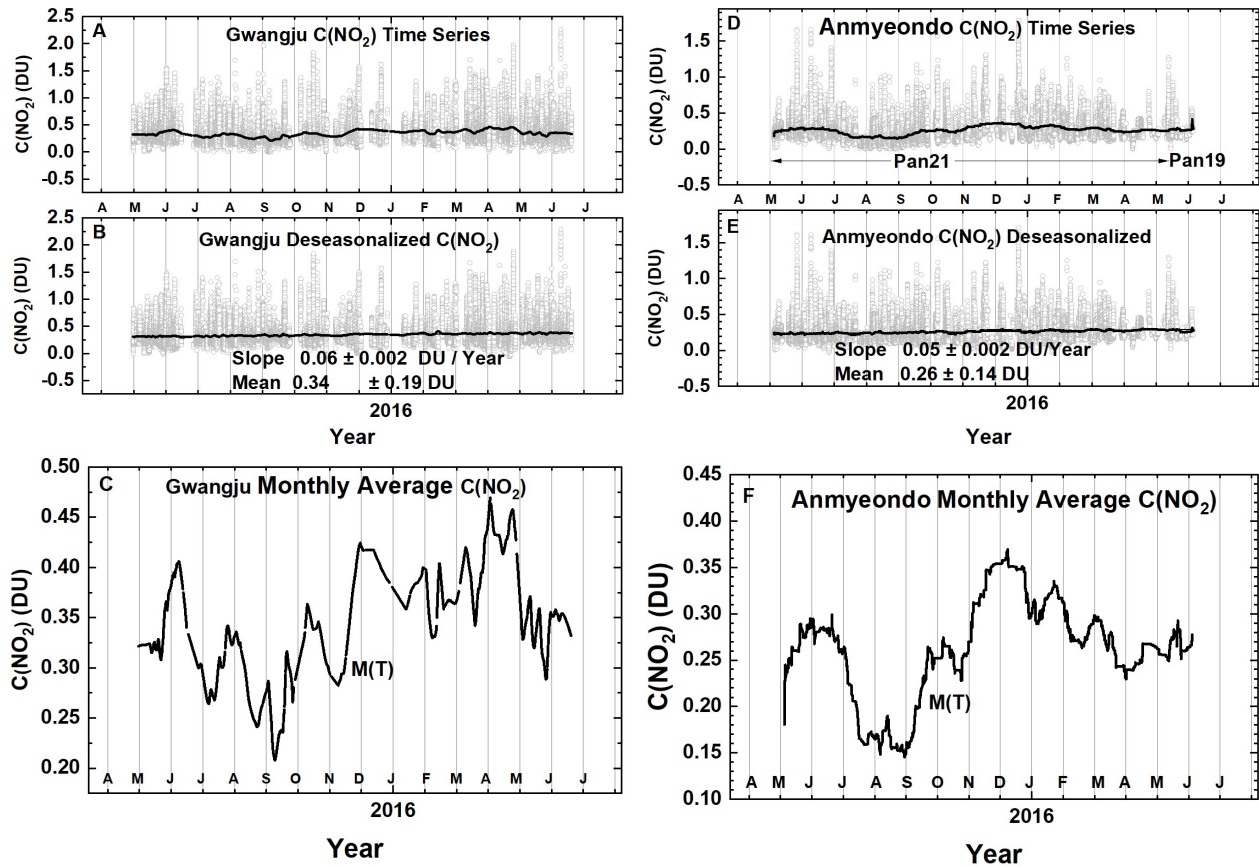


Fig. 6 Approximately 1 year of daily column $C(\text{NO}_2)$ amount data (Panels A and D) and the monthly running average amount (dark plot in Panels A and D). The data are from GIST at Gwangju and Anmyeondo. Panels A and D are the original time series with one data point every 80 seconds, panels B and E are the deseasonalized time series. Panels C and F are an expanded scale of the monthly running averages $M(t)$ of $C(\text{NO}_2)$ that are identical to the solid lines in panels A and D. The vertical extent (panels A, B, D, and E) on a given day is the range of diurnal variation from early morning to late afternoon.

873

874

875 **F06**

876

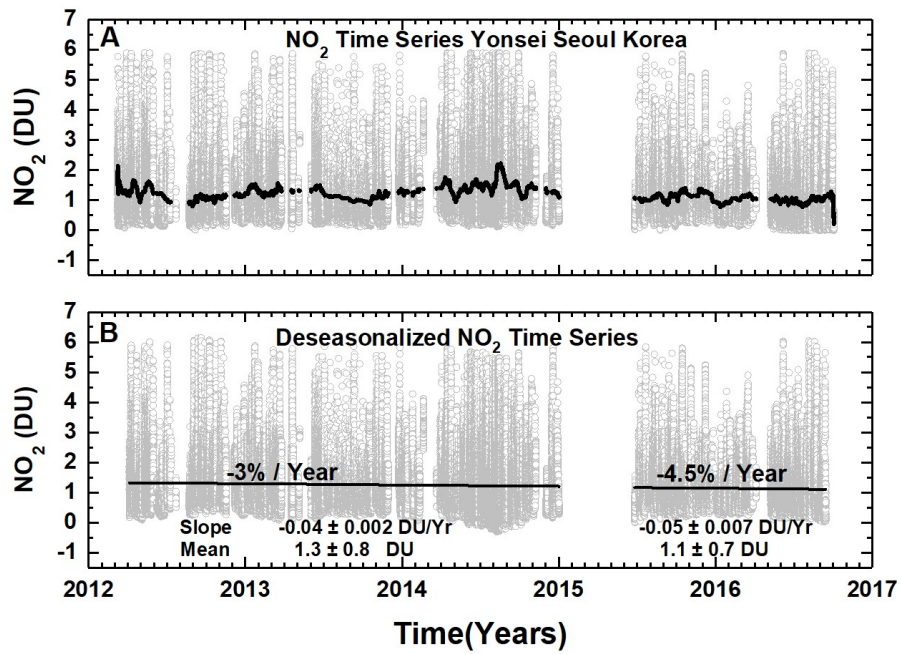


Fig. 7 (A) NO₂ time series at Yonsei University in Seoul NO₂(grey) and (B) deseasonalized time series. Combined slope = -0.05 ± 0.001 DU/Year and Mean = 1.2 ± 0.8 DU or the decrease is -4 ± 0.08 % / Year. Seoul has no clear seasonal cycle.

877

878 **F07**

879

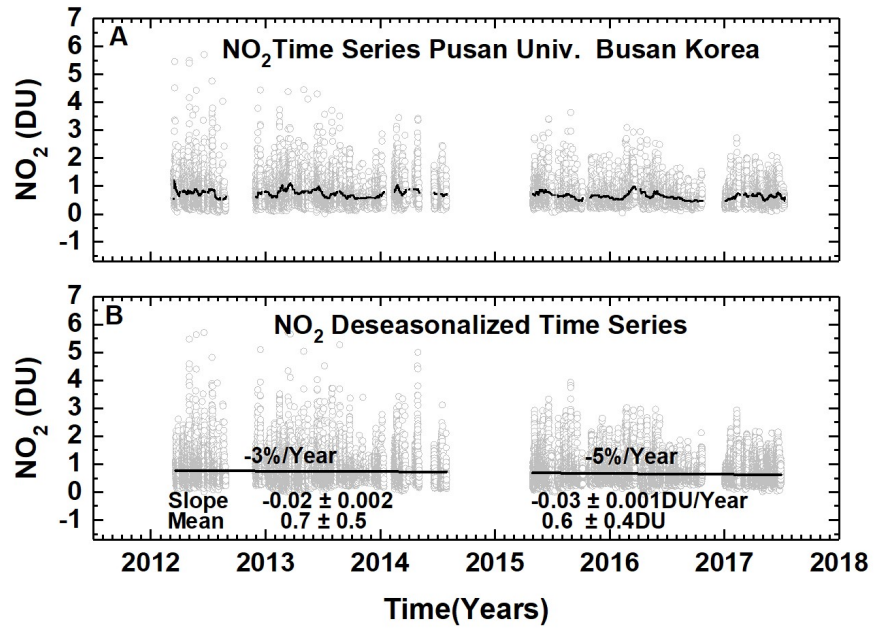


Fig. 8 (A) Pusan University in Busan NO₂ daily time series (grey) and (B) deseasonalized time series with linear trends.

880

881 **F08**

882

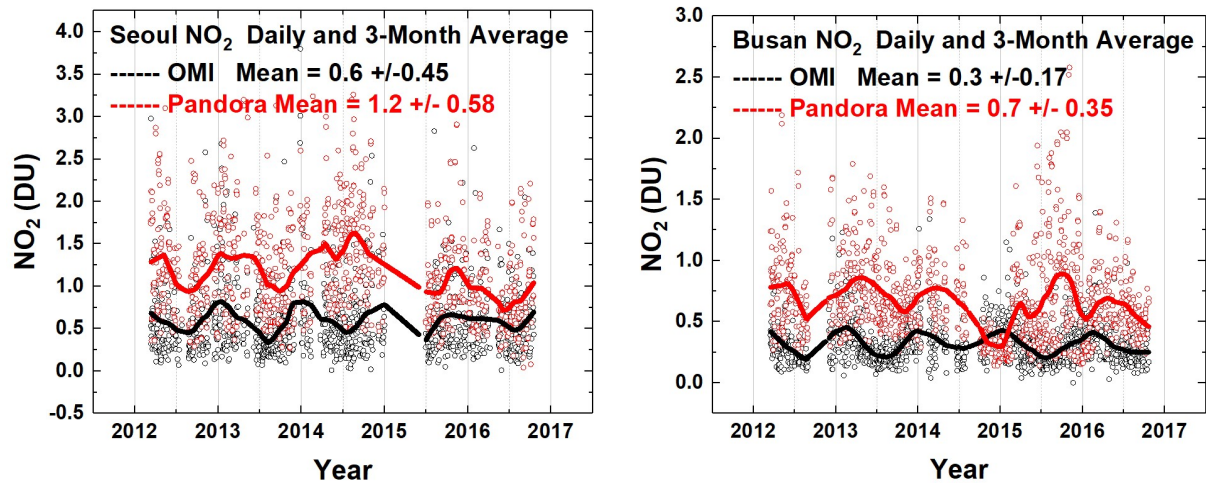


Fig. 9a Comparisons between the daily values of C(NO₂) for OMI (black) and PSI (red) at Seoul and Busan for a 5-year period. Solid lines show the average seasonal variation (Lowess(0.1)), see also Fig. 9b. Linear interpolation is used where there are missing data points.

883

884 **F09a**

885

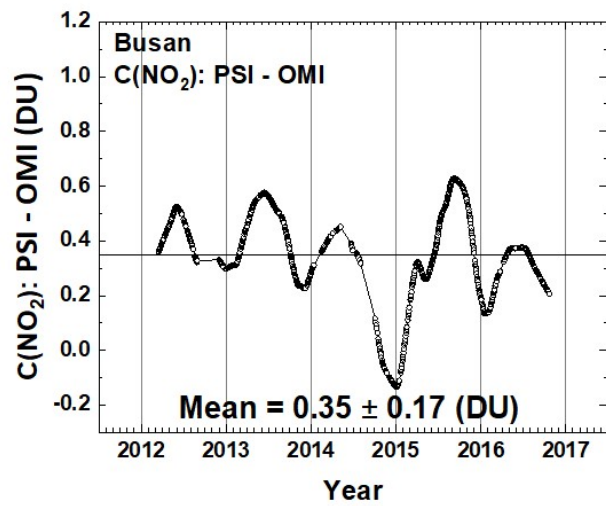
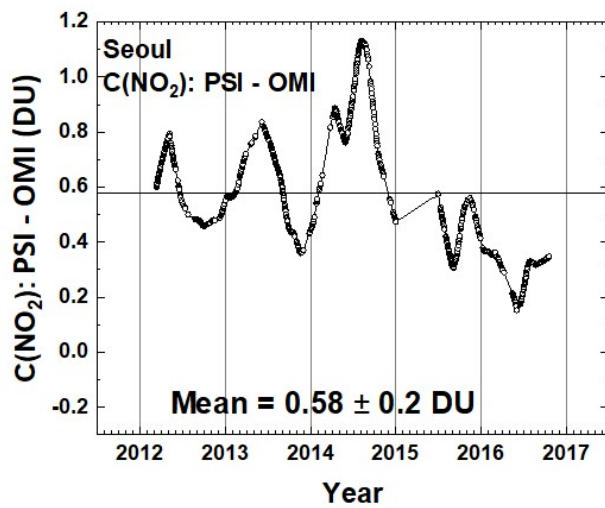
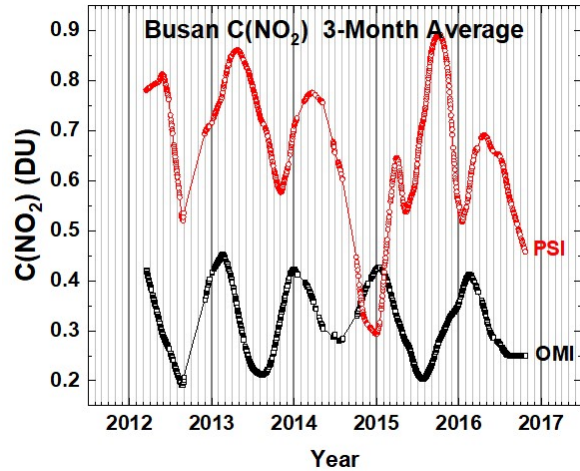
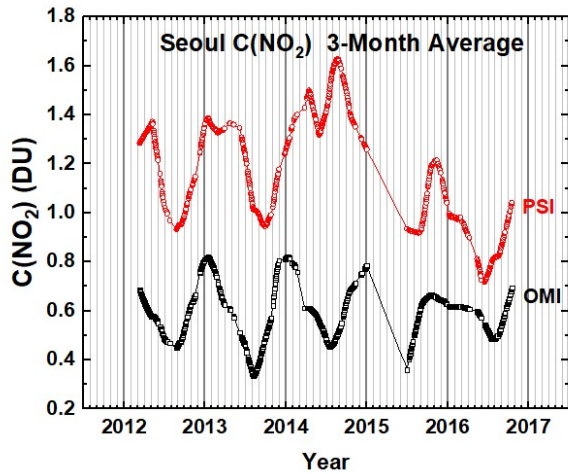


Fig. 9b Comparisons between the seasonal averages for $C(\text{NO}_2)$ from OMI (black) and PSI (red) at Seoul and Busan for a 5-year period. The lower panels show the seasonal difference between the PSI and OMI. The individual data points are shown derived from a Lowess(0.1) smoothing, approximately a 3-month running averages of the daily data. Interpolation has been used where there are missing data points.

886

887 **F09b**

888

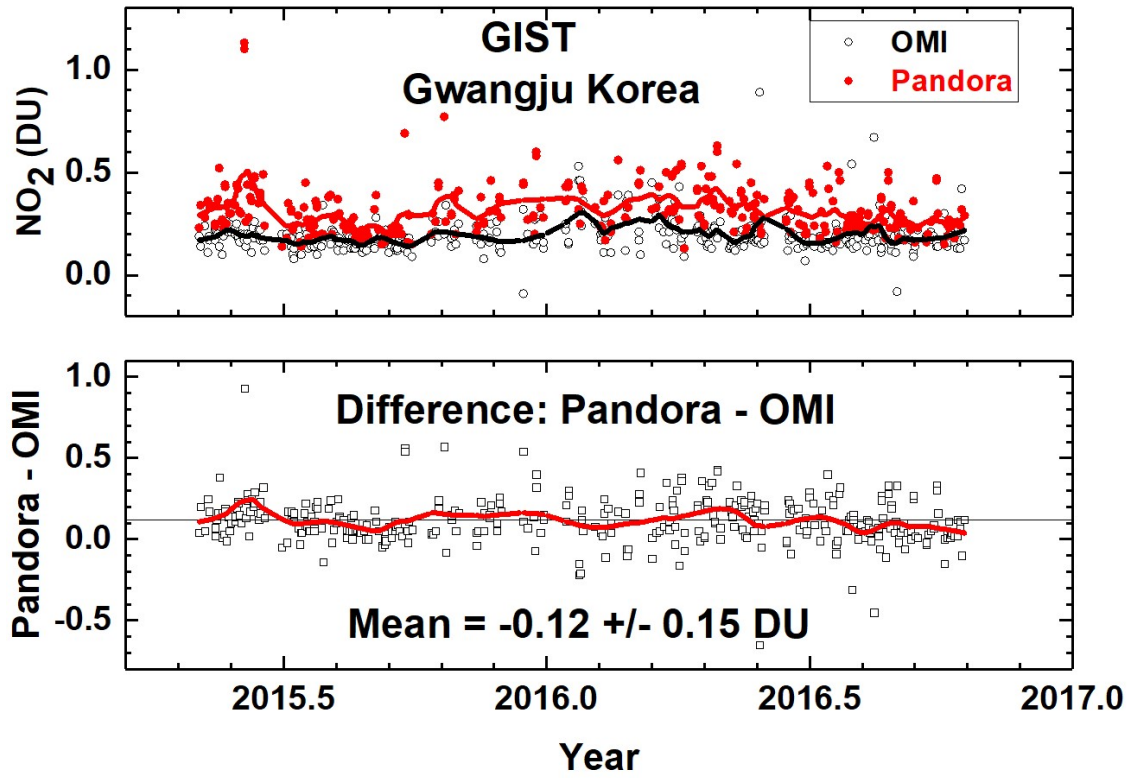


Fig. 10 C(NO₂) time series from Pandora (red) and OMI (black) for GIST University in Gwangju Korea and their differences. The comparison is formed from time coincidences between Pandora and OMI.

889

890 **F10**

891

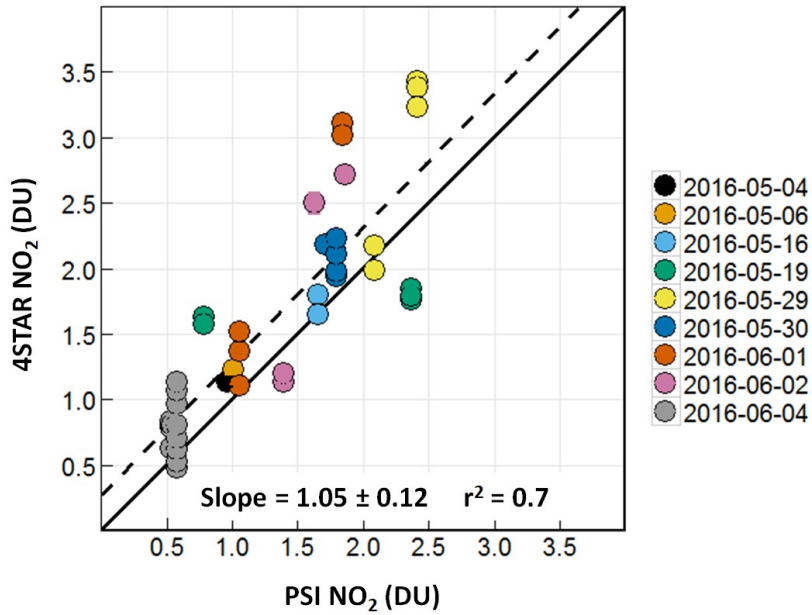


Fig. 11 A correlation plot of C(NO₂) from 4STAR onboard the DC-8 compared to the C(NO₂) amount measured by the PSI at Olympic Park on nine different days. The solid black line is the 1:1 line drawn for reference. The dashed line represents the data linear fit, with a slope of 1.05, and a correlation coefficient $r^2 = 0.7$, as shown on the plot.

892

893 **F11**

894

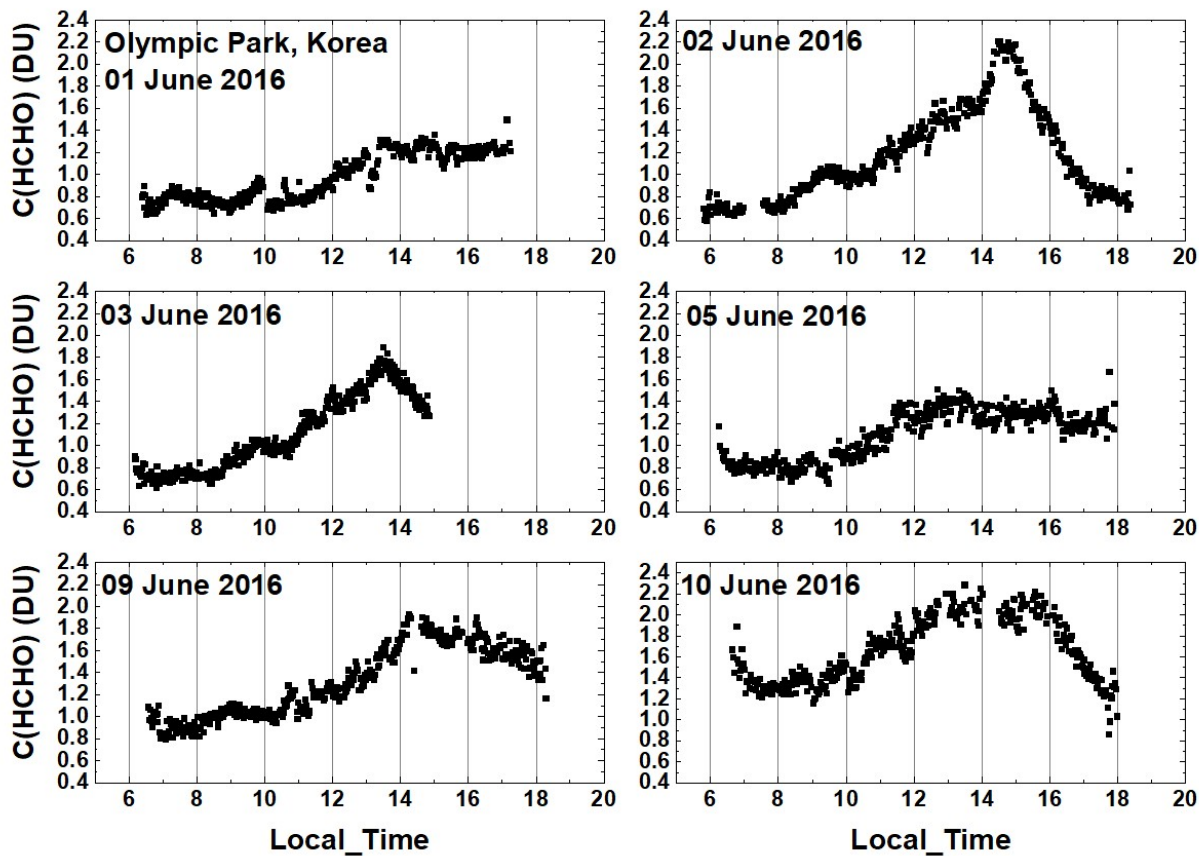


Fig. 12 C(HCHO) from PSI at Olympic Park for 6 days in June 2016. C(HCHO) on 2 June 2016 has a peak value of 2.3 DU at 14:30 hours.

895

896 **F12**

897

898

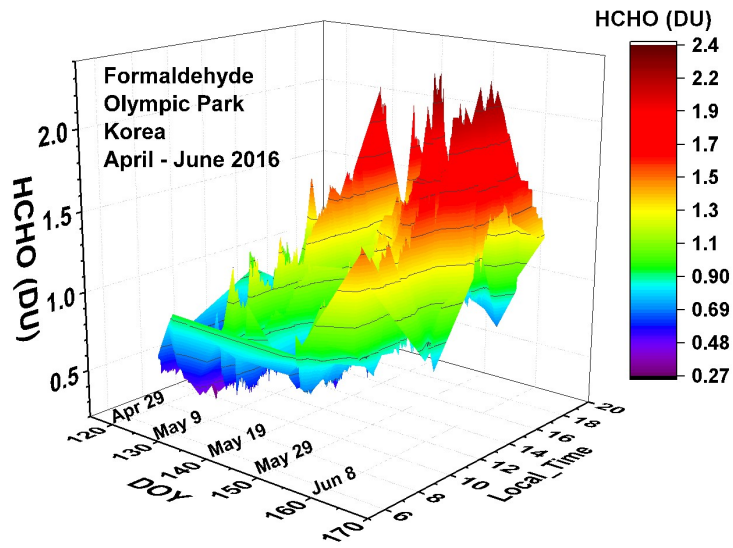


Fig. 13 Pandora measured formaldehyde amounts vs day of the year and local time for 29 April 2016 to 11 June 2016 in Olympic Park.

899

900 **F13**

901

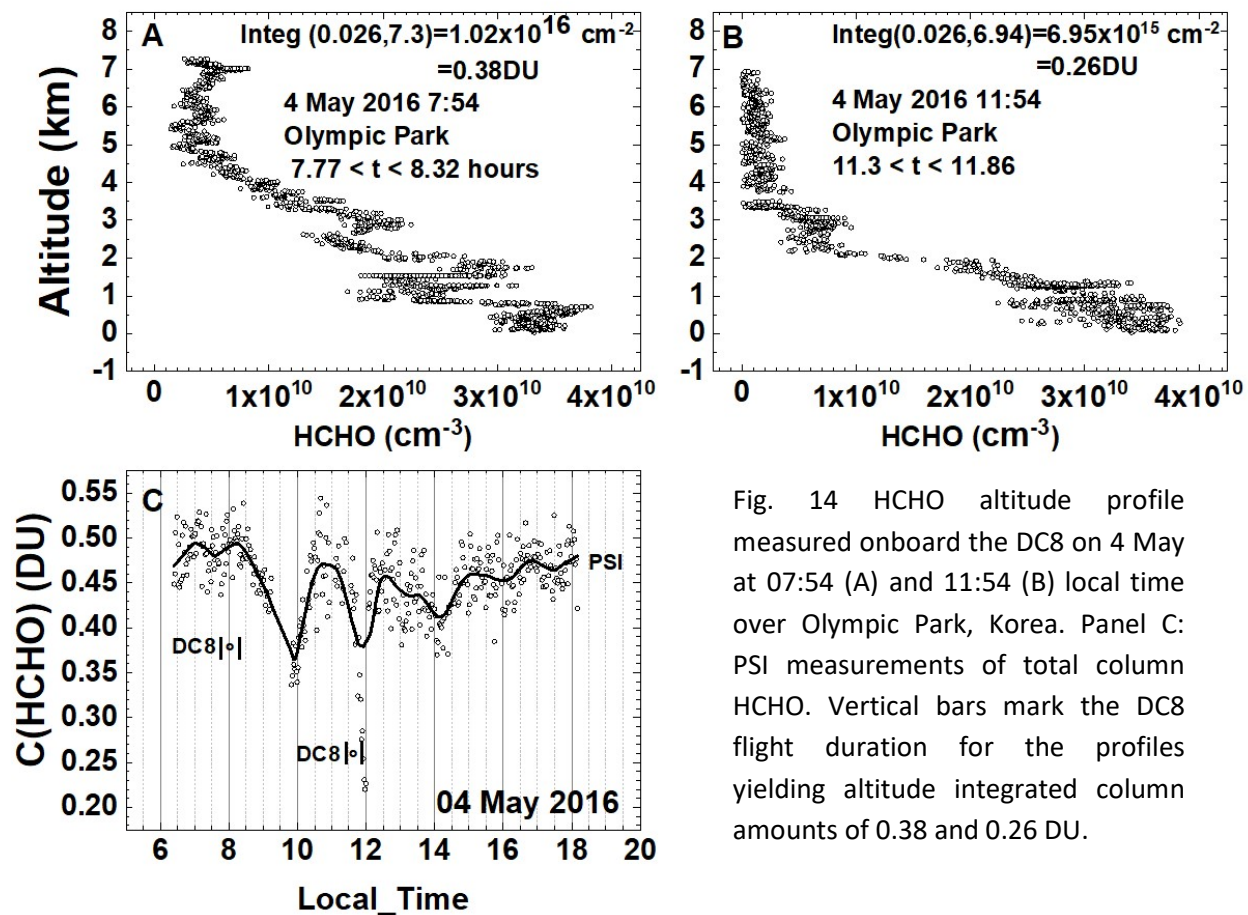


Fig. 14 HCHO altitude profile measured onboard the DC8 on 4 May at 07:54 (A) and 11:54 (B) local time over Olympic Park, Korea. Panel C: PSI measurements of total column HCHO. Vertical bars mark the DC8 flight duration for the profiles yielding altitude integrated column amounts of 0.38 and 0.26 DU.

902

903 **F14**

904

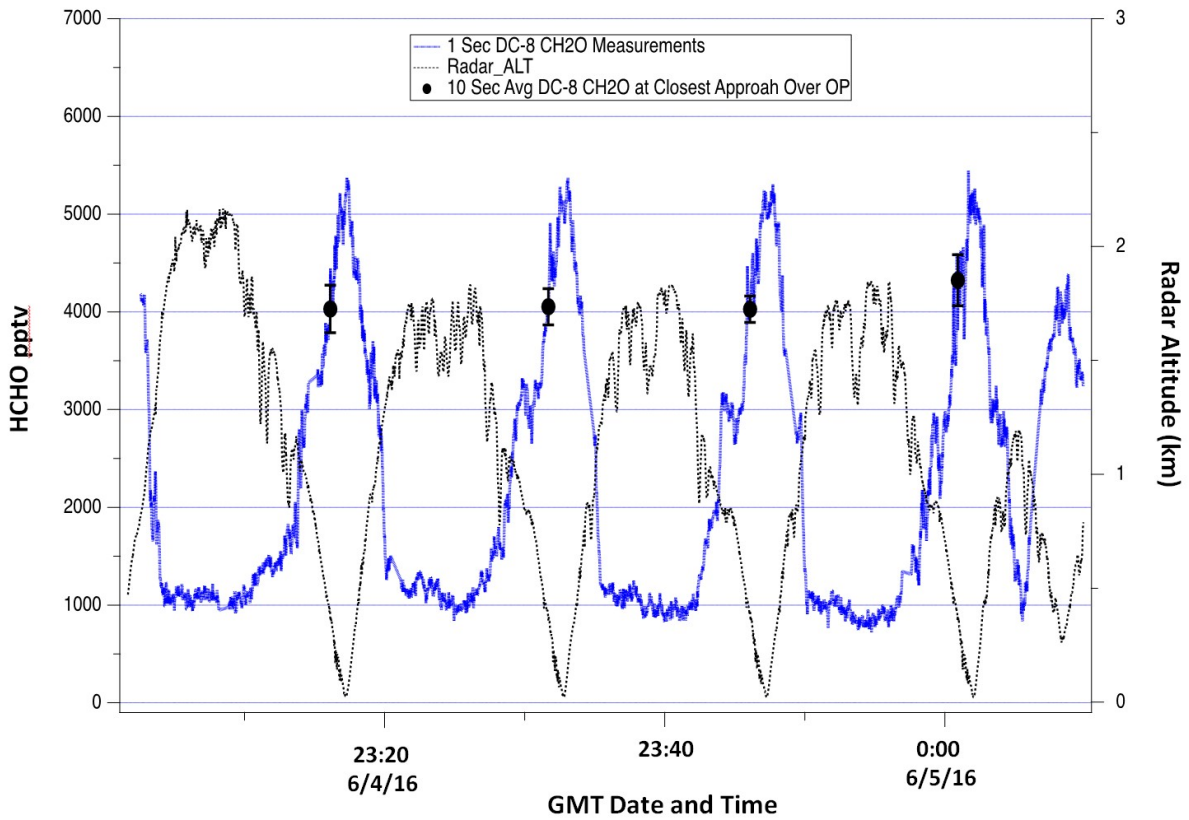


Fig. 15 DC-8 HCHO measurements over Olympic Park on June 4. The continuous blue profiles show the 1-second HCHO data while the black points with error bars show the 10-second average and standard deviation of this data at points of closest approach above the Olympic Park site.

905

906 **F15**

907

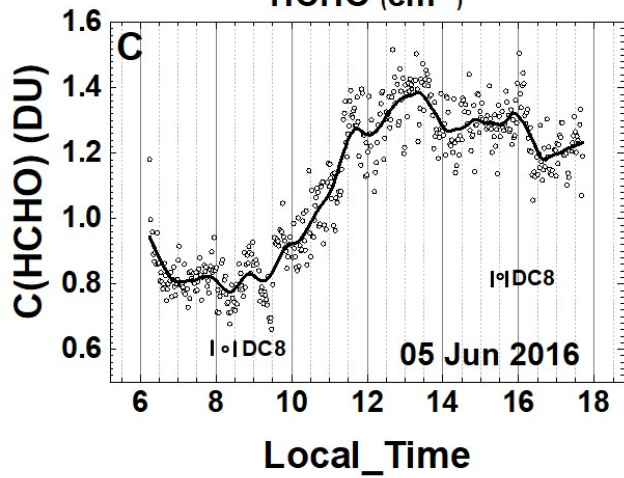
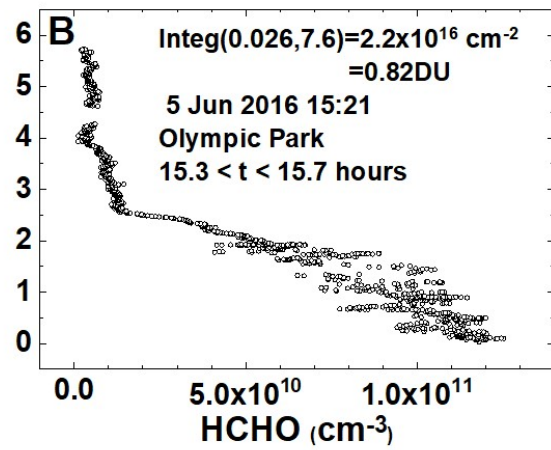
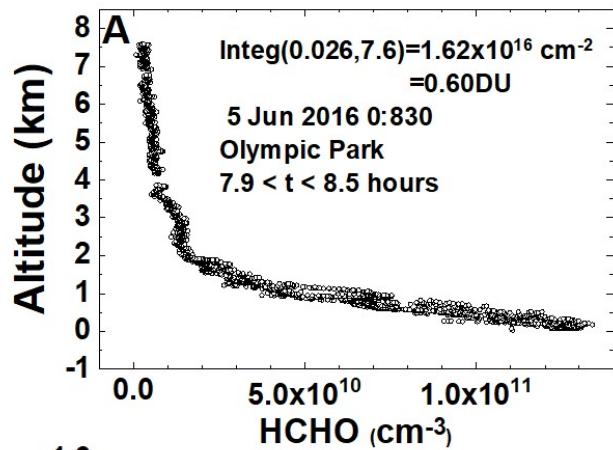


Fig. 16 HCHO altitude profile measured onboard the DC8 on 5 June at 8:30 (A) and 15:21 (B) local time over Olympic Park, Korea. Panel C: PSI measurements of total column HCHO. Vertical bars mark the DC8 flight duration for the profiles yielding column amounts of 0.60 and 0.82 DU.

908

909 **F16**

910

911

912

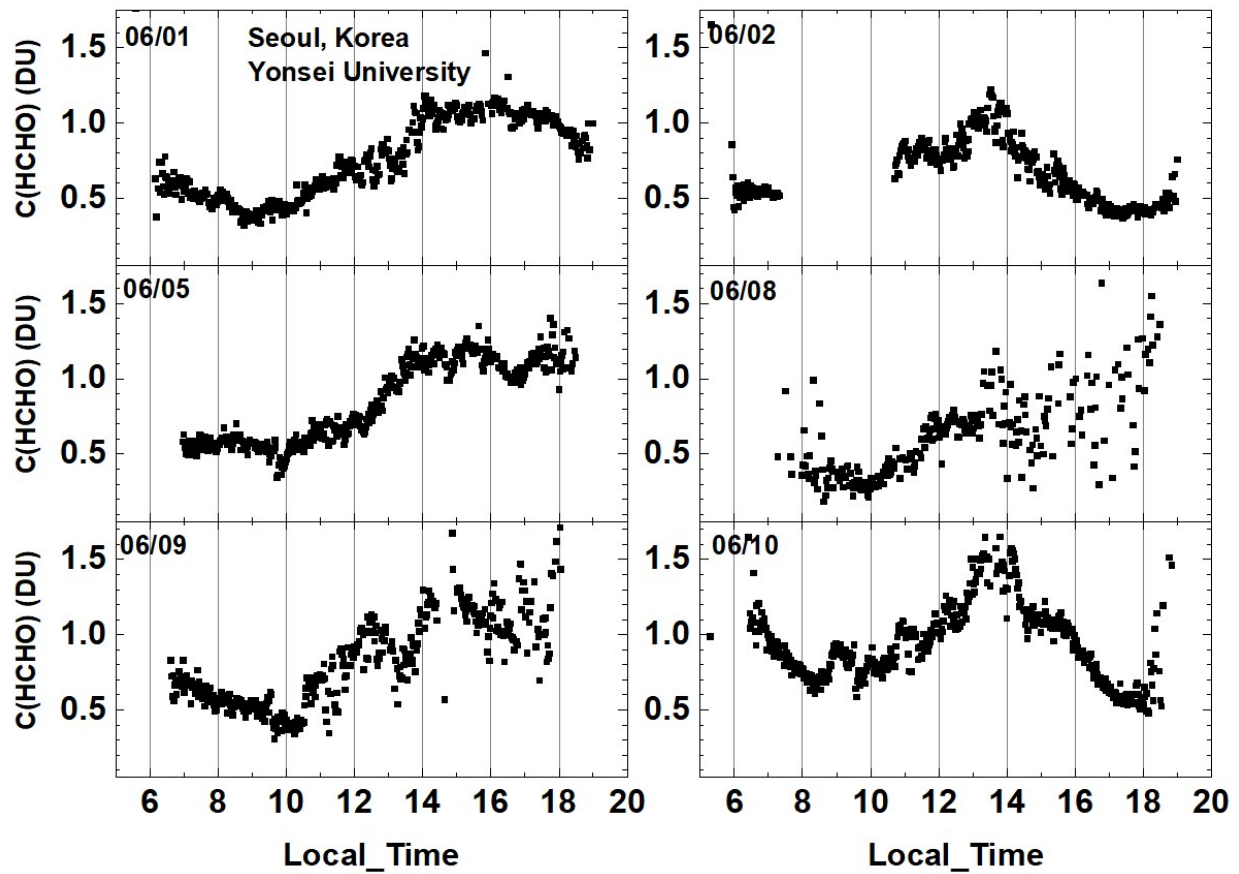


Fig. 17 Total column HCHO from Pandora Yonsei University, Seoul for 6 days in June 2016. C(HCHO) on 2 June 2016 has a peak value of 1.2 DU at 13:30 hours.

913

914 **F17**

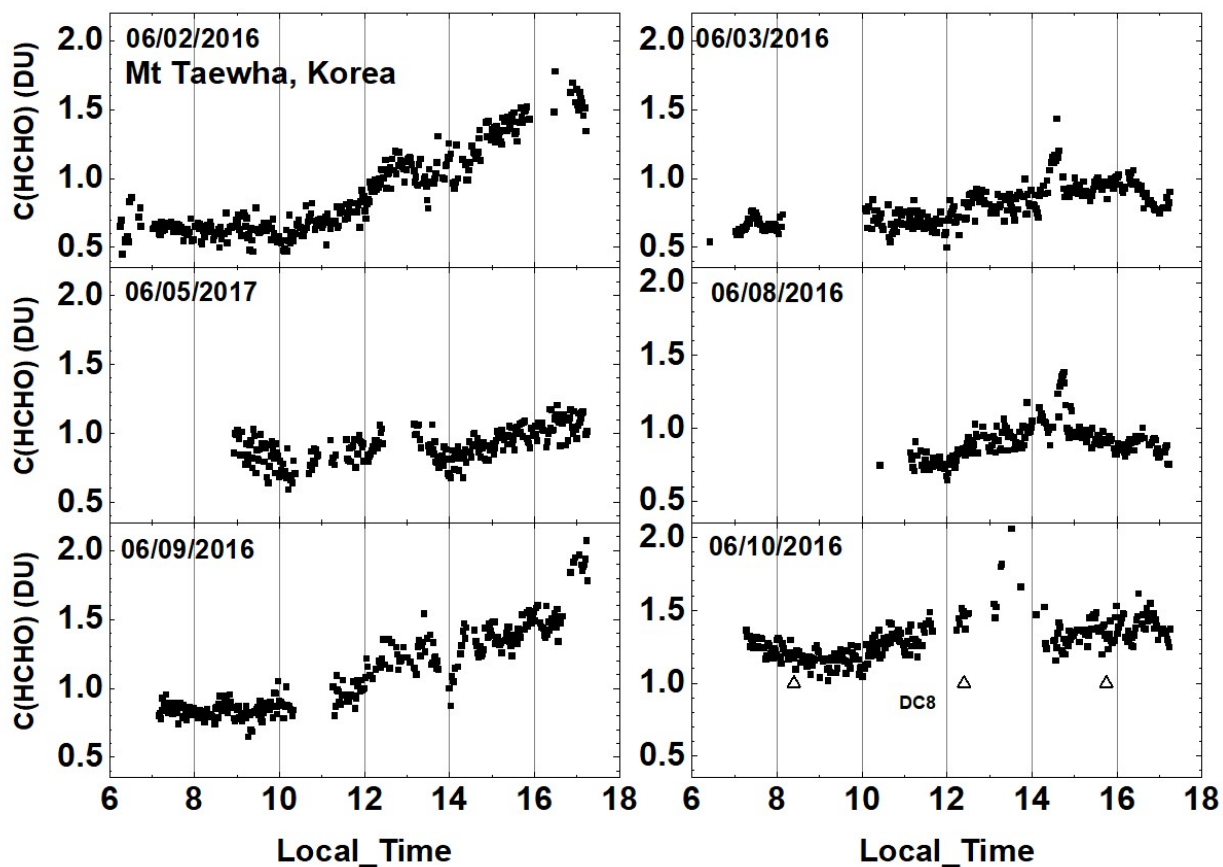


Fig. 18 Total column HCHO from Pandora at Taehwa Mountain for 6 days in June 2016. C(HCHO) on 2 June 2016 has a peak value of 1.7 DU at 16:20. △ are DC8 measurements on 10 June

915

916 **F18**

917

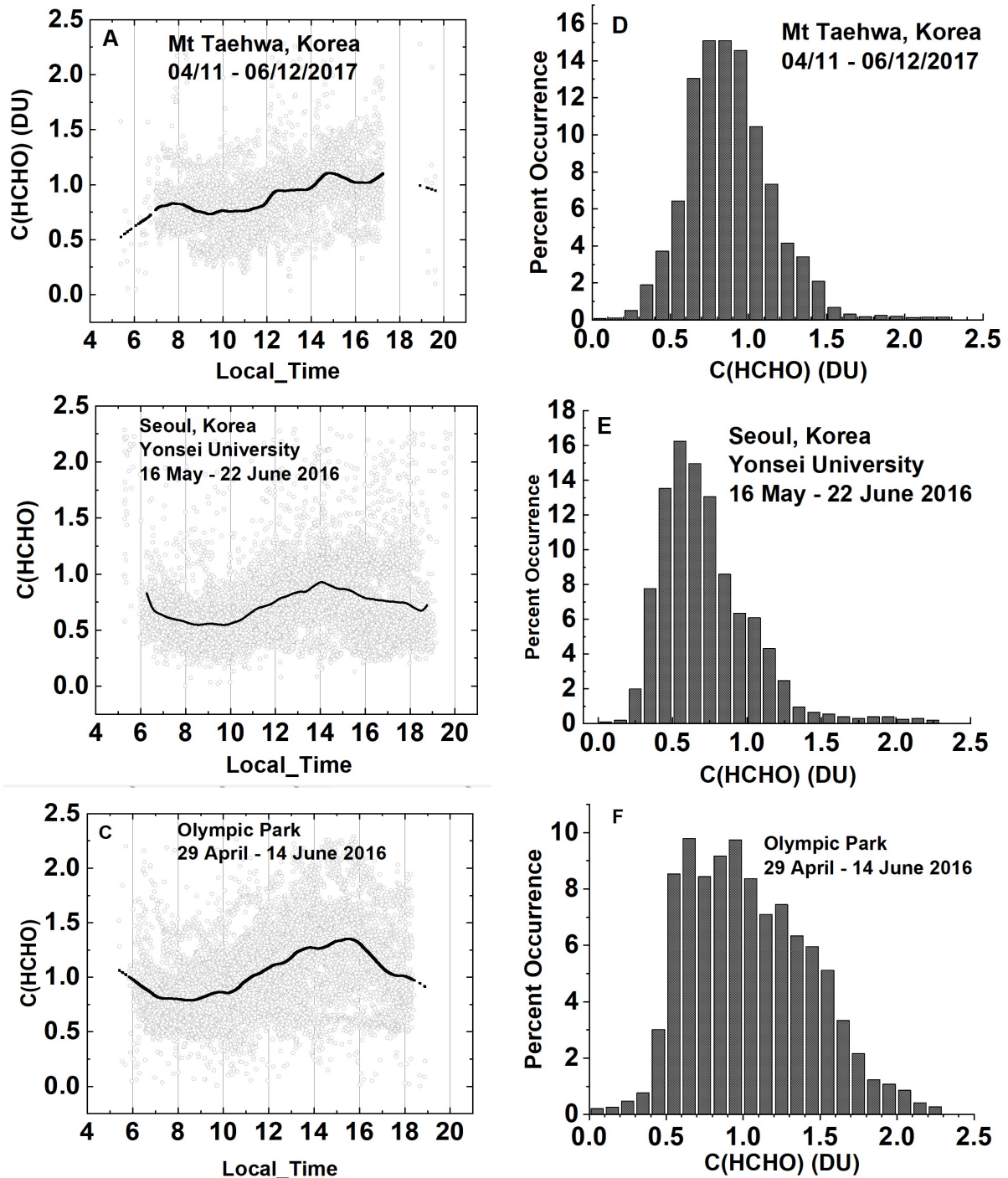


Fig. 19a Summary of total column HCHO for the stated dates during the KORUS-AQ campaign. The solid line is a Lowess(0.1) fit to the data. The sharp cutoffs in panel A, B, and C were caused by obstructions of the direct sun from the PSI FOV in the afternoon.

918

919 **F19a**

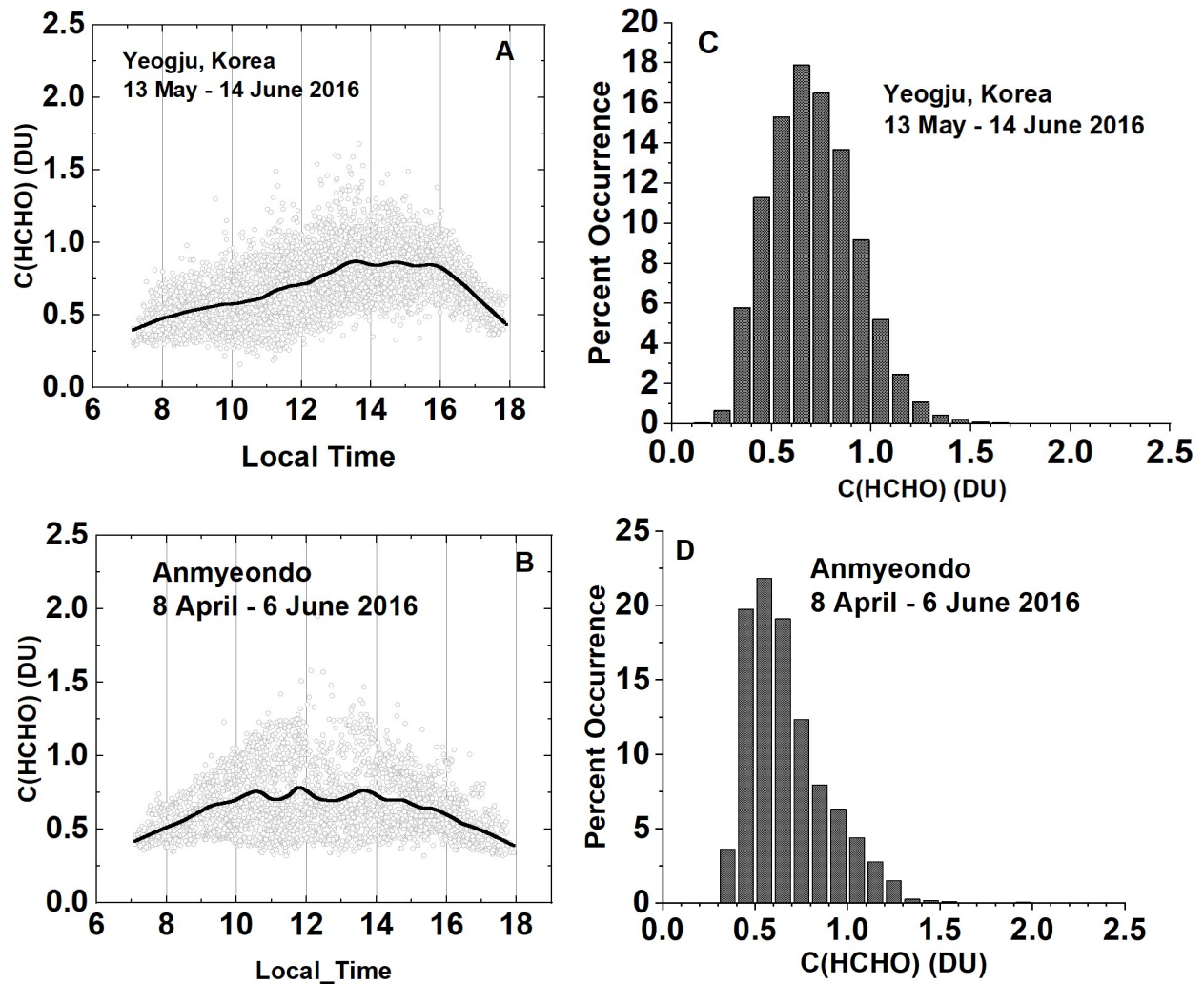


Fig. 19b Summary of total column HCHO for the stated dates during the KORUS-AQ campaign. Panels A and B represent the daily variation at a given local time. The solid line is a Lowess(0.1) fit to the data. Panels C and D show the frequency of occurrence (%) for different amounts of HCHO.

920

921

922 **F19b**

923

924

925

926

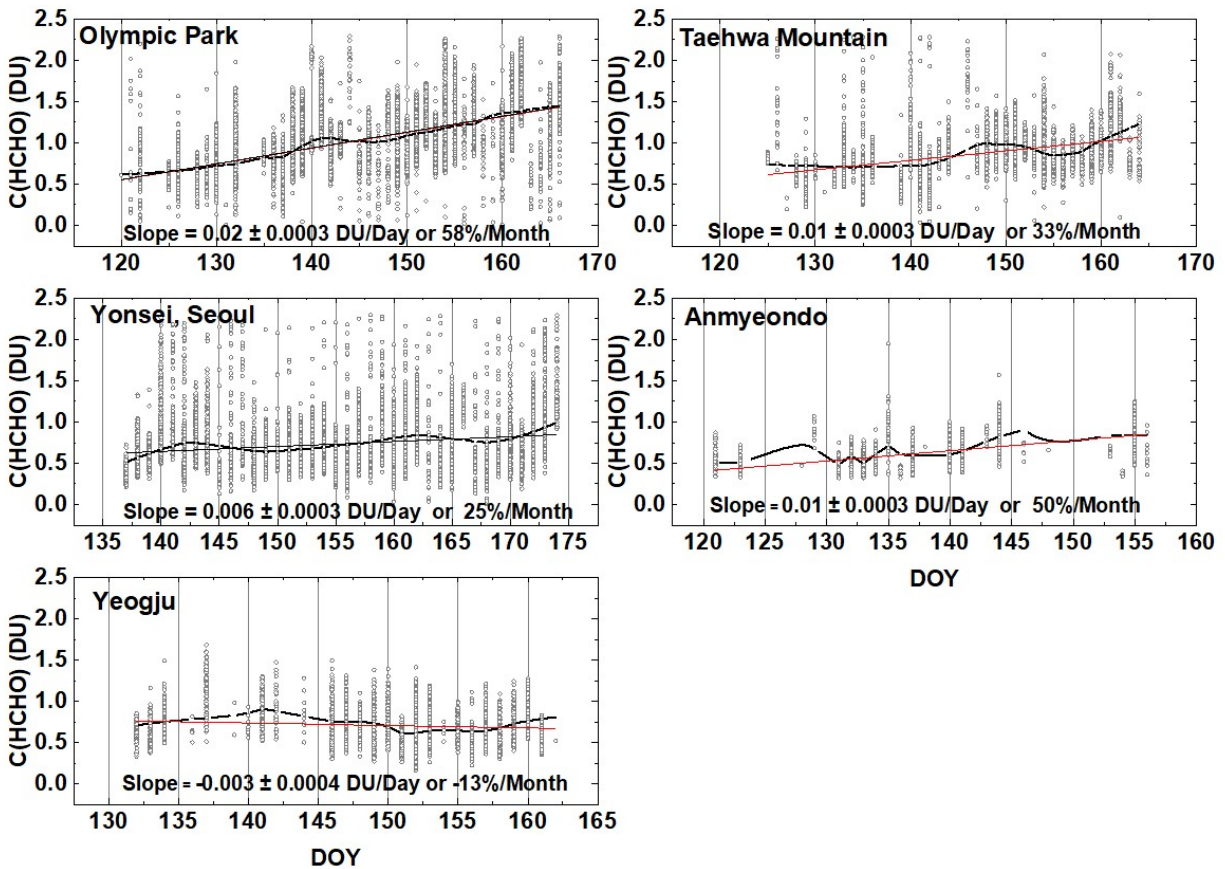


Fig. 20 The springtime change in C(HCHO) over about a 40 day period depending on the site. The “vertical bars” are the diurnal variation within each day of data. The thicker red curve is a Lowess(0.3) fit to the data, while the thin red line is a linear least squares fit. The Lowess(0.3) fit is approximately a 10-day local least-squares average.

927

928 **F20**

929

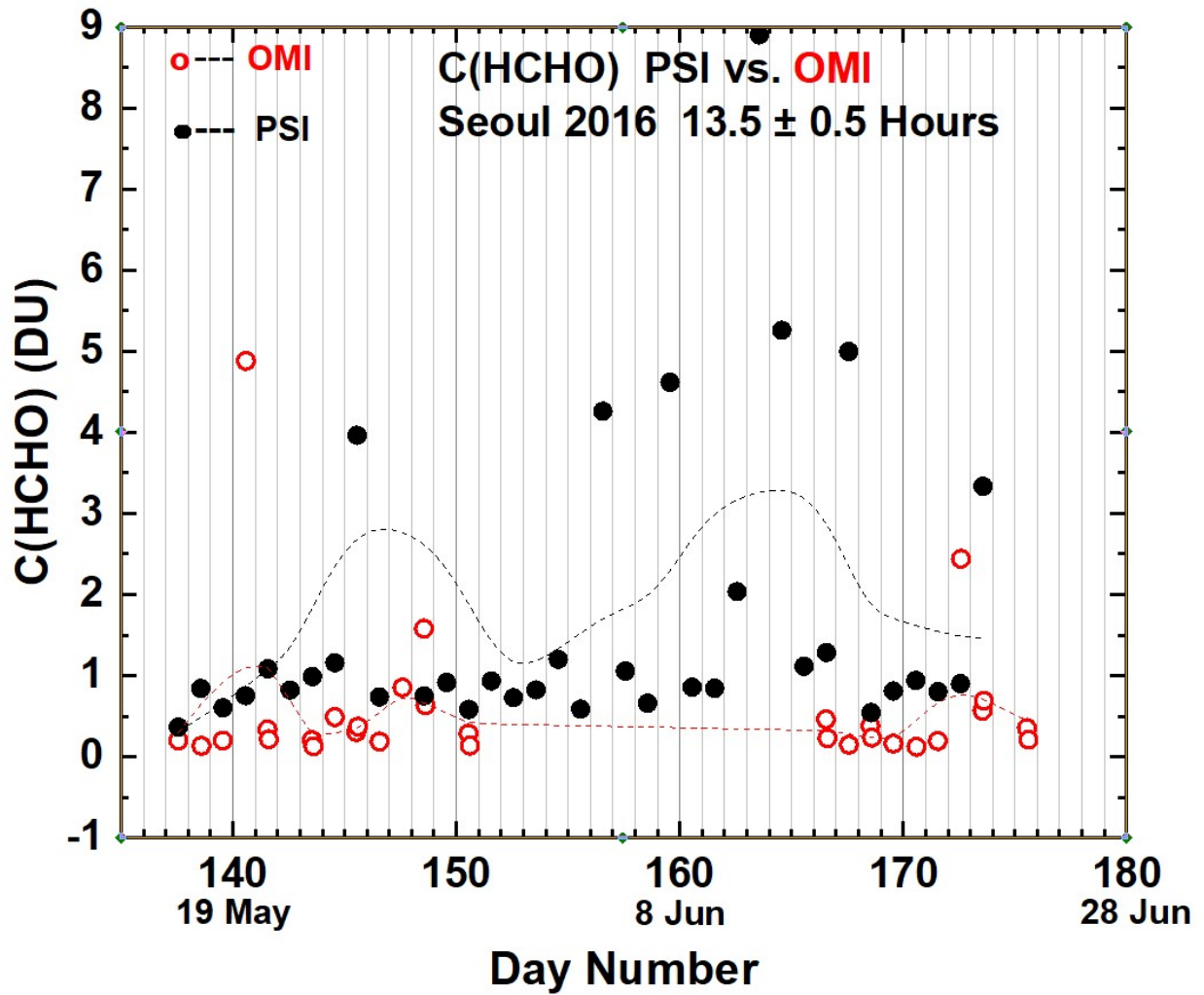


Fig. 21 Compare PSI • and OMI ◯ retrievals of C(HCHO) at 13.5 ± 0.5 hours. OMI overpass data, V03, are from <https://avdc.gsfc.nasa.gov/index.php?site=1113974256&id=81>

930

931 **F21**

932

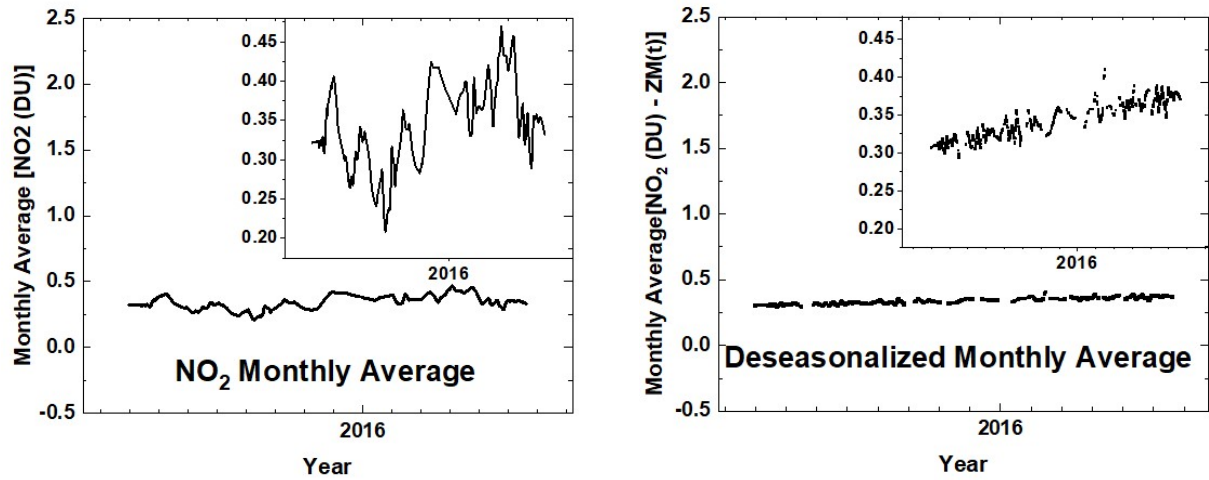


Fig. A1 An illustration of the deseasonalization (right panel) of the monthly running average of NO₂ (left panel) shown in Fig. 6. The insets are magnifications of the main plots.

933

934

935 **FA1**